

Copyright
by
Erin Nancy Eastwood
2011

The Dissertation Committee for Erin Nancy Eastwood Certifies that this is the approved version of the following dissertation:

**RECONSTRUCTING ENVIRONMENTAL FORCINGS ON
AEOLIAN DUNE FIELDS: RESULTS FROM MODERN, ANCIENT,
AND NUMERICALLY-SIMULATED DUNES**

Committee:

Gary Kocurek, Supervisor

David Mohrig

Meinhard Bayani Cardenas

Omar Ghattas

Andreas CW Baas

**RECONSTRUCTING ENVIRONMENTAL FORCINGS ON
AEOLIAN DUNE FIELDS: RESULTS FROM MODERN, ANCIENT,
AND NUMERICALLY-SIMULATED DUNES**

by

Erin Nancy Eastwood, B.S.

Dissertation

Presented to the Faculty of the Graduate School of
The University of Texas at Austin
in Partial Fulfillment
of the Requirements
for the Degree of

Doctor of Philosophy

The University of Texas at Austin

December 2011

Dedication

For Andy.

I succeeded because of your unconditional love and unfailing support.

"I came here last year and found these canyons, and
they feel like the heart of the world to me."

~John Otto

"The Grand Canyon is... the gulf of silence, widened in the desert; it is all
time inscribing the naked rock; it is the book of earth."

~Donald Culross Peattie

Acknowledgements

My family has been an unwavering source of support and believed in me even when I doubted myself. My parents were never more than a phone call or email away, providing guidance and encouragement. My fiancé Andy listened to me whine and complain and put up with my sky-high stress levels that I'd bring home every night. He taught me what it means to be balanced, and to let go and not worry about the things I can't control. Andy reminded me that there is life outside my PhD and that family comes before everything else. Meg is always there for me, with a quick, witty thought to make me laugh. She has been the best roommate, sister, and friend -- patient, supportive and caring. Kenny is the most wonderful father-in-law and friend -- always supportive and will bend over backwards to help anyone & everyone out! Dustin has been completely supportive and a good friend.

I would like to thank my supervisor, Gary, for teaching me to stand up for my scientific ideas and to think on my feet. You taught me to read the rocks, and for that I will be eternally grateful and forever changed. David Mohrig provided "glorious" encouragement and support -- I will always be grateful for your assistance that kept me going. Joanna Nield has been an incredible mentor, research collaborator, and friend; thanks for hosting me at the University of Southampton, opening my eyes to the world of modeling, and for teaching me to ride the PhD rollercoaster. I will always have wonderful memories from London & Soton. Andreas Baas graciously hosted me at King's College London for a year and taught me to navigate a modeling project without getting lost on tangents. Bayani Cardenas introduced me to the powerful yet complicated world of FLUENT. Omar Ghattas provided mathematical and modeling advice, and proved to be an excellent role model for balancing exercise with work. Ron Blakey planted the seeds for the path I chose -- thank you for introducing me to the red rocks of Sedona, the beaches and estuaries of Rocky Point, Mexico, and the 3500 m of aeolian section on the Colorado Plateau. Chuck Barnes introduced me to the world of geology -- without him I wouldn't be here. I would like to thank Philip Guerrero for his friendship and assistance in all matters related to UT. Philip, you truly are "the man with all the answers" and none of us would survive this journey without you.

I have made the best friends of my life here in Austin -- smart, funny, beautiful people always available with a solution or a laugh. Fellow geology graduate students provided assistance and support, and have proven to be great sounding boards for new scientific ideas: Audrey, Ryan, Travis, Brandon, Glen, Jeff, Aymeric, Lindsay Jo, Jamie, and Eric. I would not have survived without our killer 'girls night' crew: Audrey, Kelly, Sara, and Julia. To the various Austinite groups that welcomed me with open arms: Jonathan and Dawn-Ashley -- our travel buddies, the Man Camp clan -- always a crazy time, and Darrell, Fr. Jamie, and Fr. Ed -- thanks for your love and prayers.

Funding for this dissertation was provided by the Jackson School of Geosciences, the National Park Service as part of the Chihuahuan Desert Network Inventory and Monitoring Program, a National Science Foundation grant to Gary Kocurek and David Mohrig, the ConocoPhillips SPIRIT scholar program, a Geological Society of America Graduate Student Research Award, BHP Billiton, and The University of Texas at Austin graduate fellowship. I am especially grateful to the National Park Service for facilitating this study: Hildy Reiser and David Bustos at White Sands National Monument and officers of the Glen Canyon National Recreational Area.

**RECONSTRUCTING ENVIRONMENTAL FORCINGS ON
AEOLIAN DUNE FIELDS: RESULTS FROM MODERN, ANCIENT,
AND NUMERICALLY-SIMULATED DUNES**

Erin Nancy Eastwood, Ph.D.

The University of Texas at Austin, 2011

Supervisor: Gary Kocurek

This dissertation combines studies of aeolian bedforms and aeolian dune-field patterns to create a comprehensive set of tools that can be used in tandem (or separately) to extract information about climate change and landscape evolution, and to identify the controls on formation for specific modern dune fields or ancient aeolian sequences. The spatial distribution of surface processes, erosion/deposition rates, and lee face sorting on aeolian dunes are each a function of the incident angle. This correlation between stratification style and incidence angle can be used to develop a “toolbox” of methods based on measurements of key suites of parameters found in ancient aeolian deposits. Information obtained from the rock record can be used as input data for different kinds of numerical models. Regional-scale paleowind conditions can be used to validate paleoclimate and global circulation models. Understanding the natural variability in the Earth’s climate throughout its history can help predict future climate change. Reconstructed wind regimes and bedform morphologies can be used in numerical models of aeolian dune-field pattern evolution to simulate patterns analogous to those

reconstructed from ancient aeolian systems. Much of the diversity of aeolian dune-field patterns seen in the real world is a function of the sediment supply and transport capacity, which in turn determine the sediment availability of the system. Knowledge of the sediment supply, availability, and transport capacity of aeolian systems can be used to predict the amount of sand in the system and where it might have migrated. This information can be extremely useful for development and production of oil and gas accumulations, where a discovery has been made but the spatial extent of the aeolian reservoir is unknown.

Table of Contents

| | |
|---|-----|
| List of Figures | xii |
| Chapter 1: Introduction | 1 |
| Chapter 2: Methodology for Extracting Wind Direction and Speed from Aeolian Cross-strata | 7 |
| Abstract | 7 |
| 1. Introduction | 8 |
| 2. Theory | 10 |
| 2.1 Reconstruction of wind direction | 10 |
| 2.2 Reconstruction of wind speed | 15 |
| 3. Study area and methods | 23 |
| 3.1 Study area overview | 23 |
| 3.2 Methods | 25 |
| 4. Data | 28 |
| 4.1 Characterization of the wind events | 28 |
| 4.2 Sediment record of the wind events | 31 |
| 5. Data analysis and discussion | 37 |
| 5.1 Dynamics that control the spatial distribution of lee surface processes | 37 |
| 5.2 Deposition/erosion rates and incidence angle | 42 |
| 5.3 Grain sorting by surface processes and modes of transport | 43 |
| 6. Conclusions | 47 |
| 7. Acknowledgements | 50 |
| 8. Mathematical Notation | 51 |
| 9. References | 52 |
| Chapter 3: Reconstructing Wind Direction and Speed for the Permian Cedar Mesa Sandstone, SE Utah | 58 |
| Abstract | 58 |
| 1. Introduction | 59 |

| | |
|---|-----|
| 2. Theory | 61 |
| 2.1 Reconstruction of Wind Direction | 61 |
| 2.2 Reconstruction of Wind Speed | 63 |
| 3. Field area and methods | 67 |
| 3.1 Permian Cedar Mesa Sandstone..... | 67 |
| 3.2 Methods..... | 69 |
| 4. Data | 71 |
| 4.1 Stratification Types | 71 |
| 4.2. Characterization of the Wind Direction..... | 77 |
| 4.3 Characterization of the Wind Speed | 81 |
| 5. Data Analysis | 87 |
| 5.1 Wind Regime Recorded in Cross-Strata | 87 |
| 5.2 Redefining Incidence Angle | 91 |
| 5.3 Predicting Stratification Type | 93 |
| 6. Application to Paleoclimate Reconstructions | 94 |
| 7. Conclusions..... | 96 |
| 8. Mathematical Notation..... | 98 |
| 9. References..... | 99 |
| Chapter 4: Modelling Controls on Aeolian Dune-Field Pattern Evolution | 104 |
| Abstract | 104 |
| 1. Introduction..... | 105 |
| 2. Methods..... | 106 |
| 2.1 Model Description | 106 |
| 2.2 Simulated Sediment State | 109 |
| 2.3 Simulated Source-Area Geometry | 112 |
| 3. Results and Discussion | 113 |
| 3.1 Simulated Bedforms..... | 113 |
| 3.2 Source-Area Geometries..... | 115 |
| 3.2.1 Point and Line Sources | 115 |
| 3.2.2 Plane Source..... | 120 |

| | |
|---|-----|
| 3.2.3 Source-Area Pattern Evolution | 122 |
| 4. Modeling Changes in Sediment Supply and Transport Capacity | 122 |
| 5. Sediment Supply and Transport Capacity Controls on Dune-field Development | 123 |
| 5.1 Simulated Patterns | 126 |
| 5.1.1 Non-development Pattern | 126 |
| 5.1.2 Barchan Pattern | 126 |
| 5.1.3 Crescentic Ridge Pattern | 127 |
| 5.1.4 Clustered Pattern | 127 |
| 5.1.5 Superimposed Pattern | 128 |
| 5.1.6 Sheet-Crescentic Ridge Pattern | 129 |
| 5.1.7 Ridge Pattern | 130 |
| 5.2 Sediment Availability Controls On Dune-field Development | 130 |
| 5.3 Bedform Clustering | 131 |
| 6. Conclusions | 134 |
| 7. Mathematical Nomenclature | 136 |
| 8. References | 137 |
| Chapter 5: Conclusions | 139 |
| Appendix A: Estimating Percentages of Grainflow and Wind Ripples, Cedar Mesa Sandstone | 144 |
| Appendix B: Maximum Set Thickness, Cedar Mesa Sandstone | 145 |
| Appendix C: Average Thickness of Individual Grainflows, Cedar Mesa Sandstone | 146 |
| References | 147 |
| Vita | 156 |

List of Figures

- Figure 2.1.** (A)-(C). Field photos and diagrammatic renderings of the seven styles of sediment transport recognized on the lee faces of White Sands dunes.
- (A) Type A – wind ripples (wr) occurring on net erosional, bypass and net depositional surfaces. (B) Type B – wind ripples and grainfall (ga). (C) Type C – wind ripples, grainfall and grainflow (gf).....13
- Figure 2.1.** (D)-(F). Field photos and diagrammatic renderings of the seven styles of sediment transport recognized on the lee faces of White Sands dunes.
- (D) Type D – grainfall only. (E) Type E – grainfall and grainflow with basal wind ripples. (F) Type F – grainfall and grainflow. (G) Type G – grainflow.14
- Figure 2.2.** Summary diagram of experimentally defined boundaries for sediment transport in creep, saltation, modified saltation, and suspension modes using $u^* / u^* c.$ and $ws / u^*.$ (A) Experimentally-derived ranges. (B) Ranges used in this study for different modes of sediment transport.19
- Figure 2.3.** (A) Location of the White Sands Dune Field in south-central New Mexico, USA. (B) Portion of the dune field within the White Sands National Monument. The resultant wind direction of N65E is from data recorded at Holloman AFB weather station KHMN. (C) Locations of Dunes 1, 2 and 3 that were monitored in this study. The lines marking the three dunes define the lee face for each bed form.....24

Figure 2.4. Maps of the lee faces of Dunes 1-3 showing the spatial distribution of sediment transport styles (Fig. 1) on each surface. Uncolored areas represent dune segments where the lee face was not defined by a brink line and were not considered in this study. The primary wind direction for each dune is indicated. Local incidence angles for each dune segment are also marked next to each lee surface. The sinuosity for entire crestline of each dune, along with the sinuosities for specific dune segments are reported. Segments of particularly high sinuosity are marked in red. The black dots mark the locations where grain size and erosion/deposition rates were measured.27

Figure 2.5. Velocity profile for wind measured by hot-wire probes at 4 cm, 10 cm, 30 cm and 80 cm above the bed at the crest of Dune 3 during the April wind event. Each point represents the average speed for a 2-hour sampling interval. The range bar on each mean velocity is +/- one standard deviation. The surface roughness height, z_0 , is the Y-intercept at 0.11 mm. Using Eq. 2, the calculated value for u^* is 0.36 m/s. The measured profile is projected up to 10m above the bed, the height at which wind data is collected at Holloman AFB. The average wind speed and wind gust measured at Holloman AFB over the same two-hour period are marked. The total range in average wind speed and wind gusts is also presented. Note that the measured profile from the White Sands dune is most closely aligned with the wind gust data from Holloman AFB.30

Figure 2.6. Transect-averaged rates for lee-face erosion/deposition plotted as a function of incidence angle. These values were calculated by taking the average vertical displacement of the lee surface measured at transects (Fig. 4) and dividing it by the number of hours of sand-transporting conditions measured at each dune. A best-fit line through the data shows a linear correlation between erosion/deposition rate and incidence angle.31

Figure 2.7. Cumulative grain-size curves for deposits at the base of lee surfaces following the March (Dune 1 & 2) and April (Dune 3) wind events. (A) Grainflow. (B) Grainfall. (C) Wind Ripples. Curves are partitioned into transport modes based on the empirical relationships shown in Figure 1. Estimates for u_* were calculated using wind data from the March or April wind event and Eq. 6. Estimates for u_{*c} were calculated using the median grain size collected and Equation 4. The representative values for settling velocity were calculated using Equation 3. Statistics given with each set of curves are mean values for these curves.32

Figure 2.8. Type of lee-face deposit (A-G, Figure 2) plotted against the incidence angle for the dune segment on which it was observed. Points are color coded by dune and the size of each symbol is related to the dune segment length where the deposit type was observed. Data points that occurred on dune segments with high local sinuosity are circumscribed by dashed ovals and represent outliers to the data ranges for deposit types E-G (Fig. 2).37

Figure 2.9. Summary diagram showing the range of incidence angles associated with each surface-process and deposit type (A-G, Fig. 2.2) after the outliers in Figure 2.8 have been removed. The ranges of observed lee-face erosion, bypass and deposition as a function of incidence angle. Rates of deposition continue to increase with increasing incidence angle (Fig. 2.6).40

Figure 3.1. Outcrop location map for the Permian Cedar Mesa Sandstone, SE Utah. Field site for this study at Hite Crossing is marked. Modified from Mountney (2006).68

Figure 3.2. Digital Elevation Model (DEM) of outcrop location at Hite Crossing, Utah. DEM was created by surveying in 23 set boundaries at cm. scale resolution across the ~1 km³ outcrop.....70

Figure 3.3. Field examples of the four arrangements of stratification types seen in the Permian Cedar Mesa Sandstone at Hite Crossing, Utah. Figure shows stratification types 1-4, with a photograph and sketch of the same location differentiating grainflow and wind ripple deposits. See text for explanation and discussion of stratification types. A 22 cm. long field book and a person are shown for scale.73

Figure 3.4. Planview bedform reconstruction of 23 sets from the uppermost sequence of the Cedar Mesa Sandstone at Hite Crossing, Utah. All bedforms are scaled and color-coded by stratification type.....75

Figure 3.5. Plot showing incidence angle vs. basal wind ripples thickness for the uppermost sequence of the Cedar Mesa Sandstone. Maximum thickness of basal wind ripples occurs at 55° incidence angles, identifying the “sweet spot” for basal wind ripple formation.77

Figure 3.6. Crest orientations calculated from 205 cross-strata dip directions and plotted on wind rose diagrams. Shown plotted together and separated by stratification type. All crest orientations are scaled and color-coded by stratification type.78

Figure 3.7. Gross-bedform normal wind rose diagram from Rubin and Hunter (1987) for the uppermost sequence of the Cedar Mesa Sandstone showing cross-strata dip directions measured in this study with net migration direction at 125°. D is the dominant wind direction from 290°, S is the subordinate wind direction from 005°. R is the resultant.80

Figure 3.8. Cumulative frequency curves for different stratification styles: grainflow, grainfall and wind ripples.82

Figure 3.9. Photographs of storm deposits in the rock record represented by grainfall deposits (ga) and unusually thick and/or coarse grainflow deposits (gf). A) Wind storm event #1: unusually coarse grainflow ($d_{50} = 203 \text{ um}$) and associated grainfall. Lens cap for scale. B) Wind storm event #2: largest accumulation of grainfall (1.3 m). Individual grainflow toes are marked by washers. Location of unusually thick grainflow deposit (8 cm) is indicated. 1.5 liter water bottle and 4 cm. washers for scale.86

Figure 3.10. All crest orientations from the uppermost sequence of the Cedar Mesa Sandstone plotted on a wind rose diagram. Each crest orientation is scaled and color-coded by stratification type. Wind directions 290° and 005° are plotted, along with orientation of erosional reactivation surfaces. The wind rose diagram is segregated into erosional (0-15°), longitudinal (15-25°), oblique (25-65°), and transverse (65-90°) sections for the 005° wind (inner diagram) and the 290° wind (outer diagram).89

Figure 3.11. Ideal bedform for the Cedar Mesa Sandstone, predicting the stratification type that will develop at all crest orientations (360-90° northern hemisphere). Bedform is a real dune taken from LiDAR data of White Sands Dune Field, New Mexico and rotated to achieve the SE net migration direction seen in the Cedar Mesa Sandstone.94

Figure 4.1. Schematic diagram of cellular model space. Sediment transport, flow separation, and avalanching rules used in algorithm are illustrated, as well as the source-to-sink sediment transport capability. Modified from Baas (1996).108

Figure 4.2. Examples of simulated and real-world dune-fields showing similar shapes and dune-field patterns. Sediment transport is from left to right in each image. All images from Google Earth unless otherwise noted. (A) Simulated barchans and barchans from the Atlantic Sahara, Morocco (27°47'N, 12°41'W). (B) Simulated crescentic ridges and crescentic ridges from Guerrero Negro, Baja, Mexico (27°51'N, 114°18'W). (C) Simulated clustered pattern and clustered pattern from Magdalena Bay, Baja, Mexico (24°48'N, 112°14'W). (D) Simulated superimposed dunes and superimposed dunes from the Algodones Dune Field, California (32°47'N, 114°56'W). (E) Simulated sheet-crescentic ridge pattern and a sheet-crescentic ridge pattern from the White Sands Dune Field, New Mexico, LiDAR image (32°48'N, 106°16'W). (F) Simulated ridge pattern or falling dune and falling dune from Candor Chasma, Mars. MOC image E03-00746 (7.01°S, 72.69°W), modified from Bourke et al. 2004.....114

Figure 4.3. Simulation of transverse point source-area geometry over 5000 iterations.

Images (A) to (C) include landscape patterns and tracings of dune crest lines at multiple time slices, illustrating the evolution of the dune field. (A) Landscape after 840 iterations and the location of the 5 equally-spaced transects used in each time slice to calculate the spacing vs. distance values in plot D. (B) Landscape after 2640 iterations and the location of the single transect through the dune field center, used to calculate the crest length vs. distance values in plot E. (C) Landscape after 6420 iterations. (D) Plots of spacing vs. distance for each time slice. (E) Plot of crest length vs. distance for each time slice. The linear regression coefficients (r^2 values) for each time slice and the number of data used are listed along the top portion of the graph. Data were smoothed using a boxcar average with a bin size of 4.....116

Figure 4.4. Simulation of transverse line source-area geometry over 20,000 iterations.

Images (A) to (C) include landscape patterns and dune crest lines at multiple time slices. (A) Landscape after 1500 iterations and the 5 transects used in each time slice to calculate the values in plot D. (B) Landscape after 7100 iterations and the transect location used to calculate the values in plot E. (C) Landscape after 20,000 iterations. (D) Plots of spacing vs. distance for each time slice. (E) Plot of crest length vs. distance for each time slice. Data were smoothed using a boxcar average with a bin size of 4.....119

Figure 4.5. Simulation of transverse plane source-area geometry over 15,000 iterations of simulation time. Images (A) to (C) include landscape patterns and dune crest lines at multiple time slices. (A) Landscape after 500 iterations and the 5 equally-spaced transects used in each time slice to calculate the spacing vs. distance values in plot D. (B) Landscape after 7500 iterations and the location of the single transect, drawn through the center of the dune field, used in each time slice to calculate the crest length vs. distance values in plot E. (C) Landscape after 15,000 iterations. (D) Plot of average spacing vs. distance for each time slice. (E) Plot of average crest length vs. distance for 6 time slices. Error bars for plots D and E are $\frac{1}{2}$ std.121

Figure 4.6. The range of landscape patterns seen in simulations as a function of the sediment supply and transport capacity of the wind. Lines of constant sediment availability separate the different pattern categories. Values of sediment availability calculated using Eqn. 4 are shown for specific (circled) simulations. (A)-(F) Transverse model simulations of pattern evolution resulting from changes in the sediment supply and transport capacity of the wind. Patterns are shown as a function of increasing sediment supply, with lowest influx at the top and greatest influx at the bottom. Each simulation was modeled on a 1000x400 grid (downwind cells x lateral cells).....125

Figure 4.7. Real world examples of clustered and superimposed patterns. Images from Google Earth. White dashed lines mark approximate location of downwind extent of each bedform cluster. (A) Compound, clustered bedforms, Lower Helmand Basin, southern Afghanistan ($30^{\circ}46'N$, $62^{\circ}06'E$). (B) Mega-compound bedform, Guerrero Negro, Baja, México ($27^{\circ}51'N$, $114^{\circ}18'W$). (C) Megabarchan, Atlantic Sahara, Morocco ($21^{\circ}14'N$, $16^{\circ}48'W$). (D) Schematic diagram for the formation of compound dunes. Top panel depicts the commonly-envisioned evolution in which a simple bedform grows large enough to support superimposed dunes. The lower panel depicts an alternate mechanism of bedform clustering with an incipient compound dune.133

Figure 4.8. Map and plan views of both real-world and simulated superimposed dunes. (A) Algodones Dune Field, California ($32^{\circ}47'N$, $114^{\circ}56'W$). (B) Simulated superimposed dunes. Note similarity of dune morphologies, patterns, and spatial scales. Simulations are explicitly associated with line source simulations. See the Simulated Patterns section for additional discussion.134

Chapter 1: Introduction

Modern and ancient dune fields have been reported on every continent, and deposits are preserved from nearly all geologic periods beginning with the late Precambrian. The best preserved aeolian record on Earth is from the Colorado Plateau (COP) in the southwestern USA, which contains a 3500 m thick composite aeolian section, ranging in age from the late Pennsylvanian through the Cretaceous and covering nearly 10^6 km². Dune fields form wherever there is a supply of loose sediment available for transport and wind energy is sufficient to transport the grains. Dune-field accumulations that formed within subsiding basins or were incorporated into a rising regional water table represent most of the preserved rock record. Aeolian systems are dynamic and the internal architecture of dune deposits reflects both internal and external controls from a broad range of processes, including tectonics, climate, sea level, groundwater levels, sediment supply, and transport capacity (i.e., wind strength). Typically, ancient aeolian sequences preserve only the basal portions of dunes that were progressively deposited over time. These preserved accumulations, however, contain a wealth of information about dune orientation, morphology, and migration, as well as the wind conditions over time.

The work in Chapters 2 and 3 was motivated by the idea that secondary air flow on the lee face of a dune is primarily a function of the incidence angle, the angle between the dune crestline and the primary wind direction. The surface processes and resultant stratification types that form on a dune lee face are the result of the secondary flow

configurations. Ancient aeolian cross-strata are the most direct record of the continental sediment transport system by wind and contain a climatic record of both wind direction and wind speed. Aeolian cross-strata are complex because most wind regimes are not unidirectional, most dunes are too large to reform with each component of the wind regime, and the wind is rarely uniform or steady. As a result, dune crests become oriented as perpendicular as possible to all constructive wind directions (i.e., gross bedform-normal crest orientation). Historically, the average dip direction of the cross-strata has simply been taken as the paleowind direction. This simplifying assumption is correct only in the case where the wind regime is unidirectional and may yield an inaccurate reconstruction of the wind regime. A goal of this research is a refined methodology for reconstructing the primary wind direction that gave rise to ancient cross-strata by constraining the ranges of styles of stratification as a function of incidence angles. In addition, wind speed, the other climatic component recorded in aeolian cross-strata, has rarely been addressed in the literature, and a goal of this research is to develop a methodology that allows for the bracketing of wind speeds by identification of modes of grain transport that characterize lee surface processes and their resultant stratification types.

Following the goals outlined above, Chapter 2 builds upon the existing understanding of aeolian dunes with new data from the White Sands Dune Field, New Mexico, to assemble a methodology to reconstruct both wind direction and wind speed from sets of aeolian cross-strata. This methodology allows for: (1) a determination of the wind direction based upon the spatial distribution and style of stratification types as a

function of the incidence angle; and (2) a determination of wind speed based upon the grain sizes within different stratification types as a function of the grain sorting that occurs on the lee face.

Chapter 2 confirms that the spatial distribution of surface processes, erosion/deposition rates, and lee face sorting are all functions of the incidence angle using data collected from three sinuous crescentic dunes during two individual wind events at White Sands National Monument, NM, in March and April 2011. Field investigations included: (1) topographic surveying the dune brinkline and the base of the lee face, (2) detailed documentation of lee-face surface processes, and (3) measurement of deposition/erosion rates along the lee face for each wind event. The goal of this study was to: (1) identify the ranges of incidence angles that different surface processes occur over (i.e., grainflow, wind ripples, grainfall), (2) document the range of incidence angles over which erosion, bypass, and deposition occur, (3) distill the lee-face stratification from the three dunes into seven unique and distinct stratification styles, and (4) identify the range of incidence angles that the seven different stratification types occur over.

Chapter 3 builds on the ideas presented in Chapter 2 and applies this new methodology to the uppermost sequence of the Permian Cedar Mesa Sandstone on the COP in the southwestern USA. The objective is to demonstrate the utility of this methodology in reconstructing the range of wind directions and wind speeds that gave rise to this portion of the Cedar Mesa dune field. Twenty-three aeolian sets of cross-strata were surveyed within the $\sim 1 \text{ km}^2$ field area, the stratification styles were mapped at a sub-meter scale, and 205 cross-strata dip directions were recorded. From these data, four

stratification types were identified and used with the associated dip directions to reconstruct the morphologies of twenty-three dunes. Results indicate that no single wind direction could account for the sequence of stratification styles observed within all the sets, but all could be accounted for by two primary winds (from 290° and 005°). In order to satisfy the gross bedform-normal crest orientation and yield net migration of the dunes to the SE as measured in the field, the west wind (290°) would have to have been twice the magnitude (in either duration or intensity) of the north wind (005°). Thirty grain size samples were analyzed in the lab and used to reconstruct the wind speed for the different grain sizes associated with different stratification styles using the methods outlined in Chapter 2. Reconstruction of wind speeds yield the “formative winds” most responsible for dune construction, and two wind storms were recognized. Both storm events were a product of the west wind (290°), indicating that the west wind (290°) blew more intensely than the north wind (005°).

The methods developed in Chapter 3 demonstrate that paleowind regimes can be reconstructed from ancient cross-strata, and these provide the most reasonable input for climatic models that propose to reconstruct regional circulation patterns. Paleocirculation models are important because they document the natural variability previously experienced by the Earth’s climate system, which can be used to help predict future climate change. This method sets a new standard for producing specific and accurate paleowind reconstructions from aeolian cross-strata that can be used to interpret past climates, predict stratification types, and validate paleoclimate models.

In addition to exploring how individual dunes migrate and change through time as a function of the paleoclimate, dune fields can also be explored as patterns that develop within a set of environmental or boundary conditions. The most basic boundary conditions for any dune field are the sediment supply, the availability of this sediment for transport by the wind, and the transport capacity of the wind. These parameters constitute the “sediment state” of a dune field as given by Kocurek and Lancaster (1999). Chapter 4 explores these parameters in a cellular automaton (CA) model. The role of this and any other numerical model is that processes that occur over geologic spans of time can be accelerated, potentially allowing for new insights into the processes themselves and patterns of dune-field development.

The simple second-generation (CA)-based source-to-sink model presented in Chapter 4 simulates aeolian dune-field development through self-organization by using a few simple, physically-based rules that do not simulate grain-scale interactions. This new model provides insight into the controlling factors on aeolian systems by changing a small number of parameters that relate to the sediment state of the system and the configuration of the sand-source area. Quantification of the components of sediment state (sediment supply, availability, transport capacity of the wind) allows for their sensitivity testing in the model, yielding insights into their respective roles in basic dune-field configurations.

Results from Chapter 4 argue that much of the diversity of aeolian dune-field patterns seen in the real world is a function of the sediment supply and transport capacity, which determine the sediment availability of the system where no other parameters

impact sediment availability. Simple bedforms are produced under lower sediment availability conditions when compared to mega-bedforms, which form under high sediment availability conditions. Extremely high sediment availability produces source areas of stored sediment. A “clustered pattern” is a newly identified dune-field morphology that may represent incipient or alternative development of superimposed dunes, in which clusters of bedforms develop superimposed dunes without requiring prior development of a large basal dune. Previous studies suggest this conclusion, and simulations presented here argue for the feasibility of forming compound dunes by bedform clustering.

Chapter 2: Methodology for Extracting Wind Direction and Speed from Aeolian Cross-strata

ABSTRACT

A methodology for reconstructing wind direction and speed from aeolian dune cross-strata arises from analysis of data from three crescentic dunes at White Sands, New Mexico, during two wind events. Each dune was surveyed, styles of lee-face sediment transport were mapped, erosion/deposition rates were measured, grain size was sampled, and the wind events were characterized by in-field measurements and comparison to records at Holloman Air Force Base (AFB) for the same period. The wind events are best characterized by shear velocities derived from average gust wind speeds. Seven sediment-transport assemblages were recognized at White Sands, each of which is well represented in the aeolian rock record, that show the variety in transport styles and surface processes that can occur on a single dune during a single wind event. Surface processes and the resultant style of stratification arise from the secondary lee-face flow, which is a function of the incidence angle formed between the local brinkline and the primary wind direction. Although local dune sinuosity, wind speed, and dune height impact the styles of stratification, incidence angle emerges as a robust tool to bracket the primary wind direction. Rates of erosion/deposition on the lee face also track with incidence angle, such that rates of deposition increase with increasing incidence angles.

Grain-size samples show that grain size is not uniform over a dune lee face, but rather the total sediment load traveling over the dune is sorted by the secondary flow and the surface transport. Grainflow is most representative of the total sediment load, whereas

grainfall is enriched in grains that traveled in incipient suspension and depleted in grains that traveled in creep. Wind ripples are the least diagnostic surface process because they may form on any lee sediment subject to traction reworking.

Wind speed can be reconstructed from the grain sizes that represent incipient suspension and creep utilizing empirically-derived relationships. Grain sizes representing incipient suspension can be obtained from grainfall and grainflow deposits, and grain sizes representing creep can be obtained from grainflow deposits. Currently, however, wind speed can only be bracketed within the overall context of the dune field because: (1) the mode of grain transport varies with wind speed, (2) the grain-size range within the dune field may be source-limited, and (3) dune height strongly impacts the basal lee-face stratification preserved in the rock record. The methodology proposed here is focused upon the identification and interpretation of single wind events as recorded in individual sets of cross-strata, and contrasts with the common practice of assuming that the mean cross-strata dip direction directly mirrors the wind direction.

1. INTRODUCTION

Aeolian dune cross-strata are the most direct record of the continental winds and house a climatic record of wind direction and wind speed. Aeolian cross-strata are inherently complex because: (1) most wind regimes are not unidirectional; (2) most dunes are too large to reorient to each component of the wind regime; (3) the wind is rarely uniform or steady; and (4) the wind (i.e., primary flow) is strongly modified (i.e., secondary flow) as it travels over dunes. In contrast, cross-strata formed by migrating dunes in rivers are more straightforward because flow direction is essentially

unidirectional. For decades geologists have used the orientation of cross-strata (i.e., strike and dip) to interpret wind direction and compared these interpretations to models of regional or global circulation (e.g., Parrish and Peterson, 1988; Loope et al., 2004; Rowe et al., 2007). In some cases, sophisticated use of the type and orientation of cross-strata and bounding surfaces have been used to infer cyclic components of the wind regime (e.g., Hunter and Rubin, 1983; Kocurek et al., 1991; Scherer and Goldberg, 2010). In other cases, the average dip direction of the cross-strata has simply been taken as the wind direction (e.g., Reiche, 1938; Curray, 1956; Tanner, 1965; Clemmensen and Abrahamsen, 1983; Loope, 1984; Dott et al., 1986; Clemmensen and Blakey, 1989; Mountney, 2006). As discussed below, this simplifying assumption is correct only in the special case where the wind regime is unidirectional, and making this assumption may yield an inaccurate and incomplete picture of the wind regime. In addition, the other climatic component recorded in aeolian cross-strata, wind speed, has only rarely been addressed (Jerolmack et al., 2006, 2011).

The purpose of this paper is to build upon the existing understanding of aeolian dunes with new data from the White Sands Dune Field in New Mexico to assemble a “toolset” for the reconstruction of both wind direction and wind speed from sets of aeolian cross-strata. Determination of the wind direction is based upon the spatial distribution of stratification types that in turn preserve a record of the incidence angle formed between the local dune crestline and the wind. Determination of wind speed is based upon the grain sizes found in the different stratification types on the lee faces of dunes.

2. THEORY

2.1 Reconstruction of wind direction

Experiments (Rubin and Hunter, 1987; Rubin and Ikeda, 1990), analytical solutions (Werner and Kocurek, 1997) and computer models (Werner, 1995; Bishop et al., 2002) all indicate that the crestlines of aeolian dunes are oriented to be as perpendicular as possible to all constructive wind directions. This “gross bedform-normal” crest orientation (terminology of Rubin and Hunter, 1987) applies to any bedform where the duration of wind from a given direction is shorter than the reconstitution time of the bedform, and applies to all but the smallest of aeolian dunes (Rubin and Ikeda, 1990). In a wind regime that is not unidirectional, therefore, wind components of the total wind regime may not strike the dune crestline at right angles. In addition, because most dunes are sinuous, a variety of incidence angles occur along the crestline for any given wind direction.

The secondary flow on the lee face of a dune is primarily a function of the incidence angle, but also of dune morphology (dune aspect ratio) and, to a lesser extent, atmospheric stability (Sweet and Kocurek, 1990; Walker and Nickling, 2003). For steep dunes during neutral atmospheric conditions that would characterize most sand-transporting events (Frank and Kocurek, 1994), secondary flow is controlled by incidence angle. Based upon a variety of dunes in nature and a rotating experimental dune, Sweet and Kocurek (1990) classified lee secondary flow as a function of the incidence angle: transverse (70-90°), oblique (10-70°), and longitudinal (0-10°). With a longitudinal configuration, the secondary lee flow is attached, undeflected, and transport is entirely by

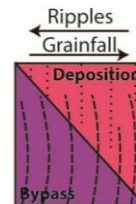
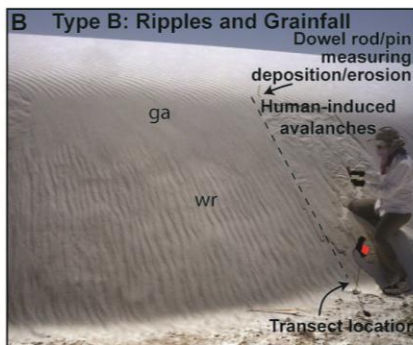
traction. As the incidence angle becomes greater (i.e., oblique) the lee flow is deflected to blow alongslope. Flow separation develops in the lee region as a 3-D vortex with components of alongslope and reversed flow (e.g., Allen, 1982). A 2-D roller vortex (Walker and Nickling, 2002) with crest-normal return flow occurs as the incidence angle approaches 90°. Based upon wind-tunnel experiments, Walker and Nickling (2003) found the same secondary flow configurations except they describe flow as attached and deflected until 70°, after which flow separation develops. Wind speed on the lee face has been found to approximate a cosine function of the incidence angle - secondary flow speed approaches the primary wind speed at longitudinal incidence angles and approaches zero at transverse incidence angles (Tsoar, 1983). The general result is the dominance of traction transport at longitudinal incidence angles, gravity-driven processes at transverse incidence angles, and the co-existence of both gravity and traction processes at oblique incidence angles.

The styles of surface sediment transport and resultant stratification types that form on a dune lee face result from the secondary flow configurations (Fig. 2.1). The basic aeolian lee-face transport processes from Hunter (1977) are: (1) *grainfall* in which grains blown passed the dune brink settle to the surface in paths that can be strongly modified by lee turbulence (Nickling et al., 2002); (2) *grainflow* in which sediment accumulating immediately down slope from the dune brink reaches the angle of initial yield, avalanches and flows down the dune slipface; and (3) *wind ripples* in which lee sediments of any origin are reworked. Grainfall and grainflow are gravity-driven processes and their exclusive presence indicates a transverse flow configuration where there is a general

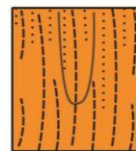
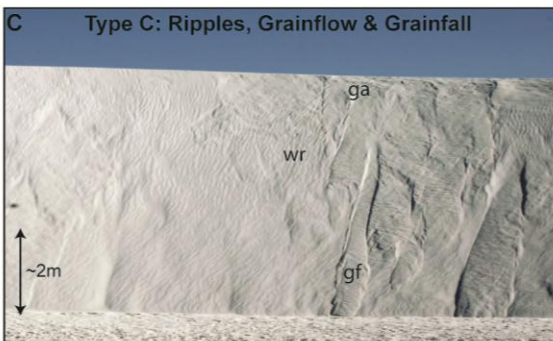
absence of traction transport (Gilbert, 1914) (Fig. 2.1F&G). Wind ripples are indicative of a flow configuration where traction transport dominates, becoming increasingly prominent with decreasing incidence angles (Fig. 2.1A&B). Lee ripples typically have crests oriented parallel to the dip of the lee face as a function of alongslope transport and gravity (Howard, 1977). With oblique flow, both grainfall/grainflow and wind ripples can occur, depending upon the spatial dominance of gravity-driven versus traction transport (Fig. 2.1C-E). Typically gravity-dominated processes on the upper lee face yield downslope to ripples migrating alongslope where traction transport dominates. In nature a variety of styles in the arrangement of stratification types occur as a function of the total wind regime, the most common configurations are shown by Kocurek (1991, see Fig. 8).



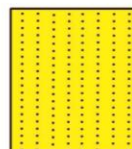
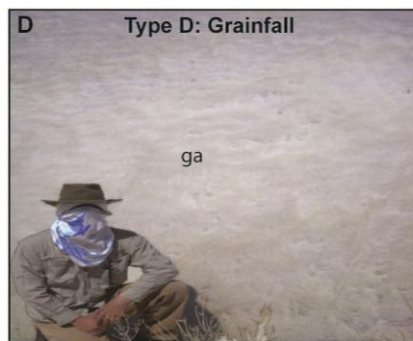
Type A
Ripples



Type B
Ripples
& Grainfall



Type C
Ripples, Grainflow
& Grainfall



Type D
Grainfall

Figure 2.1. (A)-(C). Field photos and diagrammatic renderings of the seven styles of sediment transport recognized on the lee faces of White Sands dunes. (A) Type A – wind ripples (wr) occurring on net erosional, bypass and net depositional surfaces. (B) Type B – wind ripples and grainfall (ga). (C) Type C – wind ripples, grainfall and grainflow (gf).

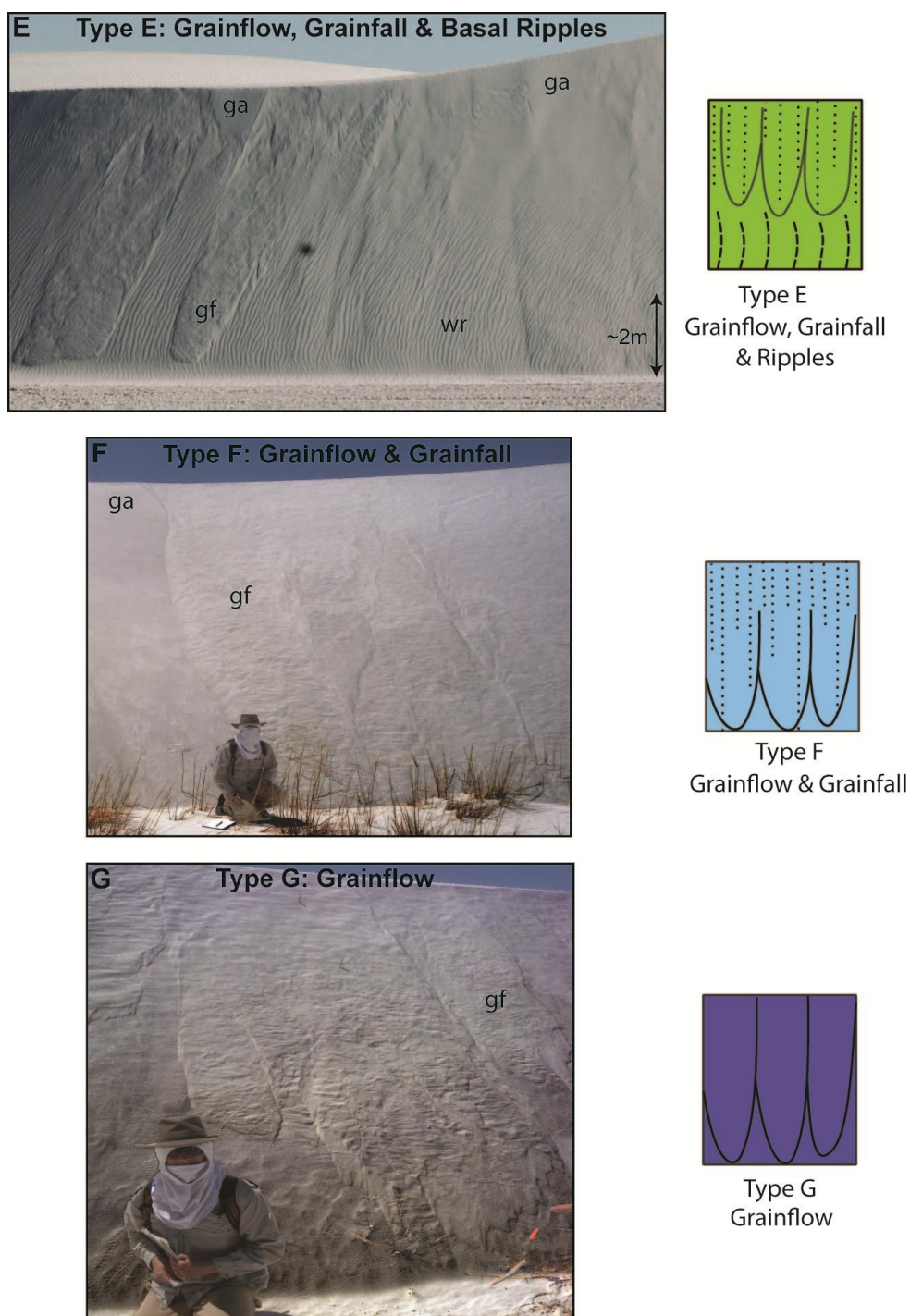


Figure 2.1. (D)-(F). Field photos and diagrammatic renderings of the seven styles of sediment transport recognized on the lee faces of White Sands dunes. (D) Type D – grainfall only. (E) Type E – grainfall and grainflow with basal wind ripples. (F) Type F – grainfall and grainflow. (G) Type G – grainflow.

In summary, the current state of understanding is as follows. Because dune crestline orientation is the product of all constructive primary winds, the average dip direction of cross-strata within a set reflects the overall dune migration direction. This is important information, for example, in determining net sand transport within a basin. Unless the wind regime is unidirectional, however, this average dip direction alone is insufficient to determine the primary wind directions. Because any given cross-strata orientation shows the local crestline orientation, a coupling of crest orientation with stratification style brackets the local incidence angle into broad categories of transverse, oblique, and longitudinal configurations. A compilation of pairs of local cross-strata orientation and stratification style all along a set reveals the overall crestline shape and orientation, and the range of incidence angles along the crestline. The correlation between incidence angle and stratification style, however, is known in only a general way. The primary goal in developing the methodology here is to provide a more precise correlation between incidence angle and style of stratification type, and to examine the extent to which other parameters may impact the distribution of sediment-transporting processes on dune lee faces.

2.2 Reconstruction of wind speed

The three end-member modes of sediment transport by the wind are creep, saltation and suspension, and these arise because of the balance between grain properties and the surface forces that cause motion (Bagnold, 1941). For sand dunes, saltation is the primary mode of transport and is characterized by grains that rise from the surface in quasi-parabolic arcs to collide with the surface and eject other grains. Saltating grains,

once ejected from the surface, are driven by fluid drag and gravity with negligible effects from fluid lift by turbulent eddies. The heaviest grains move in creep, characterized by sliding, rolling or short hops, and are driven by the combination of fluid stresses acting on grains and the kinetic energy transfer associated with impacts from other saltating grains. The lightest grains are suspended, carried into the flow when vertical velocities associated with turbulent eddy motions exceed particle fall velocities, and have only rare contact with the bed. In nature, however, there is significant gradation between the end-member modes of transport, especially between *pure* saltation and *pure* suspension. This gives rise to motions best described as modified saltation and incipient suspension (e.g., Nishimura and Hunt, 2000; Nino et al., 2003).

Attempts to characterize sediment transport all utilize basic relationships between fluid forces and grain properties. Fluid forces are characterized by the shear stress, τ , exerted on the bed by the flowing fluid. Because shear stress is difficult to measure directly, friction or shear velocity, u_* , is commonly used:

$$u_* = \sqrt{\tau/\rho_f} \quad (1)$$

where ρ_f is the density of the moving fluid. Shear velocity is then typically derived from a measured velocity profile by application of the “law of the wall”

$$u_z = \frac{u_*}{\kappa} \ln\left(\frac{z}{z_0}\right) \quad (2)$$

where u_z is the wind speed at height z above the surface, κ is von Karman’s constant (equal to 0.4 in neutral atmospheric conditions), and z_0 is the surface roughness height where zero velocity associated with turbulent flow occurs (Frank and Kocurek, 1996).

Neglecting sorting, the transportability of a grain is a function of properties such as volume, shape and density. These properties can be characterized by the grain settling velocity, w_s , and the critical shear velocity, u_{*c} , to initiate movement. Bagnold (1941) observed that once grain motion is established, saltation continues and creep begins to occur at a u_* lower than that required to initiate motion as a result of momentum transfer from the impact of saltating grains. From wind tunnel data, this critical impact-augmented shear velocity, u_* , is approximately $0.7u_{*c}$ (Bagnold, 1941; Nishimura and Hunt, 2000).

Although developed for grains settling in water, the equation by Ferguson and Church (2004), as modified by Jerolmack et al. (2006), can be applied to air:

$$w_s = \frac{(s-1)gd^2}{C_1\nu+(0.75C_2(s-1)gd^3)^{1/2}} \quad (3)$$

where $s = \rho_s/\rho_f$ is the relative density of sediment where ρ_s is the sediment density, g is the acceleration due to gravity, d is the nominal grain diameter, ν is kinematic viscosity for the fluid, and C_1 and C_2 are constants with values of 18 and 1, respectively, for natural sand.

We follow Jerolmack et al. (2006) in adopting the equation by Shao and Lu (2000) for u_{*c} , which is based upon data from Iversen and White (1982) for a range of grain sizes that includes most aeolian sand:

$$u_{*c} = \sqrt{0.0123 \left(sgd + \frac{3 \times 10^{-4} kg/s^2}{\rho_f d} \right)}. \quad (4)$$

Given values for w_s , u_{*c} , and u_* , the range of near-bed conditions associated with the different modes of sediment transport have been described as a function of the ratios u_*/u_{*c} and w_s/u_* , as summarized in Figure 2.2. Values of u_*/u_{*c} inherently best serve to address the boundary between creep and saltation. Bagnold (1941) originally described that grains begin to saltate once u_{*c} is exceeded (i.e., $u_*/u_{*c} > 1$), but creep (and saltation) may continue until $u_*/u_{*c} = 0.7$ (Fig. 2.2). Using high-speed videos, Nishimura and Hunt (2000) found that particle trajectories in saltation begin to be distorted by turbulent eddies when $u_*/u_{*c} \geq 1.5$. This change in grain paths, although described by Nishimura and Hunt (2000) as the onset of suspension and adopted as such by Jerolmack et al. (2006, 2011), is probably best described as the onset of modified saltation. This change in grain paths would not be ordinarily detectable in the field, and is not a practical definition for suspension. In this study we adopt the relationship that creep occurs at

$$0.7 \leq \frac{u_*}{u_{*c}} \leq 1.0, \quad (5)$$

after which saltation occurs with an upper limit that is best characterized by the ratio w_s/u_* (Fig. 2.2).

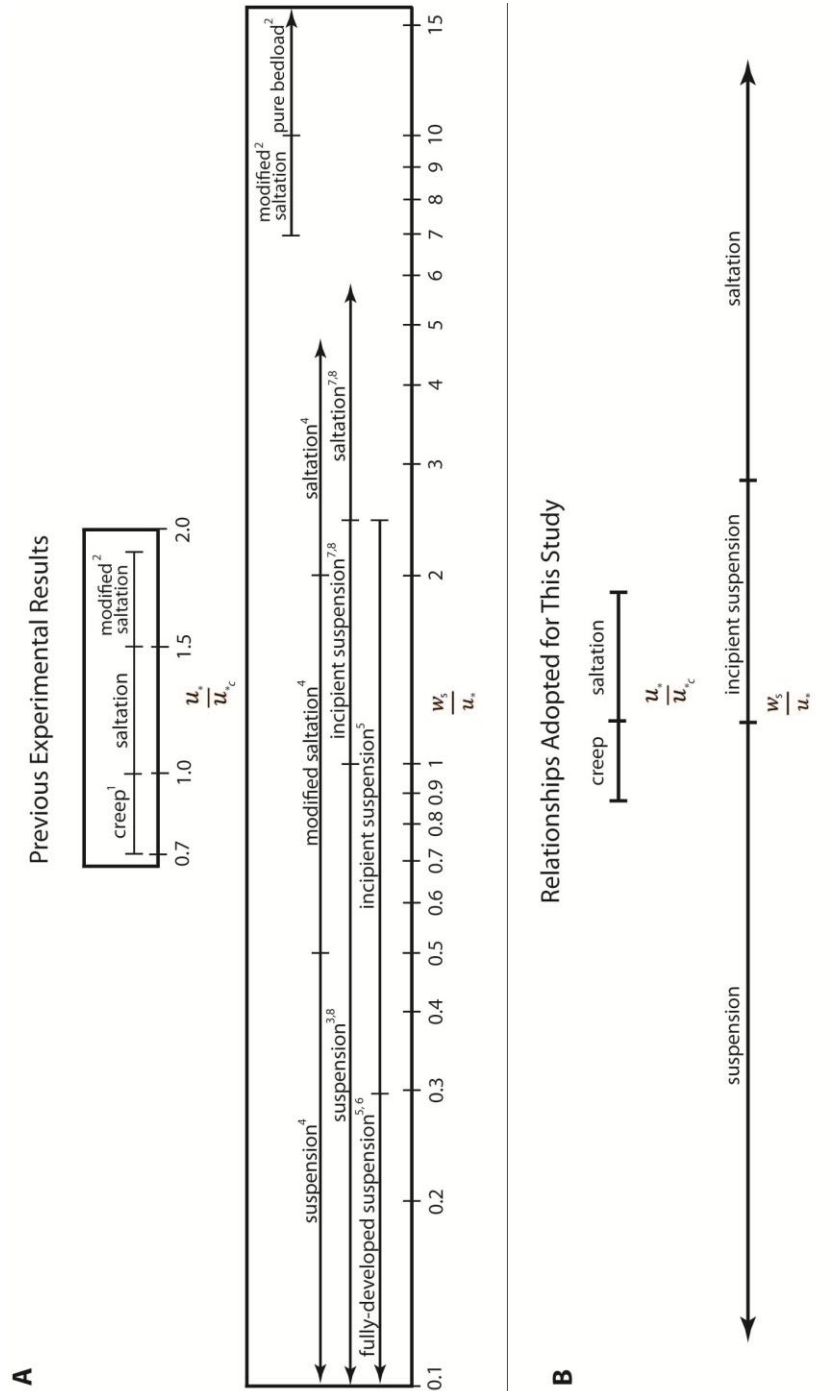


Figure 2.2. Summary diagram of experimentally defined boundaries for sediment transport in creep, saltation, modified saltation, and suspension modes using u_{*i}/u_{*c} . (A) Experimentally-derived ranges. (B) Ranges used in this study for different modes of sediment transport.

Values of w_s/u_* are most appropriate to define divisions in the gradation between saltation and suspension because the downward grain settling velocity must be balanced by the upward velocities tied to turbulent eddies, which scale with shear velocity at small distances above the bed (e.g., Bagnold, 1966; Grass, 1971; Nino et al., 2003). Attempts to define this gradation in both air and water, summarized in Figure 2.2, are subject to differing experimental methods and terminology, as well as making judgmental determinations within a clearly gradational process. The onset of deviations in saltation paths (described above) by Nishimura and Hunt (2000) begins when $w_s/u_* \approx 10$, with greater values of the ratio reflecting pure saltation. More conservatively, Shao (2000) gives the boundary between saltation and modified saltation as $w_s/u_* = 2$, with suspension occurring when $w_s/u_* < 0.5$. Using high-speed videos for transport in water, Nino et al. (2003) give the boundary between saltation and incipient suspension at $w_s/u_* = 2.5$, and the boundary between incipient suspension and full suspension at $w_s/u_* = 1$. These values reconcile with earlier works by van Rijn (1984) and Laursen (1958) where significant numbers of grains are advected into the flow interior by turbulent eddies when $w_s/u_* = 2.5$, and by Bagnold (1966) where a measurable concentration profile of suspended sediment develops at $\frac{w_s}{u_*} = 1$. Laursen (1958) and Smith and Hopkins (1972) argue that the transition to suspension transport is complete when $w_s/u_* = 0.3$.

For field studies, a definition of suspension based upon a measurable sediment concentration profile is the most appropriate definition for the onset of suspension, and we adopt suspension as occurring when

$$\frac{w_s}{u_*} \leq 1. \quad (6a)$$

All experimental work agrees that the transition from saltation to suspension is well underway in the range of $w_s/u_* = 2.0 - 2.5$, and we adopt incipient suspension as occurring when

$$1 < \frac{w_s}{u_*} \leq 2.5. \quad (6b)$$

Modified saltation would be largely undetectable from saltation in the field, and we combine these modes of transport using the definition that pure saltation is tied to conditions where

$$\frac{w_s}{u_*} \geq 2.5, \quad (6c).$$

whereas Jerolmack et al. (2011) adopt $w_s/u_* \geq 3.0$ for this same boundary.

Given ranges of u_*/u_{*c} and w_s/u_* associated with modes of grain transport, the basis for our approach is the hypothesis that the total grain population traveling over a dune is sorted on the dune lee face as a function of lee-surface transport processes (see section 2.1). Because the preserved aeolian rock record almost exclusively represents the lowermost portion of the dune lee face (Rubin and Hunter, 1982; Kocurek, 1981), we are concerned with the grain-size range in the stratification types that are found there. Although grains traveling in saltation can have trajectories that extend to basal portions of small aeolian dunes, we hypothesize that any grainfall accumulating on the basal lee of larger dunes is enriched in grains that traveled in incipient suspension and is depleted in grains that traveled in creep. In contrast, grainflow is hypothesized to be most representative of the entire transport range of grains traveling over the dune. Because lee

wind ripples reflect traction reworking of any grain population that has passed the dune brink, forming on finer-grained grainfall deposits as well as coarser-grained grainflow deposits, we hypothesize that wind ripples possess the least diagnostic distributions of grain sizes. Lee ripples, however, are likely to be concentrated in the coarser-grain fraction where traction transport is sustained or, especially, where net deflation is occurring on the lee face.

Our approach in determining wind speed largely follows that of Jerolmack et al. (2006, 2011), also at White Sands, but with some differences. First, we use a finer division of the sediment range between pure saltation and pure suspension because the pure suspension load is not directly involved in dune dynamics, and grainfall is hypothesized to be enriched in grains that traveled in incipient suspension. Second, as given above, we adopt somewhat different limits for the modes of grain transport. Third, Jerolmack et al. (2011) use a surface roughness height, $z_o \sim 10^{-4}$ m for the entire dune field, which was determined experimentally on coarse-grained ripples at White Sands by Jerolmack et al. (2006). We use a z_o based on sand ripples located on the dunes, and this should be more representative of the entire field. Fourth, whereas Jerolmack et al. (2011) systematically sampled dune stoss, crest, and lee face, we sampled stratification types on the basal lee portions of dunes in order to test the hypothesis that the total grain population is sorted by lee surface processes. In turn, lee-surface processes give rise to stratification types that can be identified in the rock record and potentially matched with a mode of transport. Fifth, the goals of this study differ from that of Jerolmack et al. (2011). As developed in Jerolmack and Brzinski (2010) and Jerolmack et al. (2011), their

goal was to determine the “dune-forming wind,” which yields a characteristic value of u_* that describes most of the work in dune-field construction using a combination of magnitude and frequency of occurrence. This parameter is important, but because dune grain size is similar throughout the Phanerozoic on Earth (e.g., Kocurek, 1996), significant ranges in wind speeds are likely to be encountered in the extremes of the grain-size range found in dune cross-strata. Our methodology is focused, therefore, upon characterization of specific wind events, the most common of which will reflect the typical wind regime.

3. STUDY AREA AND METHODS

3.1 Study area overview

Data for this study were collected from the gypsum dune field within White Sands National Monument, New Mexico, during March and April, 2011 (Fig. 2.3). The White Sands Dune Field is situated within the Tularosa Basin and consists of a core of crescentic and barchan dunes, which is rimmed to the north, east and south by parabolic dunes. To the west the dune field yields abruptly to an extensive gypsum plain, Alkali Flat. Further to the west, occupying the lowest elevations of the basin are active playa lakes, Lake Lucero being the largest. Analysis of the decades-long wind regime recorded at nearby Holloman Air Force Base (AFB) by Fryberger (2003) and Jerolmack et al. (2011) yields a 060° and 065° resultant, respectively (Fig. 2.3). Dominant winds are from the WSW and are strongest during the winter-spring. A second mode of winds from the N-NW occurs during the fall and winter, and a third mode of winds from the S-SE occurs during the spring-summer.

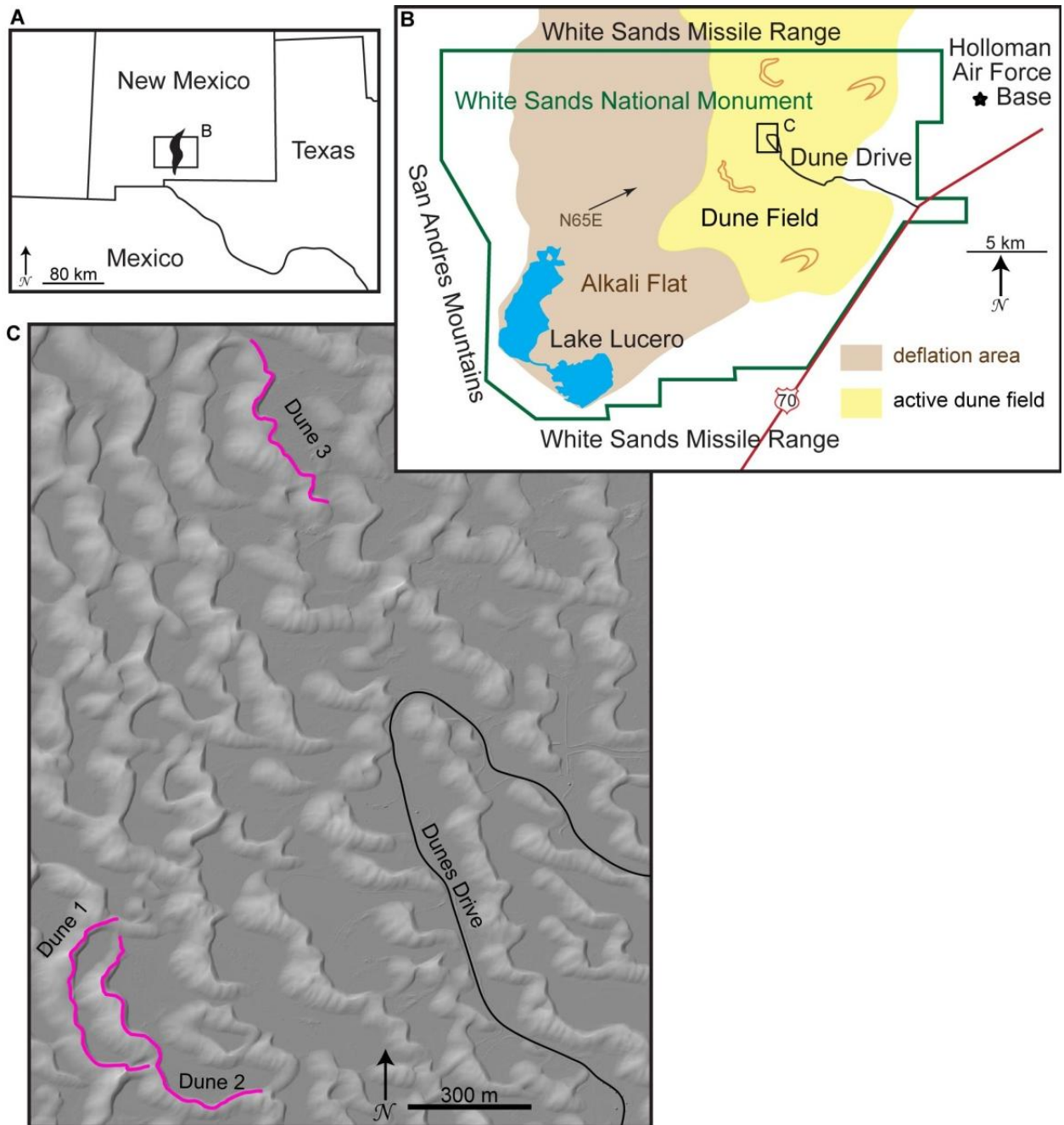


Figure 2.3. (A) Location of the White Sands Dune Field in south-central New Mexico, USA. (B) Portion of the dune field within the White Sands National Monument. The resultant wind direction of N65E is from data recorded at Holloman AFB weather station KHMN. (C) Locations of Dunes 1, 2 and 3 that were monitored in this study. The lines marking the three dunes define the lee face for each bed form.

Aspects of the White Sands Dune Field have been addressed in a number of studies, and a much fuller description and interpretation of its history, geomorphology, and sedimentology is given collectively by Kottowski (1958), McKee (1966), McKee and Douglass (1971), Allmendinger (1972), McKee and Moiola (1975), Fryberger (2003), Langford (2003), Jerolmack et al. (2006), Kocurek et al. (2007), Langford et al. (2009), Ewing and Kocurek (2010), Reitz et al. (2010), Szykiewicz et al. (2010), and Jerolmack et al. (2011).

3.2 Methods

Three crescentic dunes were chosen for this study because of their relatively high sinuosity (Figs. 2.3C, 2.4). The brink line and lee-face base for each dune was surveyed using a Trimble S3 (2") Robotic Total Station during calm periods before sand-transporting wind events. During the surveying process, dowel rods (3 mm in diameter) were set into the dune lee faces at ~ 2 m intervals from the base of the lee face to the dune brink; the spacing of these transects was such that representative segments of the curving dune lee faces were sampled (Fig. 2.4). Dune sinuosity, s , was calculated based upon the surveys using the definition that $s = L / L'$, where L is the measured brinkline length and L' is the straight-line distance (Fig. 2.4). Points of divergence in the lee-face secondary flow-field were used as the end points for the dune segments on which sinuosity was calculated (Fig. 2.4). Surface sediment-transport processes were mapped along the entire lee face at a sub-meter scale for Dunes 1 and 2 after the March wind event, and along Dune 3 after the April wind event. Primary wind directions were determined by the average orientation of wind ripples on the stoss slopes of the dunes, and compared to that

recorded at Holloman AFB during the same intervals. The incidence angle for each approximately straight-line segment of the lee face was determined based upon the primary wind directions (Fig. 2.4). The amount of deposition/erosion that occurred on the lee faces during the wind events was measured from the dowel rods and these changes in surface elevation were converted to rates by dividing by the known duration of each sand-transporting wind event. Grain-size samples were taken at each dowel location. Care was taken to sample the entire lamina/stratum formed by a given process, such that the entire thickness of wind ripples and grainflow tongues were taken. Grainfall was sampled by scraping off and collecting only those grains from the immediate surface.

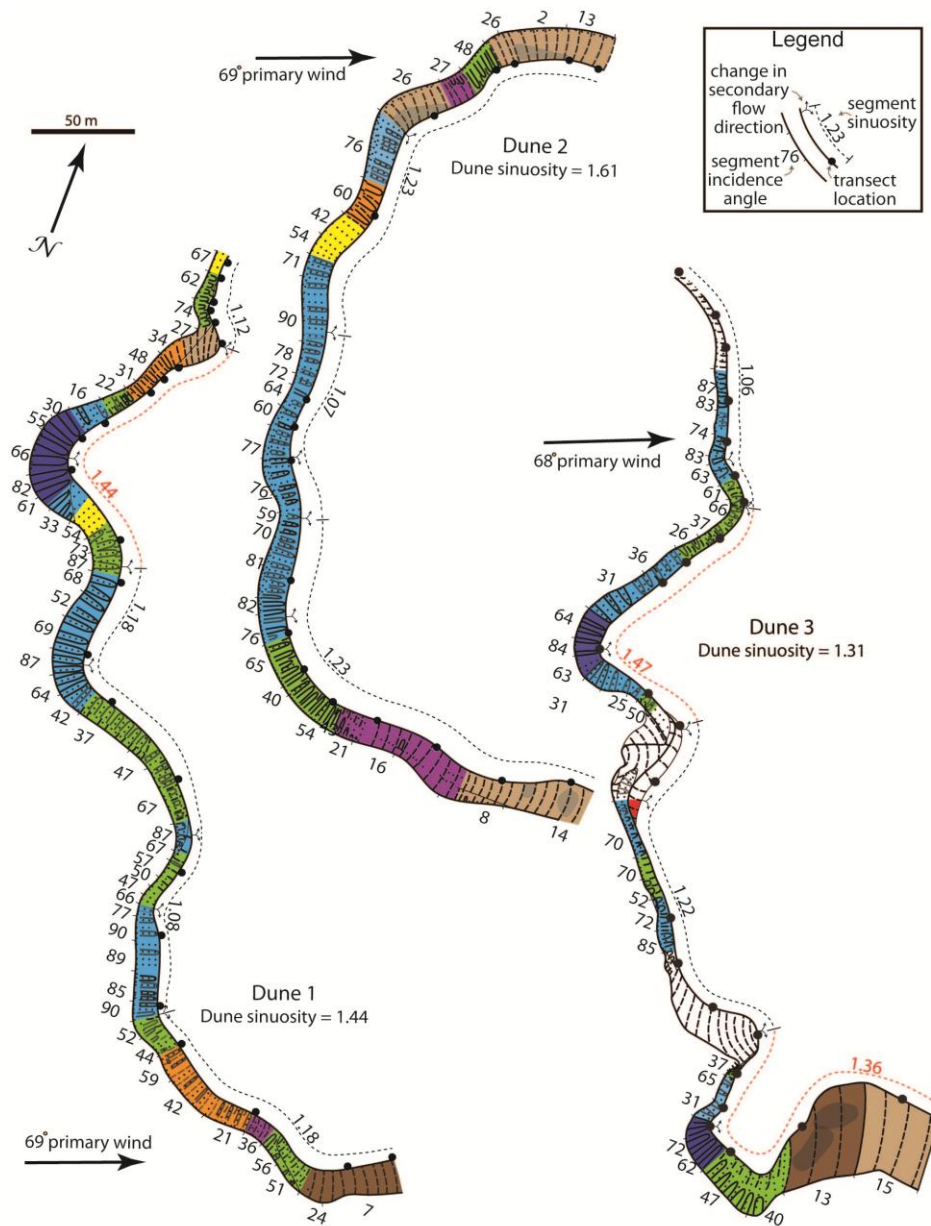


Figure 2.4. Maps of the lee faces of Dunes 1-3 showing the spatial distribution of sediment transport styles (Fig. 1) on each surface. Uncolored areas represent dune segments where the lee face was not defined by a brink line and were not considered in this study. The primary wind direction for each dune is indicated. Local incidence angles for each dune segment are also marked next to each lee surface. The sinuosity for entire crestline of each dune, along with the sinuosities for specific dune segments are reported. Segments of particularly high sinuosity are marked in red. The black dots mark the locations where grain size and erosion/deposition rates were measured.

Grain-size analysis was performed using a Retsch Technology CamSizer (www.retsch-technology.com), which digitally images and measures most grains in each sediment sample. Thus, errors associated with measuring grain size using this device are significantly less than sieving techniques. The grain-size distribution for each sediment sample is composed of 50 bins spaced logarithmically over the diameter range 0.032 - 2.5 mm.

During the April wind event, wind speed was measured over a 2 hour period using hot-wire anemometers mounted on a staff at heights of 4 cm, 10 cm, 30 cm, and 80 cm above the bed near the crest of Dune 3. This wind profile was subsequently compared to the wind record for the same time interval recorded at Holloman AFB. The Holloman data at a height of 10 m and consist of average wind speed and direction over 2 minute intervals, and the maximum wind gust during 10 minute intervals.

4. DATA

4.1 Characterization of the wind events

The primary wind direction determined by the orientation of wind ripples was 069° for the March wind event, and 068° for the April wind event (Fig. 2.4). These values compare to 061° and 059° , respectively, as recorded at Holloman AFB. These differences are not surprising because: (1) Holloman AFB is situated ~ 11 km east of the study area, closer to the Sacramento Mountains and may not experience exactly the same wind regime as the dune field; and (2) dune topography may affect the orientation of the near-bed flow. The average orientation of the stoss-slope wind ripples is taken as the more

accurate indicator of the wind over the dunes, especially as it relates to the incidence angle and is used in our analysis.

The wind velocity profile obtained during the April wind event shows the average $u_* = 0.36$ m/s as measured by hot-wire probes and calculated using Equation 2, with $z_o = 0.11$ mm (Fig. 2.5). This is, in fact, essentially the same z_o as calculated by Jerolmack et al. (2006) for coarse-grained ripples. Wind data recorded at Holloman AFB during the same interval shows an average wind speed of 6.5 m/s, with an average wind gust speed of 10.3 m/s (Fig. 2.5). The projection of our velocity profile to a height of 10 m (i.e., the height at which data are collected at Holloman AFB) yields 9.5 m/s, which is between the average and gust values at Holloman AFB, but closer to the gust range. In fact, using the average gust speed at 10 m measured at Holloman AFB and the calculated $z_o = 0.11$ mm in Equation 2 yields $u_* = 0.38$ m/s during the 2 hour anemometer recording period. Because sand transport, q , roughly scales with u_* as $q \approx u_*^3$ (Bagnold, 1941), sand-transporting wind events may be best characterized by the average wind gust speed, as reported by meteorological stations. The average wind gust speed for the entire April wind event was 12.1 m/s, yielding $u_* = 0.44$ m/s. If applied to the March wind event, when the average wind gust speed was 9.4 m/s, $u_* = 0.35$ m/s. These values of shear stress are adopted here as characterizing their respective wind events. The “formative shear velocity” $u_{*f} = 0.39$ m/s for the White Sands Dune Field determined by Jerolmack et al. (2011) falls between the u_* values for our March and April events.

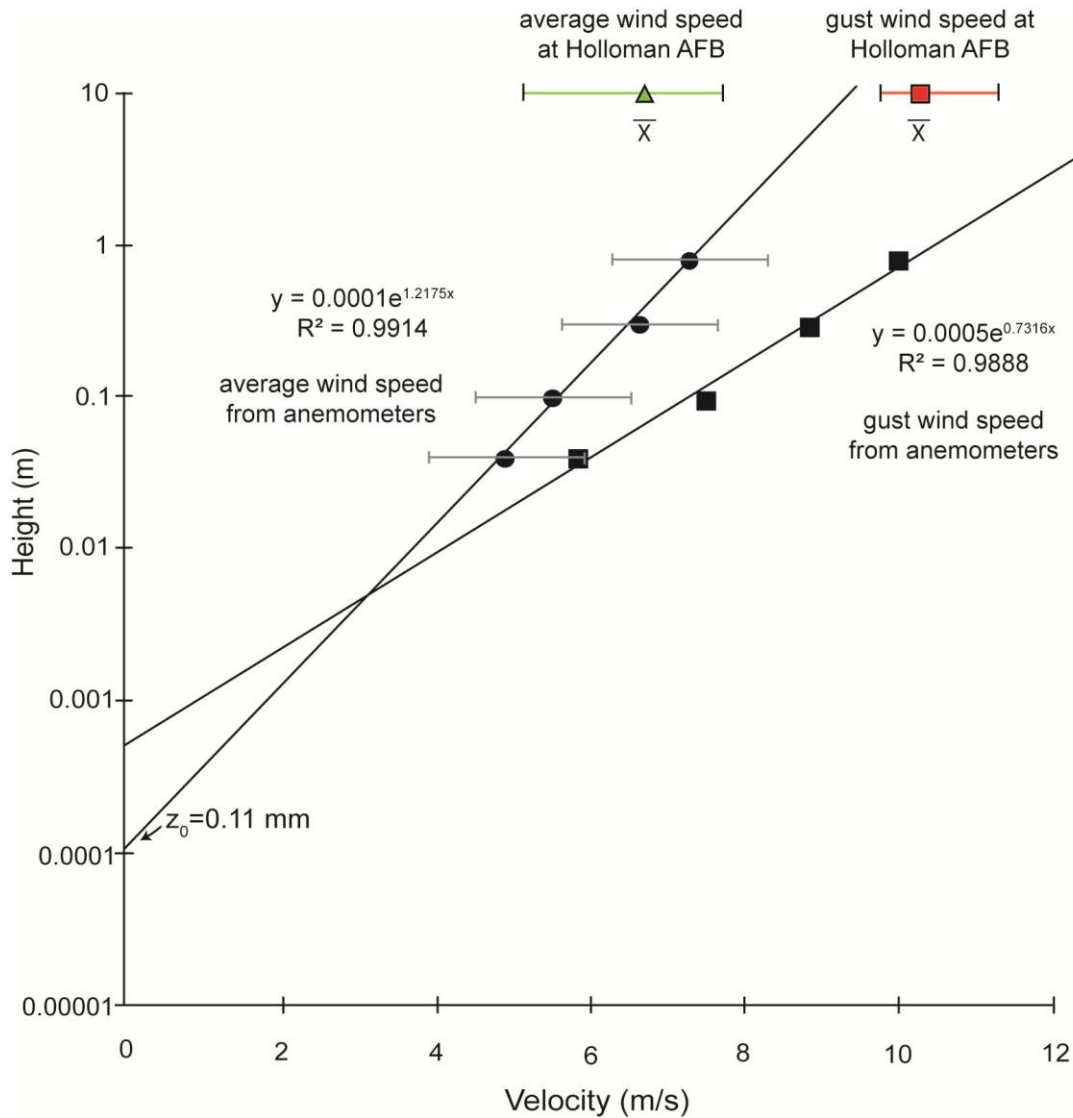


Figure 2.5. Velocity profile for wind measured by hot-wire probes at 4 cm, 10 cm, 30 cm and 80 cm above the bed at the crest of Dune 3 during the April wind event. Each point represents the average speed for a 2-hour sampling interval. The range bar on each mean velocity is +/- one standard deviation. The surface roughness height, z_0 , is the Y-intercept at 0.11 mm. Using Eq. 2, the calculated value for u_* is 0.36 m/s. The measured profile is projected up to 10m above the bed, the height at which wind data is collected at Holloman AFB. The average wind speed and wind gust measured at Holloman AFB over the same two-hour period are marked. The total range in average wind speed and wind gusts is also presented. Note that the measured profile from the White Sands dune is most closely aligned with the wind gust data from Holloman AFB.

4.2 Sediment record of the wind events

Given the primary wind directions for the two wind events, a range of incidence angles from 2° – 90° occurs on the three dunes as a function of local dune orientation (Fig. 2.4). The sinuosity of individual dune segments ranges from 1.06 – 1.47, as compared to 1.18 – 1.61 for the dunes as a whole (Fig. 2.4). The deposition/erosion rate is plotted by incidence angles in Figure 2.6. Grain size of the samples, partitioned by surface process, is plotted as cumulative frequency curves in Figure 2.7.

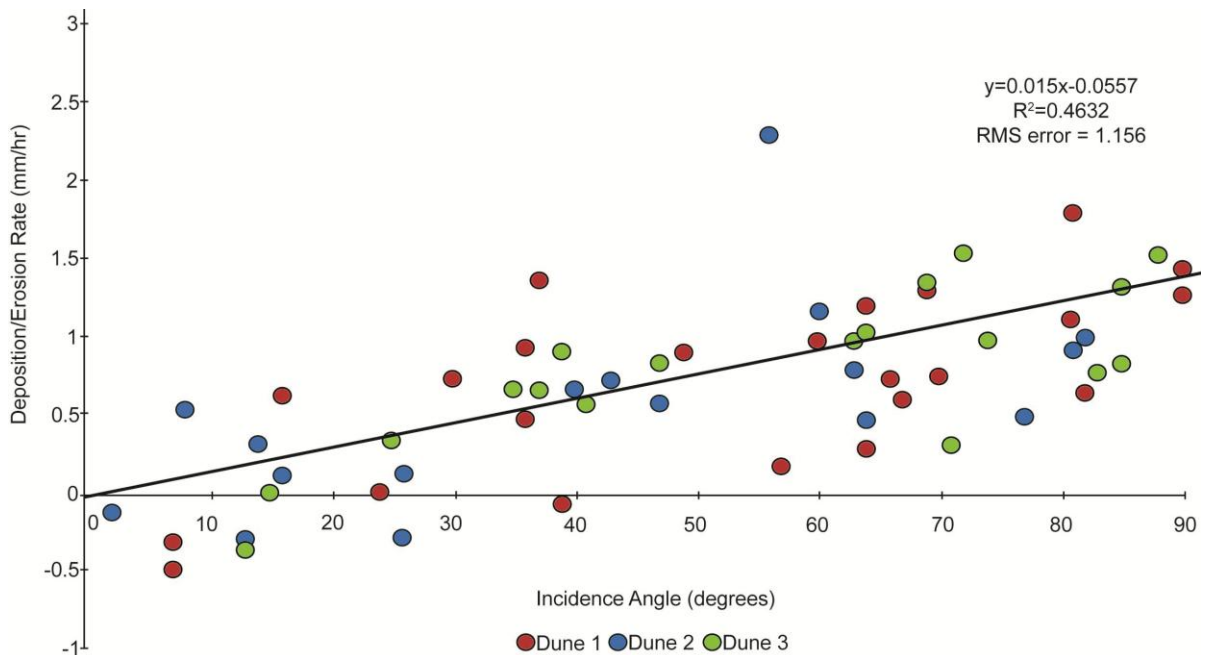


Figure 2.6. Transect-averaged rates for lee-face erosion/deposition plotted as a function of incidence angle. These values were calculated by taking the average vertical displacement of the lee surface measured at transects (Fig. 4) and dividing it by the number of hours of sand-transporting conditions measured at each dune. A best-fit line through the data shows a linear correlation between erosion/deposition rate and incidence angle.

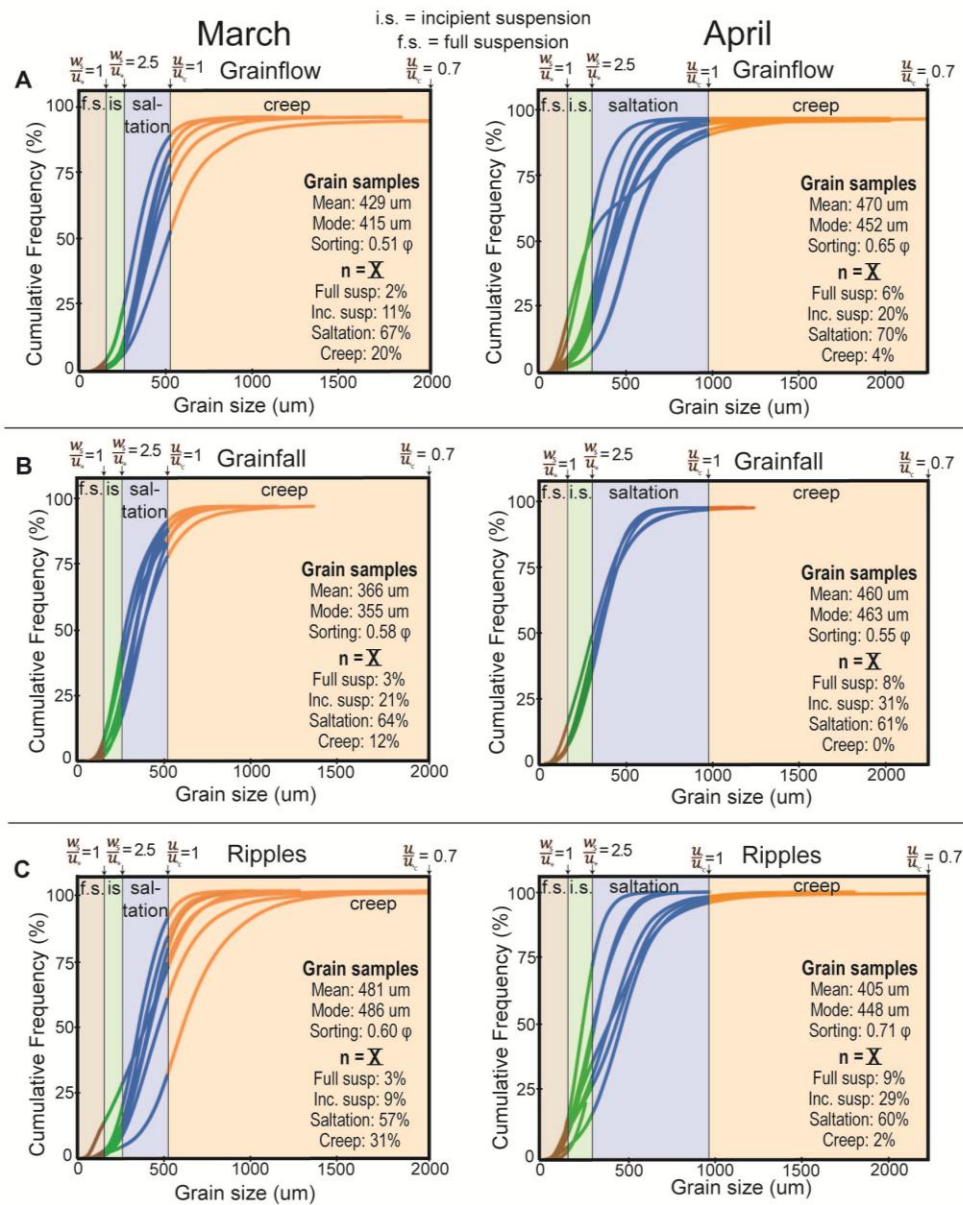


Figure 2.7. Cumulative grain-size curves for deposits at the base of lee surfaces following the March (Dune 1 & 2) and April (Dune 3) wind events. (A) Grainflow. (B) Grainfall. (C) Wind Ripples. Curves are partitioned into transport modes based on the empirical relationships shown in Figure 1. Estimates for u_* were calculated using wind data from the March or April wind event and Eq. 6. Estimates for u_{*c} were calculated using the median grain size collected and Equation 4. The representative values for settling velocity were calculated using Equation 3. Statistics given with each set of curves are mean values for these curves.

Our initial mapping of surface processes revealed many variations of the three basic surface processes. For example, areas of wind ripples varied significantly in the sharpness and definition of the ripples as a result of their formation time and presence/absence of blanketing grainfall. Grainflow varied from pristine to subdued (“ghosts”) where it had been blanketed by grainfall or partly reworked by wind ripples. In most cases, these variations represent surface processes at different stages of development. Ultimately, the variations were distilled into seven basic styles of surface processes, which are designated as Type A–G in Figure 2.1. Each type would be recognizable in the rock record as a style of stratification type. The White Sands examples are illustrated in Figure 2.1 and plotted by incidence angle in Figure 2.8.

Type A (wind ripples) characterized entire segments of lee faces, ranging from those experiencing erosion to bypass to deposition (Fig. 2.1A), but the face was always dominated by traction transport. At White Sands, ripples on erosional surfaces that typically exposed weakly-cemented dune cross-strata were coarser grained than those on depositional surfaces. Wind-ripple stratification is probably the most common stratification type in the aeolian rock record (e.g., see Figs. 3-4 Hunter, 1981; Fig. 8 Kocurek and Dott, 1981), and consists of the translent strata of Hunter (1977); the very thin, subcritically-climbing variety referred to as “pin-stripe laminations” by Fryberger and Schenk (1988).

Type B (wind ripples and grainfall) occurred on surfaces of bypass to deposition and is characterized by grainfall on the upper lee face passing downward to wind ripples (Fig. 2.1B). This stratification style shows a mix of gravity-driven and traction-driven

process. Grainfall is largely prevented from building to the angle of initial yield and avalanching by the alongslope reworking of wind ripples. At White Sands, Type B ranged from patchy grainfall on mostly-rippled lee surfaces to lee surfaces mostly covered by grainfall with subdued basal wind ripples. The representation of this stratification style in the rock record is a function of original dune size and preserved set thickness. Grainfall typically reaches the base of the lee face on small dunes, but does not reach the base on large dunes. On small dunes, Type B shows a dominance of grainfall deposits in the upper portion of the set passing downward to interlaminated wind ripple and grainfall laminae, the former commonly showing a high angle of climb (e.g., see Figs. 5A&6 Hunter, 1981; Fig. 19 Hunter and Richmond, 1987; Fig. 3A Kerr and Dott, 1988). On large dunes, or where only the most basal lee face has been preserved, Type B may be indistinguishable from Type A except for the intercalation of some grainfall laminae.

Type C (wind ripples, grainflow and grainfall) typically represented a more depositional surface than Type B and one that was influenced more by gravity-driven processes (Fig. 2.1C). Either higher rates of grainfall or less traction reworking by wind ripples allowed the grainfall deposits to build to the point of avalanching, yielding grainflow tongues. Wind ripples, however, reworked the entire surface between avalanches, and dominated on lower portions of the lee face. Type C is common in the rock record, represented by grainflow cross-strata that both intertongue with bottomsets of ripple laminae and are intercalated with ripple laminae that extend to the top of the sets

(e.g., see Fig. 11C Blakey and Middleton, 1983; Fig. 21 Hunter and Richmond, 1987; Fig. 5A Mountney and Jagger, 2004).

Type D (grainfall) is characterized by lee faces showing only grainfall deposits, which may extend as aprons onto the interdune floor (Fig. 2.1D). This stratification style should be inherently ephemeral because the grainfall will either build to the angle of initial yield and avalanche (Type F) or will be reworked by wind ripples (Type B). At White Sands this stratification style occurred along tapering portions of prograding depositional slipfaces (i.e., sections generating cross-strata). Although not common, cross-strata consisting largely of grainfall laminae have been described in the rock record (e.g., see Fig. 5B Hunter, 1981; Fig. 6A Clemmensen and Abrahamsen, 1983).

Type E (grainflow, grainfall, and basal ripples) is similar to Type C, with the important difference that wind ripples occur only at the base of the lee face (Fig. 2.1E). Type E, therefore, represents a gravity-dominated slipface except for the basal portion where traction still dominates. In the rock record, this stratification style is identified by grainflow cross-strata that intertongue with bottomsets of ripple laminae (e.g., see Figs. 3A&C Chandler et al., 1989; Fig. 11 Clemmensen and Blakey, 1989). Ripple laminae intercalated with the grainflow strata, a characteristic of Type C, are largely absent.

Type F (grainflow and grainfall) is characterized by slipfaces in which grainfall mantles some or most of the surface between avalanches and wind ripples are absent (Fig. 2.1F). The extent to which grainfall is carried down the lee face is a function of dune size, wind speed and lee turbulence. In the rock record, Type F is represented by grainfall laminae intercalated with grainflow cross-strata (e.g., see Figs. 5&6 Kocurek

and Dott, 1981; Fig. 6B Clemmensen and Abrahamsen, 1983), but it may be indistinguishable from Type G where slipface height or other factors precluded grainfall on the lower lee face.

Type G (grainflow) is characterized by slipfaces where pristine avalanche tongues extended from the lee base to the dune brink (Fig. 2.1G). The difference between Type G and Type F is that grainfall was confined to the uppermost slipface in Type F, and the frequency of avalanching in Type G was much greater than in Type F. Type G is common in the rock record and consists of sets of cross-strata composed exclusively of grainflow strata (e.g., see Fig. 6D Hunter, 1981; Fig. 10 Kocurek et al., 1991; Fig. 5B Loope, 1984; Fig. 6A Taggart et al., 2010).

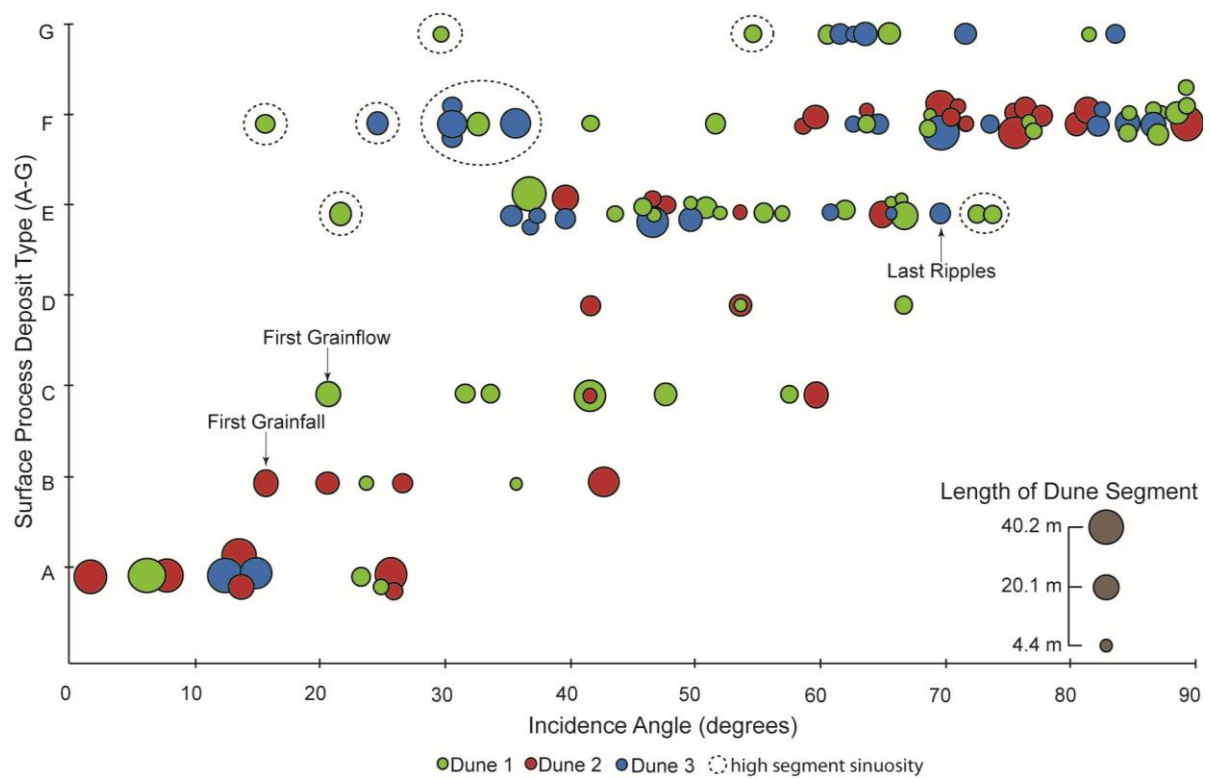


Figure 2.8. Type of lee-face deposit (A-G, Figure 2) plotted against the incidence angle for the dune segment on which it was observed. Points are color coded by dune and the size of each symbol is related to the dune segment length where the deposit type was observed. Data points that occurred on dune segments with high local sinuosity are circumscribed by dashed ovals and represent outliers to the data ranges for deposit types E-G (Fig. 2).

5. DATA ANALYSIS AND DISCUSSION

5.1 Dynamics that control the spatial distribution of lee surface processes

The purpose in mapping surface processes on the lee faces of the dunes after the wind events was to: (1) document the range of surface processes that occur during a single wind event; (2) explore the sediment-transport mechanics, especially as a function of incidence angle, that give rise to this range and its spatial distribution; and (3) provide

a basis for the reconstruction of paleowind directions from the spatial distribution of stratification types within sets of aeolian cross-strata.

Figure 2.4 clearly illustrates the diversity of surface processes that occur along the lee faces of sinuous dunes during single wind events. The simple plotting of styles of surface processes (Types A–G) by incidence angle in Figure 2.8 shows that although each stratification style occurs over a considerable range of incidence angles, there is a general trend in which moving from Type A all the way through to Type G corresponds to progressively higher angles of incidence. Wind ripples (Type A) dominate at low incidence angles, and grainflow and grainfall (Types F and G) dominate at high incidence angles. Between these end-members there is a progression in the first occurrence of gravity-driven surface processes, grainfall at 16° and grainflow at 22° , and the last occurrence of traction wind ripples appear at 70° . This progressive change from traction-dominated to gravity-dominated sediment transport also connects Types B–E to incidence angle (Fig. 9).

In addition to the control of incidence angle on the positioning of stratification styles (Fig. 2.8), their distribution was also explored in terms of lee-face segment length (Fig. 2.4) and lee-face sinuosity (Fig. 2.4). No distinct trends in the pattern of secondary-flow development emerge when segment length alone is considered. Long segments are common as outliers, and both long and short segments occur within concentrated clusters of points (Fig. 2.8). However, segments of local high sinuosity (dashed circles in Fig. 2.8) represent outliers, as seen in the low incidence angles for Types F–G, and the highest and lowest incidence angles for Type E. The sinuosity in these areas ranges from 1.31–1.61

(in red on Fig. 2.4), whereas the sinuosity in other areas ranges from 1.06–1.23 (in black on Fig. 2.4). This observation argues that high dune sinuosity may skew the distribution of surface processes. Characteristic secondary flow may be retarded where incidence angle changes rapidly because of dune curvature, and/or there is a lag in surface processes as secondary flow changes rapidly.

Data from the three dunes allow us to establish the relationships between incidence angle and lee-face surface processes for both low and high sinuosity dunes. Not surprisingly, these relationships are tighter for dunes and dune segments with lower sinuosities. Pure traction transport, as evidenced by wind ripples exclusively, occurs up to incidence angles of 16° , at which point grainfall begins to occur on the upper portion of the lee face. On the other end of the spectrum, although exclusively gravity-driven processes (Types F–G) can characterize a slipface with incidence angles as low as 43° , most occur at incidence angles $\geq 60^\circ$ (Fig. 2.8) and the last occurrence of wind ripples is at 70° . Type G, which occurs exclusively on concave segments of the lee face, is the most transverse configuration in which the concentration of grainfall on the uppermost lee face causes a high frequency of avalanching. Type E, which occurs at incidence angles of 37° – 70° , represents the classic oblique configuration in which a slipface of grainfall and grainflow sits above a wind ripple plinth (Fig. 9). The relationships are not as tight for high sinuosity cases. Type F and G occur at incidence angles between 16° and 36° . Wind ripples occur at incidence angles as high as 75° .

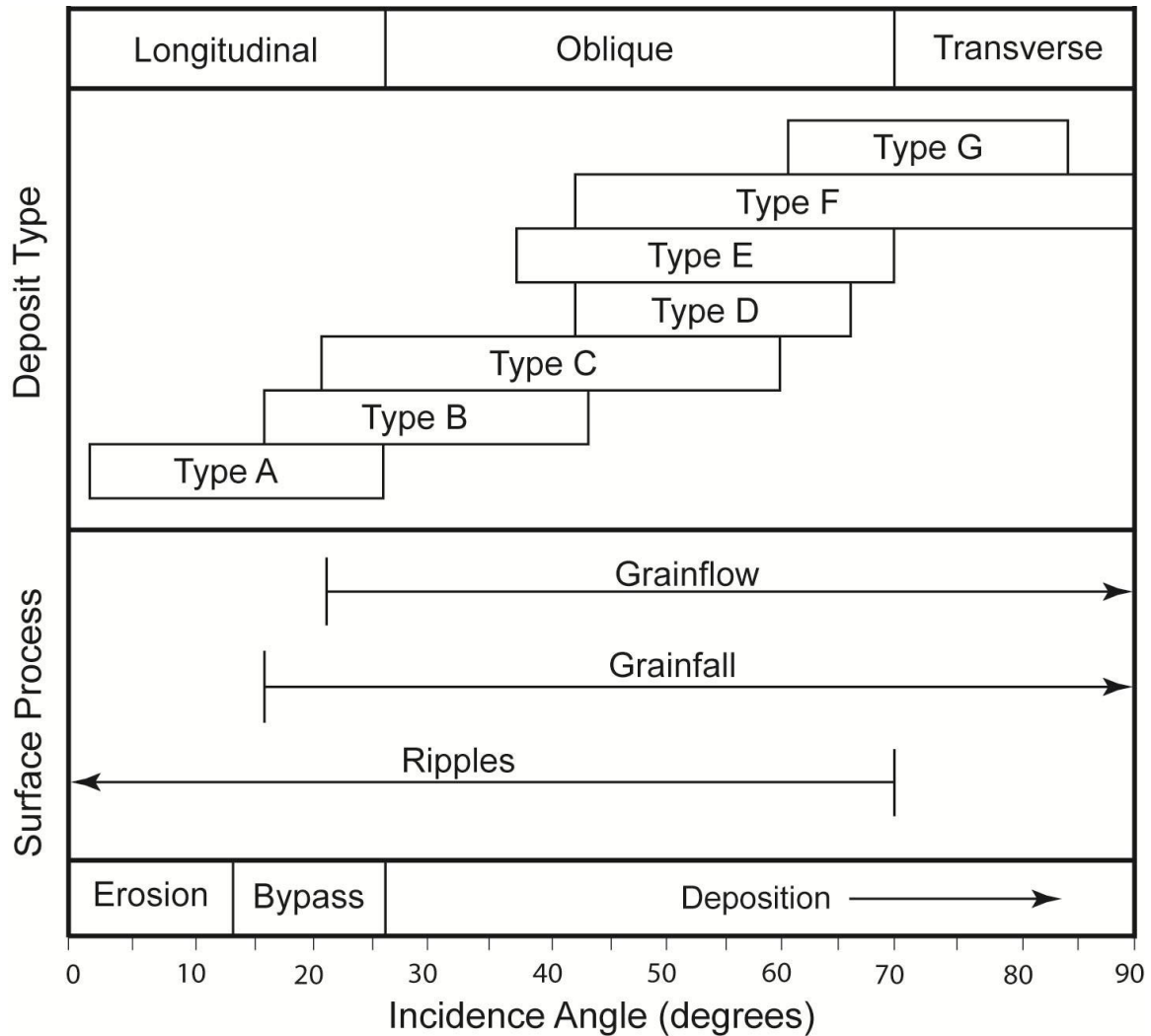


Figure 2.9. Summary diagram showing the range of incidence angles associated with each surface-process and deposit type (A-G, Fig. 2.2) after the outliers in Figure 2.8 have been removed. The ranges of observed lee-face erosion, bypass and deposition as a function of incidence angle. Rates of deposition continue to increase with increasing incidence angle (Fig. 2.6).

These relationships compare to previous work in the following ways. Sweet and Kocurek (1990) define longitudinal flow as 0-10°, characterized by attached flow where lee wind speeds approach that of the primary wind. They characterized transverse flow as well-developed flow separation, low lee wind speeds, and the absence of traction

transport that occurs from 70-90°. Sweet and Kocurek (1990) define oblique flow as occurring between 10–70°, characterized by components of both gravity-driven and along-slope traction transport. We re-define longitudinal secondary flow as 0-26°, characterized by surface processes (primarily wind ripples) experiencing erosion and bypass conditions. Incidence angles between 26-70° describe oblique flow, consisting of depositional deposits of grainflow, grainfall, and wind ripples. Transverse secondary flow characterizes incidence angles between 70-90°, characterized by grainflow and grainfall deposits and an absence of wind ripple deposits (Fig. 9).

The impact of wind speed in the development of lee surface processes can only be evaluated in a general way with our data. In agreement with earlier conclusions (Hunter, 1981; Hunter and Richmond, 1987; Kocurek, 1991), the White Sands data argue that the abundance of grainfall and the distance it is carried down the lee face increases with wind speed. For example, whereas grainfall commonly extends to the base of small dunes with transverse flow configurations, the presence of grainfall at the base of large dunes is taken as representing a storm event (Kocurek, 1991). For the White Sands data, the lee face of Dune 3, which represents the higher wind speed event, is enriched in basal grainfall and grainflow processes (Types E-G, Fig. 2.4). In contrast, the lee faces of Dunes 1-2, which represent the lower wind speed March event, exclusively show examples of Types B-C, where wind ripples actively rework grainfall and grainflow deposits. Dune 3 has a lower sinuosity (1.31) than Dunes 1-2 (1.44 and 1.61, respectively, Fig. 2.4), thus presenting an overall more transverse orientation. However, Type C (where wind ripples rework the entire lee face) will likely shift to Type E (basal wind

ripples only) at higher wind speeds where the intensity of grainfall on the upper lee faces overwhelms traction processes that would give rise to wind ripples.

This study does not address impact of lee-face height, as the dunes studied all had similar heights (average brink heights for Dune 1: 10.6m, Dune 2: 9.7 m, Dune 3: 9.1 m). For a given wind speed, grainfall becomes progressively difficult to transport down to the base of the lee face as dune height increases. The primary effect would be the convergence of Type F (grainfall and grainflow) toward Type G (all grainflow), especially in the rock record where only the lower lee face is preserved. Conversely, for a given dune height, the presence/thickness of grainfall at the base of the lee face should increase with wind speed, such that Type F occurs and is an indicator of wind storm events for large dunes represented primarily by Type G.

5.2 Deposition/erosion rates and incidence angle

As evident from Figure 2.6, deposition on the lee face is not uniform and generally follows with stratification styles. Erosion is largely restricted to portions of the lee face dominated by wind-ripple traction transport (Type A) in longitudinal flow where the incidence angle is $\leq 13^\circ$. Greatest amounts of deposition are associated with stratification types F and G at incidence angles close to 90° . The average rate of deposition/erosion increases linearly with incidence angle (Fig. 2.6). The variability about this trendline is best characterized using the root mean square error for the data set. This error is comparable to a standard deviation about the mean for the case where mean values are predicted using the equation $Erosion/Deposition Rate = 0.015 mm/hr \times Incidence Angle - 0.056 mm/hr$ (Fig. 2.6). The computed value for root mean square error

is 1.156 mm/hr. At any particular incidence angle the naturally occurring variability in this system is producing a spread in predicted deposition/erosion rates that is 89.3% of the greatest rate measured during the two studied wind events.

The spatially varied rates of deposition/erosion on the dune lee face show the net sand flux on the lee face as a function of a given primary wind direction. Each such portion of the wind regime causes a change in dune shape and migration direction, evident in seasonal changes in the dunes at White Sands where particular wind directions dominate (Kocurek et al., 2007). It is the cumulative sum of all the wind components that yields the net dune migration direction with dune shape largely conserved.

5.3 Grain sorting by surface processes and modes of transport

The purpose in the grain-size sampling of the basal lee surface processes was to (1) identify the mode of grain transport based upon a set of equations derived from experimental data, (2) examine the extent of grain sorting hypothesized to occur in the development of lee surface processes, and (3) provide a basis for the reconstruction of paleowind speeds from the grain-size distribution of stratification types in the aeolian rock record.

Given $u_* = 0.44$ m/s for the April wind event and using the median value of the relationship to describe creep motion (Equation 5), the smallest grain traveling in creep during the April wind event was 840 μm . All grains larger than 840 μm traveled in creep, up to the largest grain size sampled at 2222 μm . Using the median values of the relationships to describe saltation and suspension in Equations 6A-C, the smallest grain predicted to travel in saltation was 292 μm . The largest grain predicted to travel in full

suspension was 158 μm . The full range of grain sizes sampled and the method of transport for each grain size in April is: (1) suspension < 158 μm ; (2) incipient suspension = 158-292 μm ; (3) saltation = 292-840 μm ; and (4) creep 840-2222 μm . For the March wind event where $u_* = 0.35$ m/s, the same methods were used to calculate the following ranges of grain sizes and the method of transport for each grain size: (1) suspension < 137 μm ; (2) incipient suspension = 137-245 μm ; (3) saltation = 245-516 μm ; and (4) creep = 516-2001 μm . These ranges are used in the division of the cumulative frequency curves for samples from the three basic stratification types for each wind event (Fig. 2.7). Using somewhat different definitions (see section 2.2), Jerolmack et al. (2011) give comparable values for the “formative wind” ($u_* = 0.39$ m/s) at White Sands as: (1) all styles of suspension < 250 μm , (2) saltation = 250-650 μm , and (3) creep = 650-1300 μm .

Regardless of stratification type or wind event, the majority (57-70%) of grains traveled in saltation under conditions at the dune crest. The other modes of transport, however, are still represented: creep (0-31%), incipient suspension (9-31%), and suspension (2-9%). In the analysis of Jerolmack et al. (2011), the predicted values for the “formative wind” at White Sands are approximately: creep (10%), saltation (80%), and suspension (10%). The effects of higher wind speeds in April compared to March are evident. In addition to the shift in the grain-size range calculated for each mode of transport, as given above: (1) full or incipient suspension accounts for 16% of all transport in March, but 31% in April, (2) saltation accounts for 63% of all transport in March and 66% in April, and (3) the creep population is reduced from 21% in March to 3% in April. Given that the grain-size range on these dunes in close proximity to each

other is approximately the same, higher wind speeds shift modes of transport from creep to saltation, and from saltation to incipient suspension. The full suspension load does shift to higher values for the April wind event, but remains as a single-digit percentage and may be considered as deposited fairly uniformly in small quantities over the entire lee face.

Although all modes of transport are represented in most of the surface process deposits sampled from both wind events, significant grain-size sorting is evident. Grainflow deposits consist of proportions of grains that traveled in creep (20% in March, 4% in April), saltation (67% in March, 70% in April), and incipient suspension (11% in March, 20% in April), and most closely approximate the total proportions for each wind event given above. Grainfall deposits are enriched in grains that traveled in incipient suspension (21% in March, 31% in April) and depleted in grains that traveled in creep (12% in March, 0% in April) compared to the total proportions for each wind event. The creep population found in the March grainfall deposits may represent coarser grains that rolled to the dune base. Overall, while the grainflow deposits are most representative of the total sediment load transported over the dunes, the grainfall deposits represent a finer subset of this population. In contrast, wind-ripple deposits show the least consistency. Ripples sampled in the March event show 31% of the grains traveled in creep, but only 2% in April; incipient suspension accounts for 9% of the sediment load for the March event, but 29% in April. The wind ripples at White Sands ranged from those developed on: (1) grainfall deposits, or (2) grainflow deposits, to (3) well-defined ripples at lower incidence angles, to (4) coarser-grained erosional ripples at the lowest incidence angles.

The finest grain-size distributions occur with ripples developed on grainfall deposits, followed by those reworking grainflow deposits (which also show the widest grain size distributions), then well-defined ripples, and the erosional ripples show the coarsest grain sizes.

For the White Sands data, the characteristic shear velocity for the March and April wind events is best defined by grainflow deposits; the finest sediment in grainflow traveled in incipient suspension and the coarsest sediment in grainflow traveled as creep. Using Equation 6B for the definition of incipient suspension, the mid grain-size points within the defined range are 193 μm for March and 225 μm for April. These representative values yield the characteristic shear velocities of 0.35 m/s for March and 0.44 m/s for April. Averaged over the grainfall samples, the representative grain size is d_{11} for March and d_{21} for April. Using Equation 5 for the definition of creep, the mid grain-size points within the defined range are 732 μm for March and 1173 μm for April. These representative values yield the characteristic shear velocities of 0.35 m/s for March and 0.44 m/s for April. Averaged over the grainflow samples, the representative grain size is d_{96} for March and d_{99} for April.

The evaluation of wind speed from ancient cross-strata has a potential for greater error because of other impacting factors. As dune height becomes greater, it is progressively more difficult to transport grainfall to the base of the lee face. Because of this the particles preserved in basal grainfall deposits may not include the sizes that were traveling in incipient suspension load at the dune crest. The creep population is limited by both the grain-size range at the source area and how far into the dune field grains

traveling in creep are transported. It is possible that there is no creep population within the interior of the dune field. These cases will lead to an underestimate for shear velocity when employing Equations 5 and 6B.

Our methodology of characterizing a wind event using the u_* at the dune crest is intended to be used in conjunction with the determination of wind direction; combined, these methodologies allow for the recognition of specific wind events recorded in sets of cross-strata. Bagnold (1941) proposed that the u_* for a given wind is approximately equal to the u_{*c} for the coarsest grains in transport. For all of our White Sands samples, the median grain sizes in creep are 582 μm for March and 1005 μm for April, which yield values of $u_{*c} = 0.37$ m/s for March and 0.48 m/s for April. These values are only slightly more than our calculated shear velocities from the average gust wind speed. Although developed for the long-term “formative wind”, the approach by Jerolmack et al. (2011) in using d_{50} as representing the characteristic grain size in saltation may also have potential for characterizing single wind events. The challenge in any approach that attempts to utilize a single grain size in reconstructing wind speed is finding the representative grain size, given the sorting that occurs on the lee face.

6. CONCLUSIONS

The methodology presented here allows for the reconstruction of wind direction and speed from aeolian cross-strata, as opposed to the determination of net dune migration direction from the average dip direction of the cross-strata. This methodology is specifically aimed at determining wind speed and direction for individual wind events. Because sets of aeolian cross-strata commonly extend tens to hundreds of meters or more

in the migration direction, a large number of specific wind events are potentially recorded in these stratigraphic records.

Mapping of sinuous dunes at White Sands demonstrates the considerable variation in styles of the basic lee-face surface processes (grainflow, grainfall, wind ripples) that occurs on single dunes during single wind events. These styles of stratification are primarily a function of the incidence angle formed between the local orientation of the dune brink and the primary wind direction, but high local dune sinuosity, wind speed, and lee-face height also impact stratification style. Seven styles of stratification were identified at White Sands and most of these are common in ancient aeolian cross-strata. Each style occurs within a range of incidence angles, and although their ranges overlap, these stratification styles can be used to bracket the primary wind direction and secondary flow configuration in ancient cross-strata. Lee faces characterized entirely by wind ripples occur at incidence angles of $0-26^{\circ}$ and generally represent attached secondary longitudinal flow and tractional grain transport. Transverse secondary flow, characterized by flow separation and gravity-driven grainfall and grainflow with the absence of wind ripples, occurs at incidence angles of $70-90^{\circ}$. Oblique secondary flow configurations show a progression from (1) grainfall subject to reworking by wind ripples ($16-43^{\circ}$), to (2) sufficient grainfall to allow for grainflow or avalanching to occur, but still subject to wind-ripple reworking ($22-60^{\circ}$), to (3) “classic” oblique configurations where grainfall/grainflow dominate the upper lee face and yield downward to a wind ripple plinth ($37-70^{\circ}$).

The rate of deposition/erosion generally increases with incidence angle, following a similar trend as stratification type and incidence angle. For our White Sands data, erosion generally occurred at incidence angles between 0-13° with the migration of coarse-grained ripples, whereas bypass or slow rates of deposition occurred at incidence angles between 13-26° where wind ripples reworked grainfall and some grainflow surfaces. The highest rate of deposition occurred with perfectly transverse secondary flow and was characterized by a high intensity of grainfall that caused frequent avalanching.

The sampling of grain size by stratification type shows that grain size is not uniform on dune lee faces, but rather is sorted by the lee secondary flow and the surface processes themselves. Grainflow strata are the most representative of the total sediment load, whereas grainfall deposits are enriched in grains that traveled in incipient suspension and are depleted in grains that traveled in creep. Although cycles have been identified based upon grain-size variations in wind-ripple strata (e.g., Kocurek et al., 1991), in general, ripple deposits are the least diagnostic of the stratification types because they may form on any lee deposit where traction transport occurs. Currently, wind speed can be estimated from the grain-size distributions of the stratification types by utilizing empirical relationships developed for the end-member modes of grain transport, but these need to be utilized within the overall context of the dune field. For the White Sands Dune Field, d_{15} for grainfall and d_{10} for grainflow are reasonable grain sizes to represent the incipient suspension load as input into Equation 6B to calculate wind speed. For the creep load, d_{97} is a reasonable grain size for input into Equation 5 to calculate wind speed. For other dune fields and ancient aeolian cross-strata, these values

provide a starting point for reconstructing wind speeds, but bracketing wind speeds by evaluating a range of grain sizes in Equations 5 and 6B may be the most reasonable approach. For example, where grainfall deposits are interpreted as representing infrequent storm events, a range of grain sizes (e.g., d_{15} , d_{25} , d_{50} , d_{75} , d_{95}) can be taken as incipient suspension and evaluated in Equation 6B. Calculated wind speeds can be compared to those for the coarsest (creep) grains (e.g., d_{95} , d_{97} , d_{99}) in contemporaneous grainflow deposits using Equation 5. A fruitful line for future research is clearly a better evaluation of the relative roles that grain-size range, wind speed, and dune height play in producing styles of stratification types and their grain size ranges.

7. ACKNOWLEDGEMENTS

This research was supported by grants from the National Park Service as part of the Chihuahuan Desert Network Inventory and Monitoring Program, from the National Science Foundation EAR-0921659, and from the Jackson School of Geosciences at the University of Texas at Austin. We thank the GEO 380R class, which helped in data collection during the April wind event. We are grateful to David Bustos and Hildy Reiser of the National Park Service for facilitating this study.

8. MATHEMATICAL NOTATION

τ = boundary shear stress

w_s = settling or terminal fall velocity of a grain

u_* = mean shear velocity or strength of the wind

u_{*c} = critical shear stress/velocity required to initiate grain motion

u_{*i} = impact shear stress/velocity required to sustain grain motion

ρ_f = density of a fluid

ρ_s = density of sediment

$s = \rho_s/\rho_f$, ratio of sediment to fluid densities

g = gravitational force, 9.81 m/s^2

d = grain diameter

C_1 = theoretical constant (equal to 18 for typical sand grains)

C_2 = constant asymptotic value of the drag coefficient (equal to 1 for typical natural grains)

ν = kinematic viscosity

κ = von Karman's constant, value = 0.4

z = elevation above bed, in m

z_0 = roughness parameter, value = 1.05×10^{-4} for this study

u_z = time-averaged velocity at height z above the bed

9. REFERENCES

- Allen, J.R.L. (1982). *Sedimentary Structures: Their character and physical basis*, Volume 2: Amsterdam, Elsevier, 663 p.
- Allmendinger, R.J. (1972), Hydrologic control over the origin of gypsum at Lake Lucero, White Sands National Monument, New Mexico. *M.S. Thesis*, New Mexico Institute of Mining and Technology, Socorro, New Mexico, 182 p.
- Bagnold, R. (1941), *The Physics of Blown Sand and Desert Dunes*, Methuen, London.
- Bagnold, R. (1966), An approach to the sediment transport problem from general physics, *Geol. Surv. Prof. Paper*, 422-I.
- Bishop, S.R., H. Momiji, R. Carretero-Gonzalez, and A. Warren (2002), Modeling desert dune fields based on discrete dynamics, *Discrete Dynamics in Nature and Society*, 7, 7-17.
- Blakey, R.C., and L.T. Middleton (1983), Permian shoreline eolian complex in Central Arizona: Dune changes in response to cyclic sealevel changes. in *Developments in Sedimentology: Eolian Sediments and Processes*, v. 38, edited by M.E. Brookfield and T.S. Ahlbrandt, p. 551-581.
- Chandler, M.A., Kocurek, G., Goggin, D.J., and L.W. Lake (1989), Effects of stratigraphic heterogeneity on permeability in eolian sandstone sequence, Page Sandstone, Northern Arizona, *AAPG Bulletin*, 73, 658-668.
- Clemmensen, L.B., and K. Abrahamsen (1983), Aeolian stratification and facies association in desert sediments, Arran basin (Permian), Scotland, *Sedimentology*, 30, 311-339.
- Clemmensen, L.B. and R.C. Blakey (1989), Erg deposits in the Lower Jurassic Wingate Sandstone, northern Arizona: oblique dune sedimentation, *Sedimentology*, 36, 449-470.
- Curry, J.R., (1956), The analysis of two-dimensional orientation data, *Journal of Geology*, 64, 117-131.
- Dott, R.H., C.W. Byers, G.W. Fielder, S.R. Stenzel, and K.E. Winfree (1986), Aeolian to marine transition in Cambro-Ordovician cratonic sheet sandstone of the northern Mississippi valley, U.S.A, *Sedimentology*, 33, 345-367.
- Ewing, R.C., and G. Kocurek (2010), Aeolian dune interactions and dune-field pattern formation: White Sands Dune Field, New Mexico, *Sedimentology*, 57, 1199-1219.

- Frank A. & Kocurek G. 1994. Effects of atmospheric conditions on wind profiles and aeolian sand transport with an example from White Sands National Monument. *Earth Surf. Proc. and Landf.* 19, 735-745.
- Ferguson, R., and M. Church (2004), A simple universal equation for grain settling velocity, *J. Sediment. Res.*, 74(6), 933-937, doi:10.1306/051204740933.
- Fryberger, S.G. (2003), Geology of White Sands National Monument web page: www2.nature.nps.gov/geology/parks/whsa/.
- Fryberger, S.G., and C.J. Schenk (1988), Pin stripe lamination: A distinctive feature of modern and ancient eolian sediments, *Sedimentary Geology*, 55, 1-15.
- Gilbert, G. K., 1914, The transportation of debris by running water: U.S. Geological Survey Professional Paper 86, 263 p.
- Grass, A.J. (1971) Structural features of turbulent flow over smooth & rough boundaries, *J. Fluid Mechanics*, 50, 233-255.
- Howard, A.D. (1977), Effect of slope on the threshold of motion and its application to orientation of wind ripples, *GSA Bulletin* 88, 853-856.
- Hunter, R.E. (1977), Basic types of stratification in small eolian dunes, *Sedimentology*, 24, 361-387.
- Hunter, R.E. (1981), Stratification styles in eolian sandstones: some Pennsylvanian to Jurassic examples from the Western Interior U.S.A. in Recent and ancient nonmarine depositional environments: models for exploration, v. 31, edited by F.G. Ethridge and R.M. Flores, p. 315-329.
- Hunter, R.E., and B.M. Richmond (1987), Daily cycles in coastal dunes, *Sedimentary Geology*, 55, 43-67.
- Hunter, R.E., and D.M. Rubin (1983), Interpreting cyclic crossbedding, with an example from the Navajo Sandstone. in *Developments in Sedimentology: Eolian Sediments and Processes*, v. 38, edited by M.E. Brookfield and T.S. Ahlbrandt, p. 429-454.
- Iverson, J.D. and B.R. White (1982), Saltation threshold on Earth, Mars and Venus, *Sedimentology*, 29, 111-119.
- Jerolmack, D.J. and T.A. Brzinski, (2010), Equivalence of abrupt grain-size transitions in alluvial rivers and eolian sand seas: A hypothesis, *Geology*, 38, 719-722.
- Jerolmack, D., D. Mohrig, J. Grotzinger, D. Fike, and W. Watters (2006), Spatial grain size sorting in eolian ripples and estimation of wind conditions on planetary surfaces:

- Application to Meridiani Planum, Mars, *J. Geophys. Res.*, *111*, E12S02, doi:10.1029/2005JE002544.
- Jerolmack, D., M. Reitz, and R. Martin (2011), Sorting out abrasion in a gypsum dune field, *J. Geophys. Res.*, *116*, F02003, doi:10.1029/2010JF001821.
- Kerr, D.R., and R.H. Dott, (1988), Eolian dune types preserved in the Tensleep Sandstone (Pennsylvanian-Permian) north-central Wyoming, *Sedimentary Geology*, *56*, 383-402.
- Kocurek, G. (1981), Significance of interdune deposits and bounding surfaces in aeolian dune sands, *Sedimentology*, *28*, 753-780.
- Kocurek, G. (1991), Interpretation of ancient eolian sand dunes, *Annu. Rev. Earth Planet. Sci.*, *19*, 43-75.
- Kocurek, G. (1996), Desert aeolian systems. in *Sedimentary Environments: Processes, Facies and Stratigraphy*, 3rd ed, edited by H.G. Reading, p. 125-133.
- Kocurek, G. and R.H. Dott (1981), Distinctions and uses of stratification types in the interpretation of eolian sand, *J. Sedim. Pet.*, *51*, 579-595.
- Kocurek, G., J. Knight, and K. G. Havholm (1991), Outcrop and semi-regional three-dimensional architecture and reconstruction of a portion of the eolian Page Sandstone (Jurassic), *SEPM Concepts in Sedimentology and Paleontology*, *3*: 25-43.
- Kocurek, G., Carr, M., Ewing, R., Havholm, K.G., Nagar, Y.C., and A.K. Singhvi (2007), White Sands Dune Field, New Mexico: Age, dune dynamics and recent accumulations, *Sedimentary Geology*, *197*, 313-331.
- Kottowski, F.E. (1958), Lake Otero: second phase in formation of New Mexico's gypsum dunes, *GSA Bulletin*, *69*, 1733-1734.
- Langford, R. (2003), The Holocene history of the White Sands dune field and influences on eolian deflation and playa lakes, *Quat. Int.*, *104*, 31-39.
- Langford, R.P., K.M. Pearson, K.A. Duncan, D.M. Tatum, L. Adams, and P. Depret (2008), Eolian topography as a control on deposition incorporating lessons from modern dunes seas: Permian Cedar Mesa Sandstone, SE Utah, U.S.A, *J. Sedim. Res.*, *78*, 410-422, doi: 10.2110/jsr.2008.045.
- Laursen, E.M. (1958), The total sediment load of streams, *Proceedings of the American Society of Civil Engineers, Journal Hydraulics Division*, *84*, 1530-1536.

- Loope, D.B. (1984). Eolian origin of upper Paleozoic sandstone, southeastern Utah, *J. Sedim. Pet.*, 54, 563-580.
- Loope, D.B., C.M. Rowe, and R.M. Joeckel (2001), Annual monsoon rains recorded by Jurassic dunes, *Nature*, 412, 64.
- McKee, E.D. (1966), Structures of dunes at White Sands National Monument, New Mexico (and a comparison with structures of dune from other selected areas), *Sedimentology*, 7, 3-69, doi:10.1111/j.1365-3091.1966.tb01579.x.
- McKee, E.D. and J.R. Douglass (1971), Growth and movement of dunes at White Sands National Monument, New Mexico, *US.G.S. Prof. Paper 750-D*, p. D108-D114.
- McKee, E.D., and R.J. Moiola (1975), Geometry and growth of the White Sands Dune Field, New Mexico. *U.S.G.S. J. Res.* 3, 59-66.
- Mountney, N.P., and A. Jagger (2004), Stratigraphic evolution of an aeolian erg margin system: the Permian Cedar Mesa Sandstone, SE Utah, USA, *Sedimentology*, 51, 713-743.
- Mountney, N.P. (2006). Periodic accumulation and destruction of aeolian erg sequences in the Permian Cedar Mesa Sandstone, White Canyon, southern Utah, USA, *Sedimentology*, 53, 789-823.
- Nickling, W.G., McKenna Neuman, C. And N. Lancaster, (2002), Grainfall processes in the lee of transverse dunes, Silver Peak, Nevada, *Sedimentology* 49, 191-209.
- Nino, Y., F. Lopez, and M. Garcia (2003), Threshold for particle entrainment into suspension, *Sedimentology*, 50, 247-263.
- Nishimura, K., and J.C.R. Hunt (2000), Saltation and incipient suspension above a flat particle bed below a turbulent boundary layer, *J. Fluid Mech.*, 417, 77-102, doi:10.1017/S0022112000001014.
- Parrish, J.T., and F. Peterson (1988), Wind directions predicted from global circulation models and wind directions determined from eolian sandstones of the western United States – a comparison, in *Sedimentary Geology* 56, edited by G. Kocurek, p. 261-282.
- Reiche, P. (1938), An analysis of cross-lamination the Coconino Sandstone, *J. of Geology*, 46, 905-932.
- Reitz, M.D., Jerolmack, D.J., Ewing, R.C., and R.L. Martin (2010), Barchan-parabolic dune pattern transition from vegetation stability threshold, *Geophys. Res. Lett.*, 37, L19402, doi:10.1029/2010GL044957.

- Rowe, C.M., Loope, D.B., Oglesby, R.J., Van der Voo, R., and Broadwater, C.E., (2007), Inconsistencies between Pangean reconstructions and basic climate controls, *Science* 318, 1284-1286.
- Rubin, D.M., and R.E. Hunter (1982), Bedform climbing in theory and nature, *Sedimentology*, 29, 121-138.
- Rubin, D. and R.E. Hunter (1983), Reconstructing bedform assemblages from compound crossbedding, in *Eolian sediments and processes*, edited by M.E. Brookfield, and T.S. Ahlbrandt, p. 407-427, Elsevier, Amsterdam, Netherlands.
- Rubin, D.M., and R.E. Hunter (1987), Bedform alignment in directionally varying flows, *Science*, 237, 276-278.
- Rubin, D.M., and H. Ikeda (1990), Flume experiments on the alignment of transverse, oblique, and longitudinal dunes in directionally varying flows, *Sedimentology*, 37, 673-684.
- Scherer, C.M.S. and K. Goldberg (2010), Cyclic cross-bedding in the eolian dunes of the Sergi Formation (Upper Jurassic), Reconcavo Basin: Inferences about the wind regime, *Palaeogeography, Palaeoclimatology, Palaeoecology*, 296, 103-110.
- Shao, Y. (2000), *Physics and modeling of wind erosion*, Atms. and Oceano. Sci. Library, 23, Kluwerk, Dordrecht.
- Shao, Y. and H. Lu (2000), A simplified expression for threshold friction velocity, *J. Geophys. Res.*, 105, 22,437-22,443.
- Smith, J.D., and T.S. Hopkins (1972), Sediment transport on the continental shelf off of Washington and Oregon in light of recent current measurements. in *Shelf Sediment Transport: Process and Patterns*, edited by D.J.P. Swift, D.B. Duane, and O.H. Pilkey. Dowden, p. 143-179, Hutchinson & Ross, Stroudsburg, PA.
- Sweet, M.L., and G. Kocurek (1990), An empirical model of aeolian dune lee-face air-flow, *Sedimentology*, 37, 1023-1038.
- Szynkiewicz, A., Ewing, R.C., Moore, C.H., Glamoclija, M. Bustos, D., and L. Pratt (2010), Origin of terrestrial gypsum dunes – Implications for Martian gypsum-rich dunes of Olympia Undae, *Geomorphology*, 121, 69-83.
- Taggart, S. Hampson, G.J., and M.D. Jackson (2010), High-resolution stratigraphic architecture and lithological heterogeneity within marginal aeolian reservoir analogues, *Sedimentology*, 57, 1246-1279.

- Tanner, W.F., (1965). Upper Jurassic paleogeography of the Four Corners region, *J. Sedim. Pet.*, 35, 534-574.
- Tsoar, H. (1983), Dynamic processes acting on a longitudinal (seif) sand dune, *Sedimentology*, 30, 567-578.
- Van Rijn, L.C. (1984), Sediment transport part I: Bed load transport, *J. Hydr. Engin.*, 110, 1431-1456.
- Walker, I.J., and W.G. Nickling (2002), Dynamics of secondary airflow and sediment transport over and in the lee of transverse dunes, *Progress in Physical Geography*, 26, 47-75.
- Walker, I.J., and W.G. Nickling (2003), Simulation and measurement of surface shear stress over isolated and closely spaced transverse dunes in a wind tunnel, *Earth Surface Processes and Landforms*, 28, 1111-1124.
- Werner, B.T. (1995), Eolian dunes: Computer simulations and attractor interpretation, *Geology*, 23, 1107-1110.
- Werner, B.T. and G. Kocurek (1997), Bedform dynamics: Does the tail wag the dog? *Geology*, 25, 727-730

Chapter 3: Reconstructing Wind Direction and Speed for the Permian Cedar Mesa Sandstone, SE Utah

ABSTRACT

A new method is applied to the uppermost sequence of the Permian Cedar Mesa Sandstone on the Colorado Plateau in the southwestern USA to reconstruct both the wind direction and wind speed. This portion of the Cedar Mesa dune field in southeastern (SE) Utah was chosen to test the utility of this new methodology because of superior outcrops and extensive previous work that documents net transport to the SE based upon the mean dip direction of the cross-strata. For the Cedar Mesa, as with other aeolian units, it is commonly assumed that the net transport direction mirrors the formative wind direction, but this is true only where the wind regime is unidirectional.

The basis for the new methodology is that most aeolian dunes are too large to reorient to each wind direction in the total wind regime. As a result, dune crests become oriented to be as perpendicular as possible to all constructive wind directions (i.e., gross bedform-normal orientation). A given wind, therefore, may strike a dune brinkline at a variety of incidence angles (the angle between the crestline and the wind) along a sinuous dune crest for a single wind direction. For each class of incident angles, characteristic secondary flow develops on the dune lee face, which, in turn, gives rise to surface processes that result in specific configurations of stratification types. The basic stratification types are: (1) wind-ripple laminae formed with traction transport, (2) grainfall strata formed by grains blown past the dune brink under the influence of lee turbulence, and (3) grainflow strata that form with avalanching of grainfall deposits.

Combined, these stratification types represent the modes of transport (i.e., creep, saltation, suspension) as a function of dune crestral wind speed.

Trial-and-error fit in the Cedar Mesa demonstrated that no single wind direction could account for the sequence of stratification styles observed along segments of crestlines, but all could be accounted for by two primary winds (from 290° and 005°). In order to satisfy the gross bedform-normal crest orientation and yield net migration of the dunes to the SE, the west wind (290°) would have to have been twice the magnitude (in either duration or intensity) of the north wind (005°). In order to determine wind speed, grain size analysis was completed for representative grainfall, grainflow, and wind-ripple deposits, and winds speeds were bracketed using well-established relationships for shear stress and mode of transport. Two wind storms were recognized. Both storm events were a product of the west wind (290°), indicating that the west wind (290°) blew more intensely than the north wind (005°).

1. INTRODUCTION

The dip of cross-strata deposits from both fluvial and aeolian deposits have long been used to infer dune migration direction (e.g., Dott and Roshardt, 1972; Hunter and Rubin, 1983; Loope, 1984; Stanesco and Campbell, 1989; Kocurek et al., 1991; Langford et al., 2008; Scherer and Goldberg, 2010). The average cross-strata dip direction is generally implied to be the net migration direction of the paleobedform. In fluvial environments, where the flow is unidirectional, the net dune migration direction is the paleoflow direction. Many people also make this assumption for aeolian environments and interpret the net dune migration direction as the paleowind direction (e.g., Reiche,

1938; Curray, 1956; Tanner, 1965; Clemmensen and Abrahamsen, 1983; Dott et al., 1986; Mountney, 2006). However, this is only true if the wind is completely unidirectional, which rarely happens in nature. Aeolian cross-strata also record information about paleowind speed, but this has rarely been addressed (Jerolmack et al., 2006; 2011).

Determination of wind direction and wind speed in ancient aeolian systems has broad but largely untapped applications in quantitatively constraining paleoclimate reconstruction for continental terrains. Arguably, aeolian sand dunes are the most direct proxies for paleowinds at the Earth's surface because sand dunes form in direct response to the surface sediment-transport system of the wind. Historically, however, paleowind information has been under-utilized as input data for numerical models describing ancient regional or global circulation and climates. Peterson (1988) compiled cross-strata dip directions from aeolian units on the Colorado Plateau (COP) and created a dataset of net migration directions spanning the Late Pennsylvanian through Jurassic periods. Paleowind directions inferred from this dataset have been used to validate global circulation models for the Pangean supercontinent. Loope et al. (2004) and Rowe et al. (2007) propose that cross-strata in the Cedar Mesa Sandstone are the product of tropical north-westerlies that seasonally blew across the equator, while Parrish and Peterson (1988) interpret these deposits as northern hemisphere subtropical anticyclones.

The new methodology described by Eastwood et al. (in review) reconstructs long-term climate variables from the aeolian rock record by calculating wind directions and wind speeds from preserved dune strata. The objective of this study is to demonstrate this

methodology by applying it to the Permian Cedar Mesa Sandstone on the COP in the southwestern USA. Results can be used to provide novel input data on regional scale paleowind conditions for application to climate models. Re-evaluation of the global circulation belts that were active on the COP during the Permian is possible using the correct interpretation of the Cedar Mesa Sandstone paleowinds.

2. THEORY

2.1 Reconstruction of Wind Direction

Experiments (Rubin and Hunter, 1987; Rubin and Ikeda, 1990), analytical solutions (Werner and Kocurek, 1997), and computer models (Werner, 1995; Bishop et al., 2002) all indicate that the crestlines of aeolian dunes are oriented perpendicular to the vector sum of all constructive winds. Any bedform, excluding the smallest aeolian dunes, exhibits this “gross bedform-normal” crest orientation (Rubin and Hunter, 1987) when the duration of the wind from a given direction is shorter than the time required for the bedform to reorient (Rubin and Ikeda, 1990). The smallest aeolian dunes are able to reorient to each change in the wind direction. Due to the various wind directions that compromise a given wind regime, medium and large dune crestlines experience a variety of incidence angles, or the angle between the dune crest and the wind. In addition, for a given wind direction, a sinuous dune crestline will experience multiple incidence angles.

The secondary flow (i.e., the dune-modified primary flow) on the lee face of a dune is primarily a function of the incidence angle but also a function of dune morphology (especially lee slope) (Sweet and Kocurek, 1990; Walker and Nickling, 2003). Based upon topographical surveying and detailed analysis of lee-face stratification

after an individual wind event, Eastwood et al. (in review) confirmed and tightened the classification of secondary flow as a function of the incidence angle made by Sweet and Kocurek (1990): transverse (70-90°), oblique (25-70°) and longitudinal (0-25°). With a longitudinal configuration, the secondary lee flow is attached and transport is alongslope. As the incidence angle becomes greater (i.e., oblique), the lee flow is deflected and flow separation occurs; some of the transport occurs alongslope, while some forms a 3-D vortex with reversed flow (e.g., Allen, 1982). At transverse incidence angles, (approaching 90°) a 2-D roller develops with flow recirculation directly up the lee face. As a result of turbulence and wind speed conditions on the lee face, traction transport dominates at longitudinal incidence angles, gravity-driven processes dominate at transverse incidence angles, and both gravity and traction processes occur at oblique incidence angles (Tsoar, 1983; Nickling et al., 2002; Walker and Nickling, 2003).

The secondary flow configurations control the surface processes and resultant stratification types that form on a dune lee face. The basic aeolian lee-face processes described by Hunter (1977) are: (1) *grainfall*, in which grains blow over the dune brink and settle on the surface (Nickling et al., 2002); (2) *grainflow*, in which a pile of sediment built on the upper lee face reaches the angle of initial yield, avalanches, and flows to the base of the slipface, and (3) *wind ripples*, in which sediments of any origin on the lee face are reworked. Grainfall and grainflow are gravity-driven processes, while wind ripples are formed by traction transport. The presence of gravity-driven processes and the absence of traction transport indicate a transverse flow configuration. Eastwood et al. (in review) confirmed that grainflow deposits develop at incidence angles between 22 and

90°, and grainfall deposits form at angles between 16 and 90°. Ripples are indicative of a flow configuration where traction transport dominates, becoming increasingly prominent with decreasing incidence angles. Ripples develop between 0 and 70° (Eastwood et al., in review). With oblique flow, both grainfall/grainflow and wind ripples can occur, depending upon the spatial dominance of gravity-driven versus traction transport. Typically, gravity-dominated processes on the upper lee face yield downslope to ripples migrating alongslope where traction transport dominates. In nature, a variety of styles of stratification types occur as a function of the total wind regime, and the most common configurations are shown by Kocurek (1991, Fig. 8).

Dune crestline orientation is the product of all constructive primary winds, and the average dip direction of cross-strata within a set reflects the overall dune migration direction. The average dip direction only represents the paleowind direction when the wind regime is unidirectional. Any given cross-strata orientation reveals the local crestline orientation. Combining the crest orientation with the stratification style that occurs at that orientation brackets the local incidence angle into broad categories: transverse, oblique, and longitudinal flow. Pairs of local cross-strata orientations and stratification styles along the length of a set reveal the overall crestline shape, orientation, and the range of incidence angles along the crestline.

2.2 Reconstruction of Wind Speed

The three end-member modes of sediment transport by the wind are creep, saltation, and suspension, and these arise because of the balance between grain properties and the forces that cause motion (Bagnold, 1941). For sand dunes, the majority of grains

move in saltation via parabolic jumps and semi-elastic collisions with the bed. The heaviest grains move in creep, rolling along the bed through collisions with saltating grains and fluid drag/lift forces. The smallest grains move in suspension, advected high into the flow and rarely make contact with the bed. Attempts to characterize sediment transport utilize basic relationships between fluid forces and grain properties. Fluid forces arise because of the shear stress, τ , exerted on the bed by the fluid. Because shear stress is difficult to measure directly, friction or shear velocity, u_* , is commonly used:

$$u_* = \sqrt{\tau/\rho_f} \quad (1)$$

where ρ_f is the density of the fluid. Shear velocity is typically derived from a measured velocity profile using the “law of the wall”

$$u_z = \frac{u_*}{\kappa} \ln\left(\frac{z}{z_0}\right) \quad (2)$$

where u_z is the wind speed at height z above the surface, κ is von Karman’s constant (equal to 0.4 in neutral atmospheric conditions), and z_0 is the surface roughness height where zero velocity occurs. For this study, we will use the z_0 from Eastwood et al. (in review), $z_0 = 1.05 \times 10^{-4}$, a value based upon sand ripples from the dunes at White Sands National Monument. This value should be representative of the entire field at White Sands.

The shape, size, and density of a grain controls how it is transported, which is best described by parameters such as the grain settling velocity, w_s , and the critical shear velocity, u_{*c} , required to initiate movement. Bagnold (1941) observed two threshold shear velocities for wind-blown sand: (1) the critical threshold required for static grains

to begin moving, u_{*c} , and (2) the impact threshold required to maintain particle motion, u_{*i} . Experimental results have shown that $u_{*i} = 0.7u_{*c}$ (Bagnold, 1941; Nishimura and Hunt, 2000).

Although developed for grains settling in water, the equation by Ferguson and Church (2004), as modified by Jerolmack et al. (2006), can be applied to air:

$$w_s = \frac{(s-1)gd^2}{C_1\nu+(0.75C_2(s-1)gd^3)^{1/2}} \quad (3)$$

where $s = \rho_s/\rho_f$ is the relative density of sediment, ρ_s is the sediment density, g is the acceleration due to gravity, d is the grain diameter, ν is kinematic viscosity, and C_1 and C_2 are constants with values of 18 and 1, respectively, for natural sand.

We follow Jerolmack et al. (2006) in adopting the equation by Shao and Lu (2000) for u_{*c} , which is based upon data from Iversen and White (1982) for a range of grain sizes that includes most aeolian sand:

$$u_{*c} = \sqrt{0.0123 \left(sgd + \frac{3 \times 10^{-4} kg/s^2}{\rho_f d} \right)}. \quad (4)$$

The ratio of the grain settling velocity to the fluid shear velocity (w_s/u_*) and the ratio of shear velocity to the critical shear velocity (u_{*i}/u_{*c}) have been used to characterize suspension, saltation, and creep (Bagnold, 1941 & 1966; Laursen, 1958; Smith and Hopkins, 1972; van Rijn, 1984; Nishimura and Hunt, 2000; Shao, 2000; Nino et al., 2003). We follow the method described by Eastwood et al. (in review) to define saltation, suspension, and creep.

Values of w_s/u_* are used to define saltation, suspension, and the gradational transition between these two end members because the downward grain settling velocity must be balanced by the upward turbulent eddies, which generally scales with shear velocity (e.g., Bagnold, 1966; Nino et al., 2003). Fully-developed suspension occurs when a measurable sediment concentration profile has developed:

$$\frac{w_s}{u_*} \leq 1. \quad (5a)$$

All experimental work agrees that the transition from saltation to suspension is well underway in the range of $w_s/u_* = 2.0-2.5$, and we adopt incipient suspension as

$$1 < \frac{w_s}{u_*} \leq 2.5. \quad (5b)$$

Modified saltation would be largely undetectable from saltation in the field, and we combine these modes of transport, using the definition that saltation begins where

$$\frac{w_s}{u_*} \geq 2.5. \quad (5c)$$

There is no definition for creep that relates the suspension and lift forces to the weight of the grain (w_s/u_*), as particles are not lifted not from the bed during creep transport. Instead, creep can be defined as a ratio between the impact shear velocity and the critical shear velocity (u_{*i}/u_{*c}), following the method of Eastwood et al. (in review). Bagnold (1941) and Nishimura and Hunt (2000) experimentally found creep to occur at $0.7u_{*c}$.

$$(0.7 \geq \frac{u_{*i}}{u_{*c}} \geq 1.0) \text{ creep} \quad (6)$$

Given ranges of u_{*i}/u_{*c} and w_s/u_* associated with modes of grain transport, the total grain population traveling over a dune is sorted on the dune lee face as a function of lee surface processes (see section 2.1). Except for the smallest of aeolian dunes, grainfall that accumulates at the base of the lee face is hypothesized to be formed by grains that experienced incipient or full suspension. In contrast, grainflow cross-strata should reflect the total transport range of grains traveling over the dune. Lee ripples reflect tractional reworking of any grains on the lee face, forming on finer-grained grainfall deposits as well as coarser-grained grainflow deposits (See Sections 2.1 and 2.2 in Chapter 2 for additional details).

3. FIELD AREA AND METHODS

3.1 Permian Cedar Mesa Sandstone

This method was tested and developed using the uppermost sequence of the Permian Cedar Mesa Sandstone in SE Utah because of the extensive previous work and excellent outcrop exposures. The Cedar Mesa Sandstone is a member of the Cutler Group of the Paradox foreland basin and is the distal, arid component of a fluvial system draining the Uncompahgre Uplift (Mountney, 2006) (Fig. 3.1). Numerous authors report a consistent cross-strata dip direction to the southeast (Poole, 1962; Loope, 1984; Peterson, 1988; Langford & Chan 1989; Stanesco & Campbell, 1989; Mountney and Jagger, 2004; Mountney, 2006; Langford et al., 2008) and interpret that the wind blew from the northwest (Loope, 1984; Langford & Chan 1989; Stanesco and Campbell, 1989; Mountney and Jagger, 2004; Mountney, 2006; Langford et al., 2008).

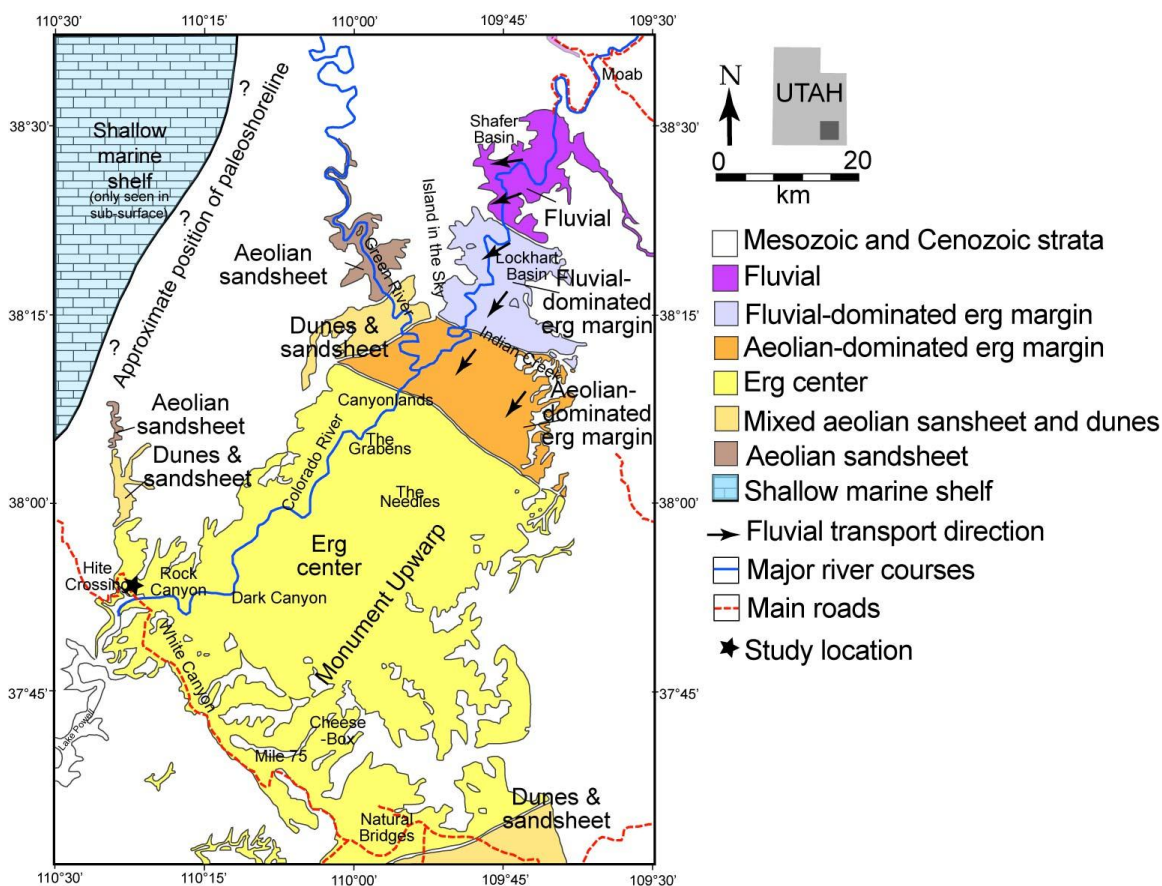


Figure 3.1. Outcrop location map for the Permian Cedar Mesa Sandstone, SE Utah. Field site for this study at Hite Crossing is marked. Modified from Mountney (2006).

The Cedar Mesa Sandstone is an Early Permian (Wolfcampian) succession of wind-blown strata exposed over an area of 8000 km² in SE Utah (Hintze, 1980; Huntoon et al., 1982; Mountney, 2006) (Fig 3.1). The unit consists of vertically-stacked sequences of aeolian deposits, each separated by a distinctive and regional erg-wide supersurface (Loepe, 1985; Mountney, 2006). The Cedar Mesa Sandstone achieves a maximum thickness of 400 m just west of Monument Upwarp but thins to approximately 200 m

near Canyonlands National Park (Stanescio & Campbell, 1989; Blakey, 1996; Nuccio & Condon, 1996; Condon, 1997). The field area for this study is located on Highway 95 at Hite Crossing, between the Colorado and Dirty Devil Rivers. The field site is approximately 1km³ and was chosen because it contains excellent three-dimensional exposures, high quality outcrops, and easily recognizable stratification types.

3.2 Methods

The stratigraphic architecture of 23 set boundaries was surveyed in the field using an Elta-4 Total Station to create a three-dimensional digital elevation model (DEM) of the outcrop (Fig. 3.2). A detailed analysis of the stratification types was conducted within each set including: thickness of individual grain flows, thickness of basal wind ripples, presence and thickness of couplets (wind ripple/grain flow packages), and presence and location of reactivation surfaces. 205 cross-strata dip directions were recorded, paying close attention to the position of each measurement within a set and the stratification type each measurement was recorded from.

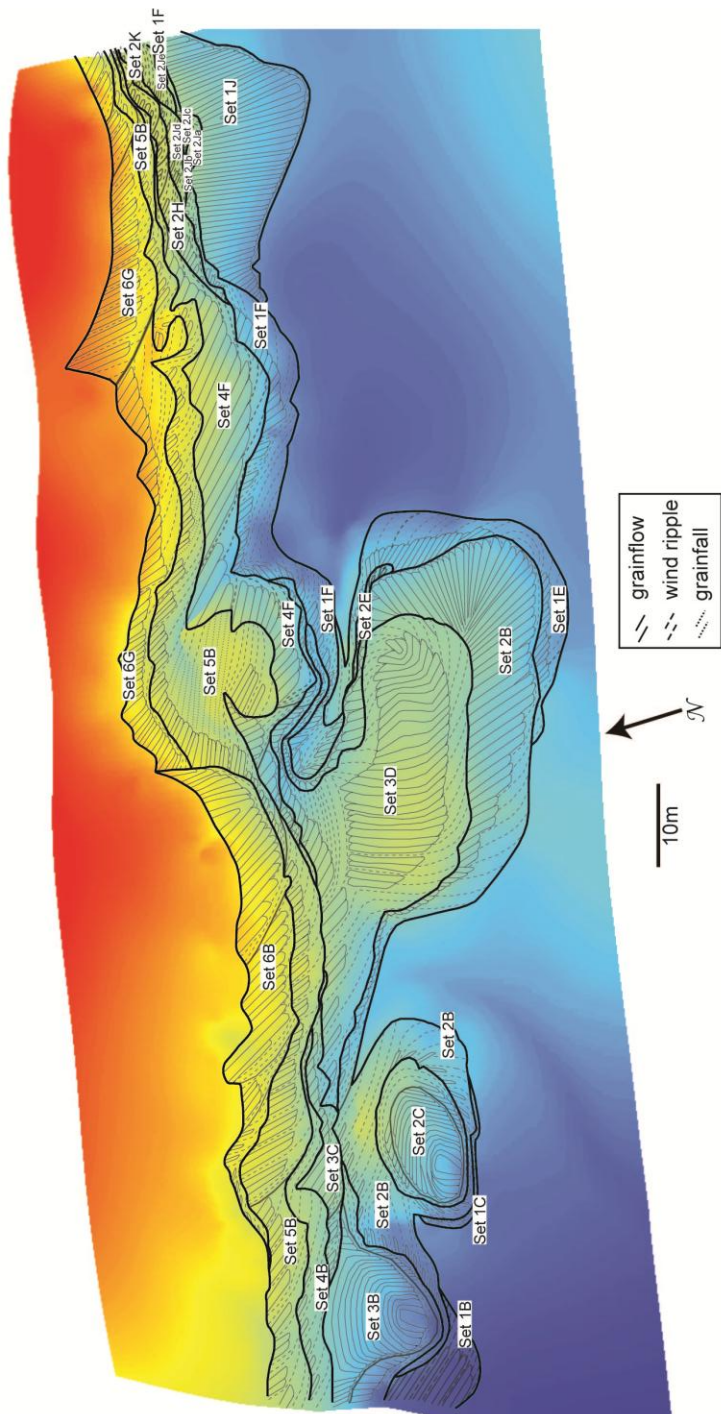


Figure 3.2. Digital Elevation Model (DEM) of outcrop location at Hite Crossing, Utah. DEM was created by surveying in 23 set boundaries at cm. scale resolution across the $\sim 1 \text{ km}^3$ outcrop.

Grain size analysis was completed for 30 samples from the Permian Cedar Mesa Sandstone, from grainfall (4), grainflow (11), and wind ripple (15) deposits. All preserved basal grainfall wedges were sampled. Grainflow deposits were sampled at the toe in order to sample the coarsest grains that collect at the toe of the flow as a result of kinematic sorting. Wind ripples were sampled from locations with well-developed packages at least 2-3 cm thick.

In the lab a Misonix sonicator was used to disaggregate rock samples via cavitation. 10% HCl acid was required to remove carbonate cement from all samples prior to sonication. Grain size analysis was performed using a camsizer by Retsch Technology, which optically measures grain size using two CCD cameras. Grains having a diameter smaller than .032 mm were not measured. Errors in size estimation are negligible compared to sieving over the measured range. Grain-size distributions were generated by measuring grain diameter, d , determined using 50 bins spaced logarithmically over the range 0.032 - 2.5 mm. Complete disaggregation of grains and dissolution of all carbonate cement was confirmed using a binocular reflecting microscope.

4. DATA

4.1 Stratification Types

All arrangements of the stratification types from the 23 sets can be represented by four configurations commonly seen in aeolian deposits (Fig. 3.3) (Kocurek, 1991). Type 1 stratification consists of low-angle wind ripple deposits and is equivalent to Type A (ripple) and Type B (ripple and grainfall) stratification types identified by Eastwood et al.

(in review). Type 2 stratification contains intercalated wind ripple and grainflow deposits with wind ripples that reach to the top of the set and is the same as the Type C (ripple, grainfall, and grainflow) stratification type identified by Eastwood et al. (in review). Note there are two varieties of the Type 2 stratification: one contains clear truncation surfaces with the grainflow deposits bevelled back, the other does not contain truncation surfaces. Type 3 stratification consists of grainflow deposits underlain by a consistent bottomset of wind ripples, and is equivalent to the Type E (grainflow, grainfall, and ripple) stratification type in Eastwood et al. (in review). Type 4 stratification consists of all, or nearly all, grainflow deposits with minor or no wind ripples at the base. A subset of Type 4 stratification consists of grainflow deposits with a basal grainfall wedge. Type 4 is the same as the Type F (grainflow and grainfall) and Type G (grainflow) stratification types of Eastwood et al. (in review). Field examples of the four stratification types are shown in Figure 3.3.

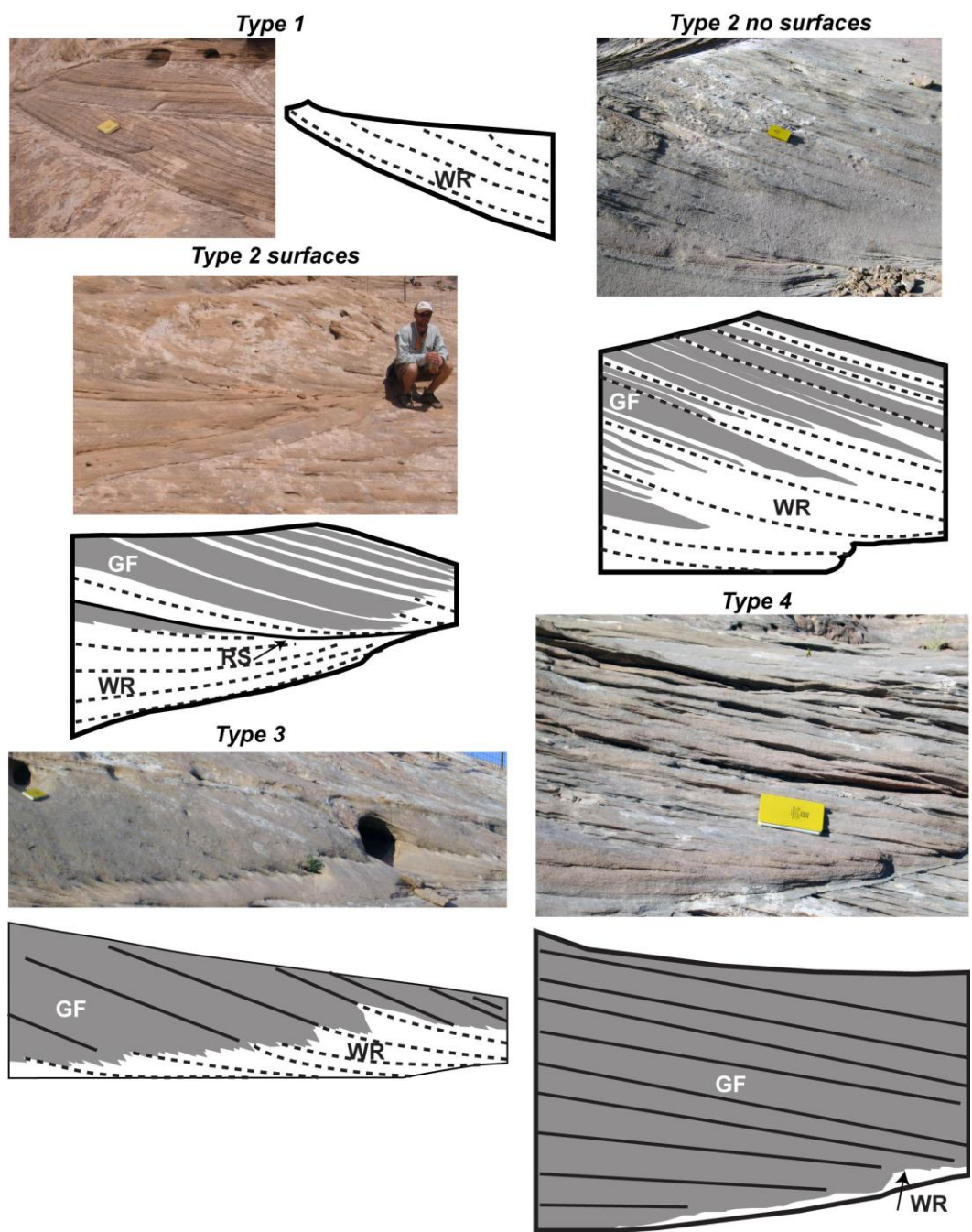


Figure 3.3. Field examples of the four arrangements of stratification types seen in the Permian Cedar Mesa Sandstone at Hite Crossing, Utah. Figure shows stratification types 1-4, with a photograph and sketch of the same location differentiating grainflow and wind ripple deposits. See text for explanation and discussion of stratification types. A 22 cm. long field book and a person are shown for scale.

The cross-strata dip direction and associated stratification types were mapped along each set with accurate spatial relationships and scaling. Cross-strata dip direction was translated into crest orientation, since the maximum dip on the lee face is perpendicular to the dune crest orientation as a result of gravity. All the above data was compiled to reconstruct the bedform shape for each set (Fig. 3.4). Using the principle of gross-bedform normal crest orientation, what wind(s) will satisfy the cross-strata orientations collected in the field?

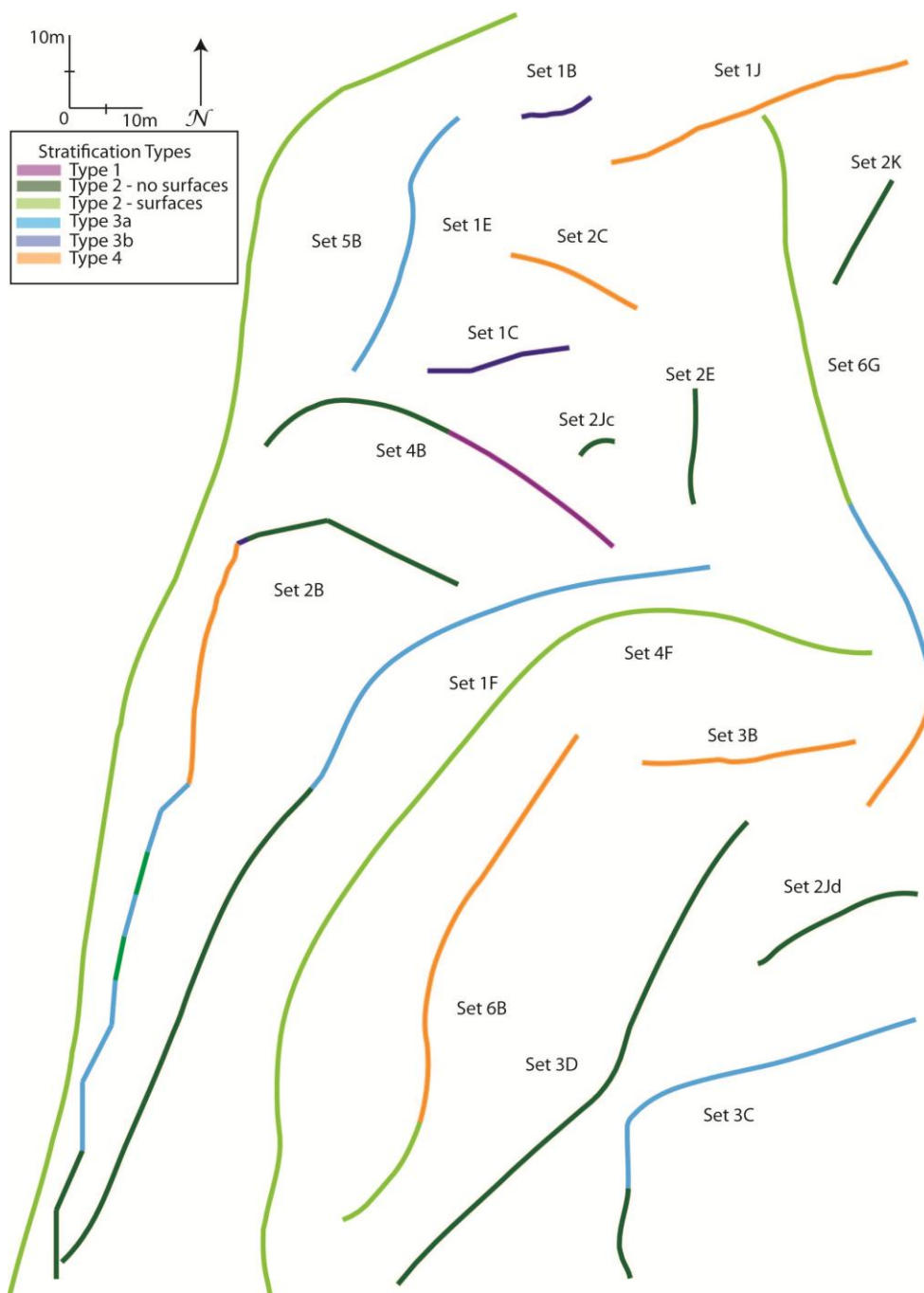


Figure 3.4. Planview bedform reconstruction of 23 sets from the uppermost sequence of the Cedar Mesa Sandstone at Hite Crossing, Utah. All bedforms are scaled and color-coded by stratification type.

Figure 3.5 plots incidence angle vs. thickness of basal wind ripples for the Cedar Mesa data and gives the incidence angles at which maximum basal wind ripples will be produced. The thickest deposits of basal ripples occur in stratification Type 3 at incidence angles ranging from 35°-75°. The maximum thickness of an individual wind ripple package occurs at a 45-55° incident angle.

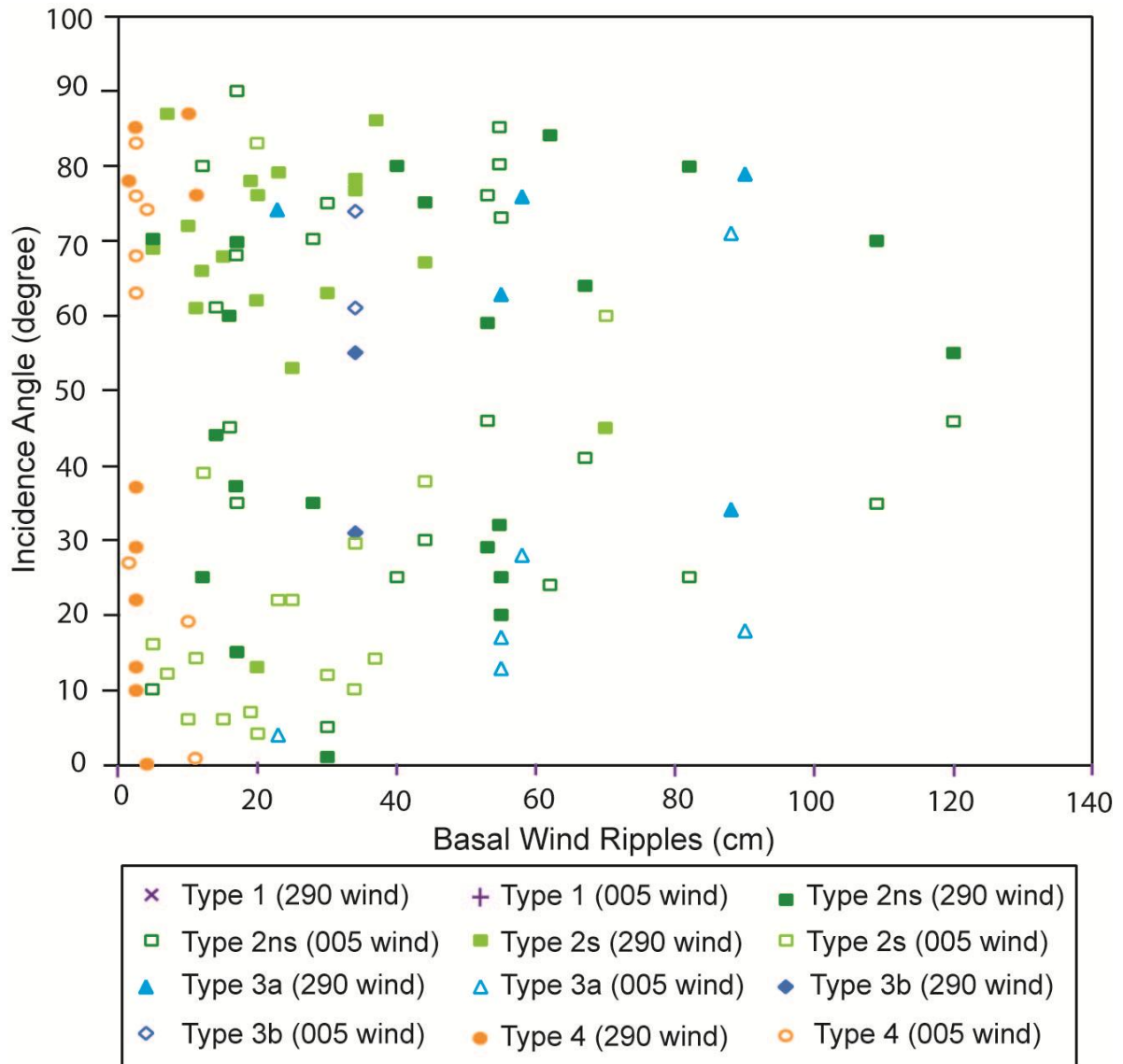


Figure 3.5. Plot showing incidence angle vs. basal wind ripples thickness for the uppermost sequence of the Cedar Mesa Sandstone. Maximum thickness of basal wind ripples occurs at 55° incidence angles, identifying the “sweet spot” for basal wind ripple formation.

4.2. Characterization of the Wind Direction

All 225 crest orientations were plotted on wind roses and color-coded according to stratification types (Fig. 3.6). When the data is separated by stratification type,

different stratification types occur at different crest orientations and have different modes. Given that different crest orientations are associated with specific stratification types, and knowing that these stratification types arise from different secondary flow processes, what wind or winds will satisfy all these crest orientations?

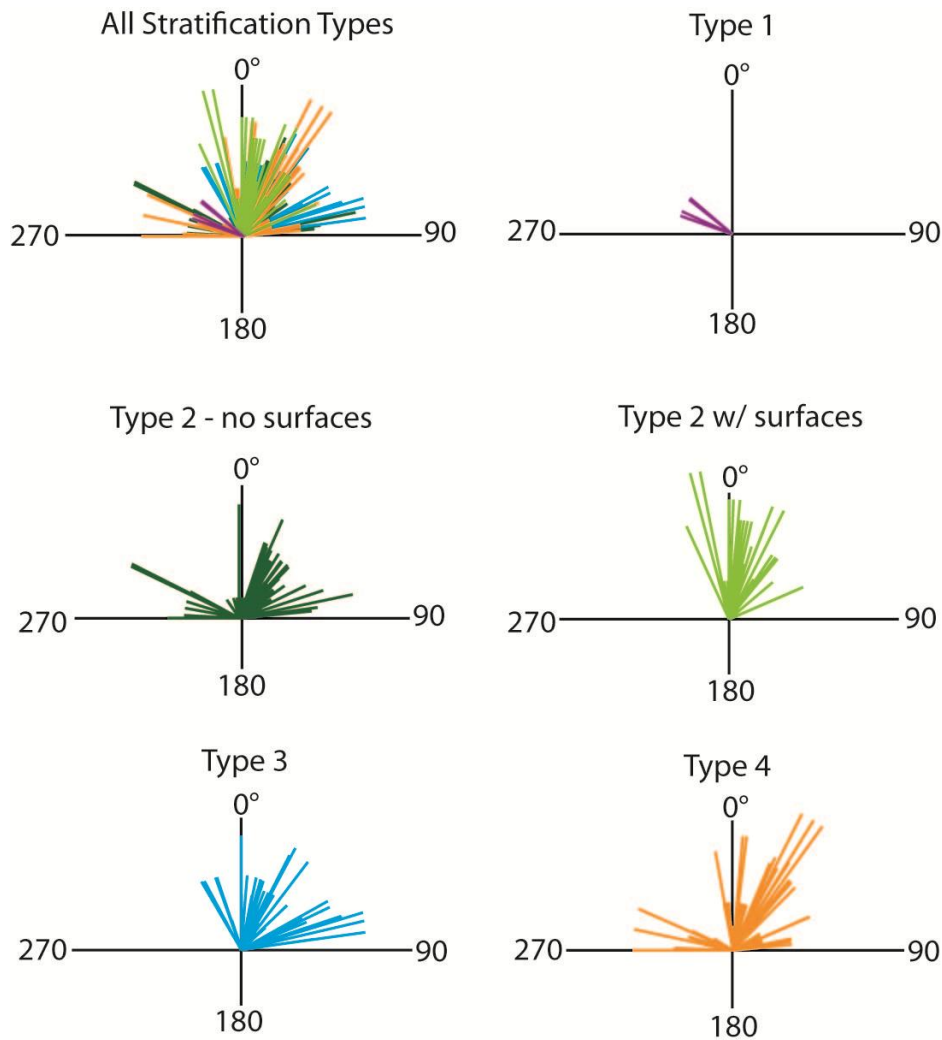


Figure 3.6. Crest orientations calculated from 205 cross-strata dip directions and plotted on wind rose diagrams. Shown plotted together and separated by stratification type. All crest orientations are scaled and color-coded by stratification type.

The first significant conclusion is that no one wind will work. When all the data are evaluated, two winds are identified that will satisfy all sets: one wind from 290° and another from 005°. These two winds produce the southeast net dune migration seen in the cross-strata dip directions. The incidence angles for both wind directions were plotted on scaled set drawings along with crest orientation segments and associated stratification types identified in the field. The proposed incidence angles produce the surface processes and associated stratification types identified in the field and confirm that these winds work for all sets.

The gross-bedform normal equation from Rubin and Hunter (1987) can be used to determine the intensity and/or frequency of two concurrent wind directions,

$$\tan \alpha = \pm R + \frac{|\cos \gamma|}{|\sin \gamma|} \quad (7)$$

where α is the angle of bedform trend (gross-bedform normal orientation), R is the transport ratio between the two wind directions (dominate and subordinate), $R = \frac{D}{S}$, and γ is the divergence angle between the two wind directions. R is positive where the divergence angle, γ , is 90-180° and R is negative where γ is 0-90°. All other angles are positive in a clockwise direction. For any dune field and combination of wind directions, if the two winds are equal in magnitude the resultant vector should exactly bisect the two wind vectors (Fig. 3.7). The resultant vector, defined by α , should equal the net dune migration direction from the cross-strata dip directions. For the Cedar Mesa erg in SE Utah, R must equal 1.6 for the resultant vector to equal the 125° net dune migration

direction measured in the cross-strata dip directions. An R value of 1.6 means that the 290° wind either (1) blew almost twice as frequently as the 005° wind, or (2) blew almost twice as intensely as the 005° wind, with respect to wind velocity.

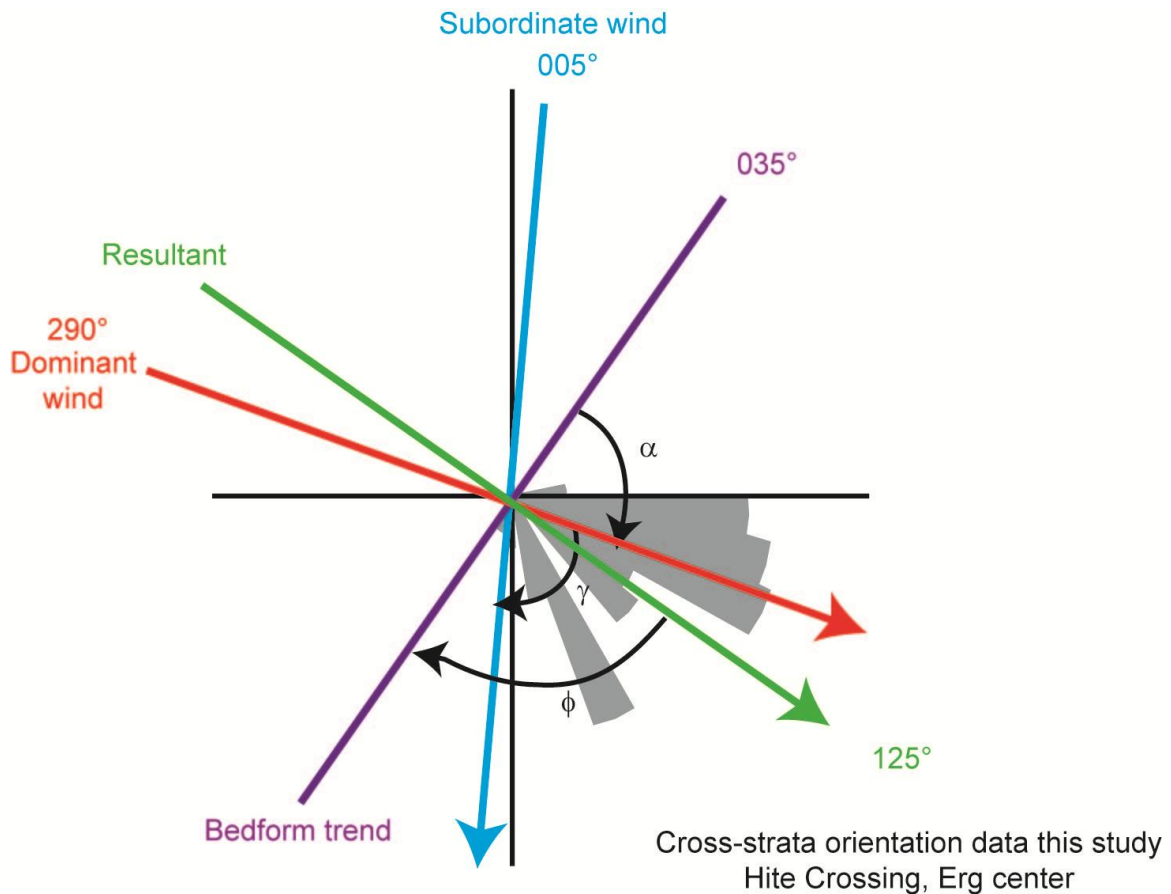


Figure 3.7. Gross-bedform normal wind rose diagram from Rubin and Hunter (1987) for the uppermost sequence of the Cedar Mesa Sandstone showing cross-strata dip directions measured in this study with net migration direction at 125° . D is the dominant wind direction from 290° , S is the subordinate wind direction from 005° . R is the resultant.

4.3 Characterization of the Wind Speed

The sampling of grain size by stratification type (Fig. 3.8) shows that grain size is not uniform on dune lee faces but is sorted by the lee secondary flow and the different surface processes. Grainflow strata represent the total sediment load, containing grains that traveled in suspension, saltation, and creep. Grainfall deposits are enriched in grains that traveled in incipient suspension and depleted in grains that traveled in creep. The composition of ripple deposits is widely variable because ripples may form on and rework any lee deposit where traction transport occurs. Currently, wind speed can be estimated from the grain-size distributions of the different stratification types using well-established empirical relationships for shear stress and modes of transport. Eastwood et al. (in review) provide the following grain sizes to calculate wind speed based on data collected at the White Sands Dune Field: d_{15} for grainfall and d_{10} for grainflow. These are reasonable grain sizes to represent the incipient suspension load for use in Equation 5b. For the creep load, d_{97} is a reasonable grain size to use in Equation 6. All wind speeds reported in the following section are calculated at 10 m above the bed using Equation 2 because 10 m represents the standard height for measuring wind direction and wind speed at weather stations. Weather stations are the most abundant and easily accessible sources of wind direction and wind speed data available to most researchers.

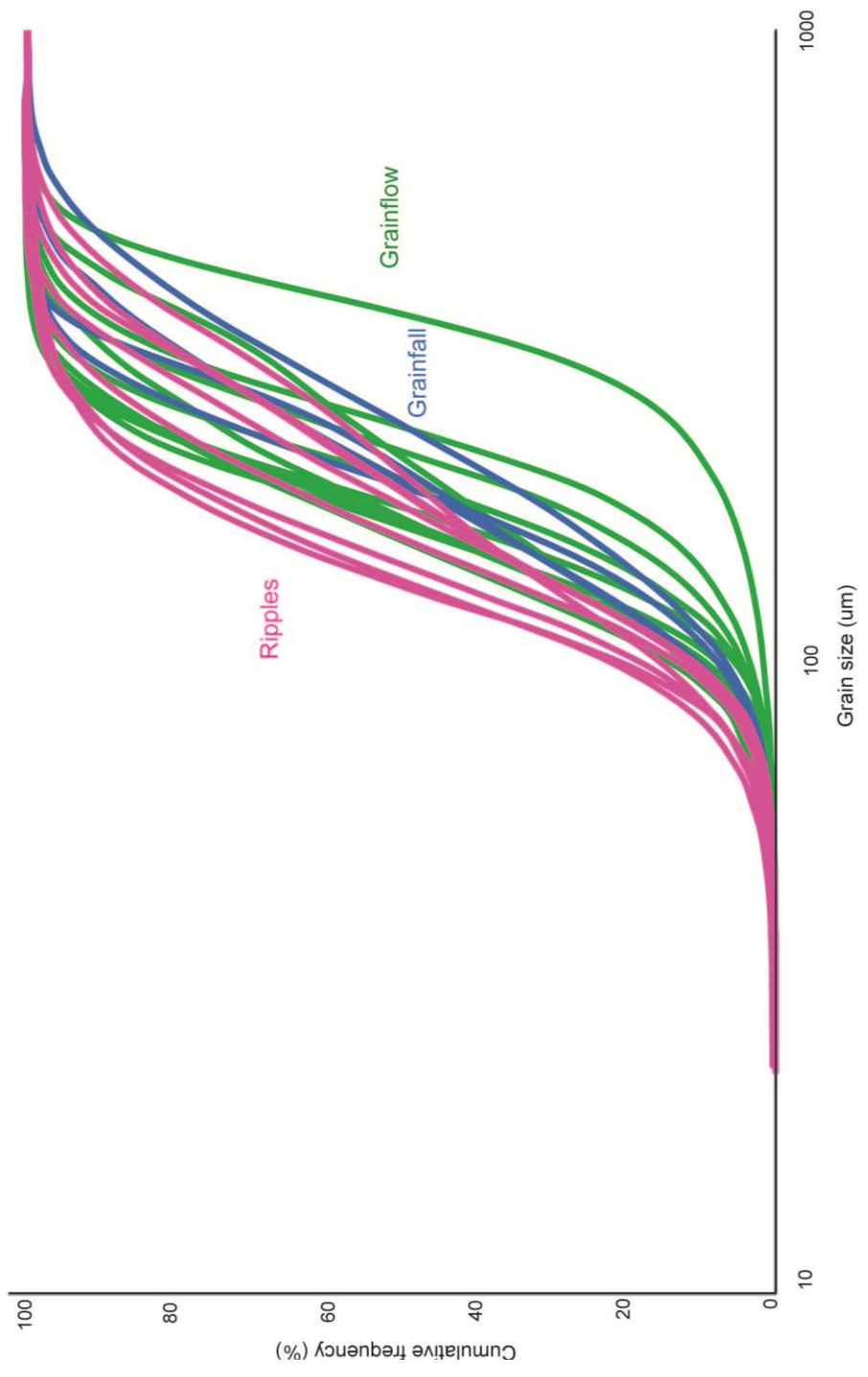


Figure 3.8. Cumulative frequency curves for different stratification styles: grainflow, grainfall and wind ripples.

For the samples taken from the Cedar Mesa Sandstone, the average d_{15} grain size from grainfall cross-strata is 118 μm . The average d_{10} grain size from grainflow cross-strata is 119 μm . The range of grain sizes traveling in incipient suspension from grainfall deposits is 110-128 μm . The range of grain sizes traveling in incipient suspension from grainflow deposits is 92-212 μm . Using Equation 5b, shear velocities range from 0.23-0.88 m/s and can be used in Equation 2 to reconstruct wind speeds ranging from 9.0-11.5 m/s (20.1-25.8 mph) for grainfall deposits, and 6.6-25.1 m/s (14.8-56.3 mph) for grainflow deposits. For the d_{97} creep population from grainflow cross-strata, the range of grain sizes is 303-549 μm . Using Equation 6, shear velocities range from 0.23-0.36 m/s and can be used in Equation 2 to reconstruct wind speeds ranging from 8.1-10.3 m/s (18.1-23.1 mph) for grains in creep. The range of overlapping wind speeds obtained from these three deposits is 20.1-23.1 mph. Jerolmack et al. (2011) used d_{50} to represent the characteristic grain size in saltation, which describes the long-term “formative wind” conditions. A “formative wind” can be calculated for the Cedar Mesa Sandstone and compared to the reconstructed wind speed conditions reported above using the parameters developed by Eastwood et al. (in review) at White Sands. The d_{50} of the Cedar Mesa Sandstone is 223 μm , which results in a $u_{*f} = 0.316$ and a wind speed of 20.3 mph at a height of 10 m above the bed. This “formative wind” speed correlates well with the range of wind speeds obtained using the White Sands parameters.

As noted by Eastwood et al. (in review), for ancient aeolian cross-strata, the grain size percentages associated with incipient suspension and creep from grainfall and grainflow deposits (i.e., d_{15} , d_{10} , and d_{97}) provide a starting point for reconstructing

paleowind speeds. However, several variables may affect the direct exportation of these percentages to the ancient rock record: (1) the mode of grain transport varies with wind speed, (2) the grain-size range within the dune field may be source-limited, and (3) dune height strongly impacts the basal lee-face stratification preserved in the rock record. As a result, reconstructing a range of paleowind speeds by evaluating a range of grain sizes in Equations 5b and 6 may be the most reasonable approach. For a given wind speed, as dune height increases, grainfall becomes increasingly difficult to transport to the base of the lee face. For a given dune height, as wind speed increases, grainfall can consist of coarser grain sizes carried in suspension. During storm conditions, when wind speeds are significantly higher than the normal “formative winds”, it is reasonable to assume that a much larger percentage of the total flow might become entrained in incipient suspension. For example, basal grainfall deposits at the base of a thick set of cross-strata very likely represent storm conditions. In this case, a range of grain sizes (e.g., d_{15} , d_{25} , d_{50} , d_{75} , d_{95}) can be taken as traveling in incipient suspension and evaluated in Equation 5b to reconstruct a range of paleowind speeds. Reconstructed wind speeds from the grainfall deposits can be compared to those for the coarsest (creep) grains (e.g., d_{95} , d_{97} , d_{99}) in contemporaneous grainflow deposits using Equation 6.

One grainflow sample from the Cedar Mesa Sandstone contains a d_{10} of 212 μm that results in a reconstructed wind speed of 56.3 mph, a large discrepancy when compared to the other reconstructed values within the 20-23 mph range. This grainflow deposit is unusually coarse and is located adjacent to a grainfall deposit preserved at the base of a 4 m set of cross-strata whose average individual grainflow is 2.5 cm. For

comparison, a 10 m tall dune at White Sands Dune Field, NM, contains set deposits 0.3-0.5 m thick with average individual grainflows < 0.5 cm thick. The set of cross-strata containing the coarse grainflow in the Cedar Mesa Sandstone is the record left by a dune significantly taller than 10m (Fig. 3.9A), and the grainfall and associated coarse grainflow are interpreted as a wind storm deposit. Under storm conditions, the potential for the percentage of the flow traveling in incipient suspension increases rapidly and use of the d_{15} no longer seems valid. It is likely that a much larger percentage of the total flow was traveling in incipient suspension during the storm event recorded in these deposits. The d_{10} of this unusually coarse grainflow indicates that grains 212 μm in diameter (d_{10}) would be traveling in incipient suspension (i.e., Equation 5b) at 56.3 mph. What percentage of the grainfall grain size distribution, traveling in incipient suspension, will produce a wind speed of 56.3 mph? A grain size of 212 μm will travel at 56.3 mph in incipient suspension, and this grain size occurs at 55% of the flow, i.e. d_{55} . Because grainfall deposits are enriched in suspended material, depleted in creep material, and only 3% of the grainfall travels in creep during normal “formative wind” conditions, it is reasonable to assume that no sediment (or less than 1%) is traveling in creep during a storm that is approximately two times the magnitude of the normal/formative wind speeds.

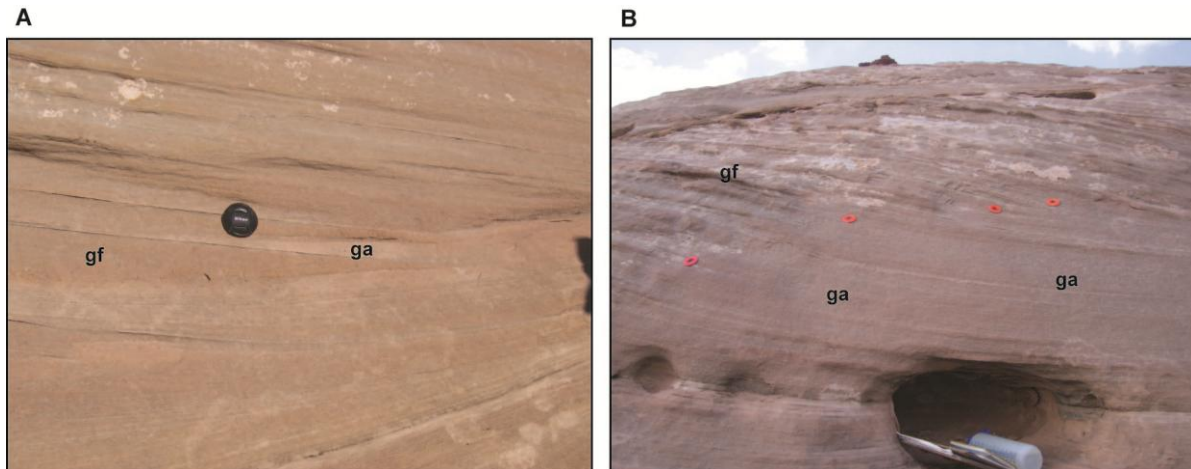


Figure 3.9. Photographs of storm deposits in the rock record represented by grainfall deposits (ga) and unusually thick and/or coarse grainflow deposits (gf). A) Wind storm event #1: unusually coarse grainflow ($d_{50} = 203 \mu\text{m}$) and associated grainfall. Lens cap for scale. B) Wind storm event #2: largest accumulation of grainfall (1.3 m). Individual grainflow toes are marked by washers. Location of unusually thick grainflow deposit (8 cm) is indicated. 1.5 liter water bottle and 4 cm. washers for scale.

The largest accumulation of grainfall identified in the Cedar Mesa is 1.3 m thick. This deposit occurs within a 4.5 m thick set of cross-strata that contains an average individual grainflow thickness of 2.6 cm (Fig. 3.9B). A grainfall deposit of this magnitude preserved at the base of a tall dune indicates a significant storm event. The d_{15} of this grainfall deposit is 128 μm , which gives a wind speed of 11.5 m/s (25.8 mph). This speed is approximately equal to the normal “formative winds” in the Cedar Mesa, but a deposit of this magnitude clearly indicates greater-than-normal wind conditions. If the parameters obtained at White Sands under-represent the wind speeds, what were the wind conditions during the storm event? There are no grainflow deposits directly associated with this second storm event to bracket the storm wind speeds. However, an

unusually thick grainflow (8 cm) is located immediately above the deposit (Fig. 3.9B). Using the parameters from White Sands, the d_{10} of the grainflow deposit is 118 μm , producing a wind speed of 10.1 m/s (22.4 mph), and the d_{97} of the grainflow is 340 μm , which results in an 8.4 m/s (18.8 mph) wind speed. These wind speeds are similar to the “formative winds” predicted for the Cedar Mesa and demonstrate a return to normal wind conditions after the storm event. A range of grain sizes and associated wind speeds are as follows: $d_{15} = 128 \mu\text{m}$, $u_{10} = 11.5 \text{ m/s}$ (25.8 mph), $d_{25} = 158 \mu\text{m}$, $u_{10} = 16.3 \text{ m/s}$ (36.4 mph), $d_{55} = 258 \mu\text{m}$, $u_{10} = 32.9 \text{ m/s}$ (73.6 mph), $d_{75} = 351.9 \mu\text{m}$, $u_{10} = 48.3 \text{ m/s}$ (108 mph), $d_{95} = 571 \mu\text{m}$, $u_{10} = 78.9 \text{ m/s}$ (176.4 mph). The d_{55} of the grainfall from the first storm event produced the correct wind speed, so applying the same percentage of the flow to incipient suspension and using the d_{55} of the grainfall from the second storm event seems reasonable. Using this assumption results in the interpretation that the 1.3 m thick grainfall deposit is the product of 32.9 m/s (73.6 mph) storm winds. Although the precise wind speed cannot be reconstructed, a grainfall deposit of this magnitude would certainly require winds greater than 35 mph and would represent more than 25% of the total flow (i.e., $> d_{25}$).

5. DATA ANALYSIS

5.1 Wind Regime Recorded in Cross-Strata

All crest orientations for Type 4, Type 3, and both varieties of Type 2 stratification are plotted on a rose diagram (Fig. 3.10). Crest orientations are color-coded by stratification type to interpret each stratification type and to determine the incidence angles at which these different stratification types occur. Crest orientations from Type 1

stratification are a product of the 005° wind, are longitudinal to the 290° wind, and represent alongslope basal wind ripples. However, orientation information obtained from Type 1 stratification will not be considered in the remainder of this paper as it is impossible to confirm whether these wind ripples represent a unique stratification type or are simply the truncated remnants of Type 3 stratification. Crest orientations between 0-40° are shared by all stratification types, with incidence angles ranging from 70-90° for the 290° wind and from 0-35° for the 005° wind. Removing these common crest orientations and evaluating the remaining data highlights the differences between these stratification types.

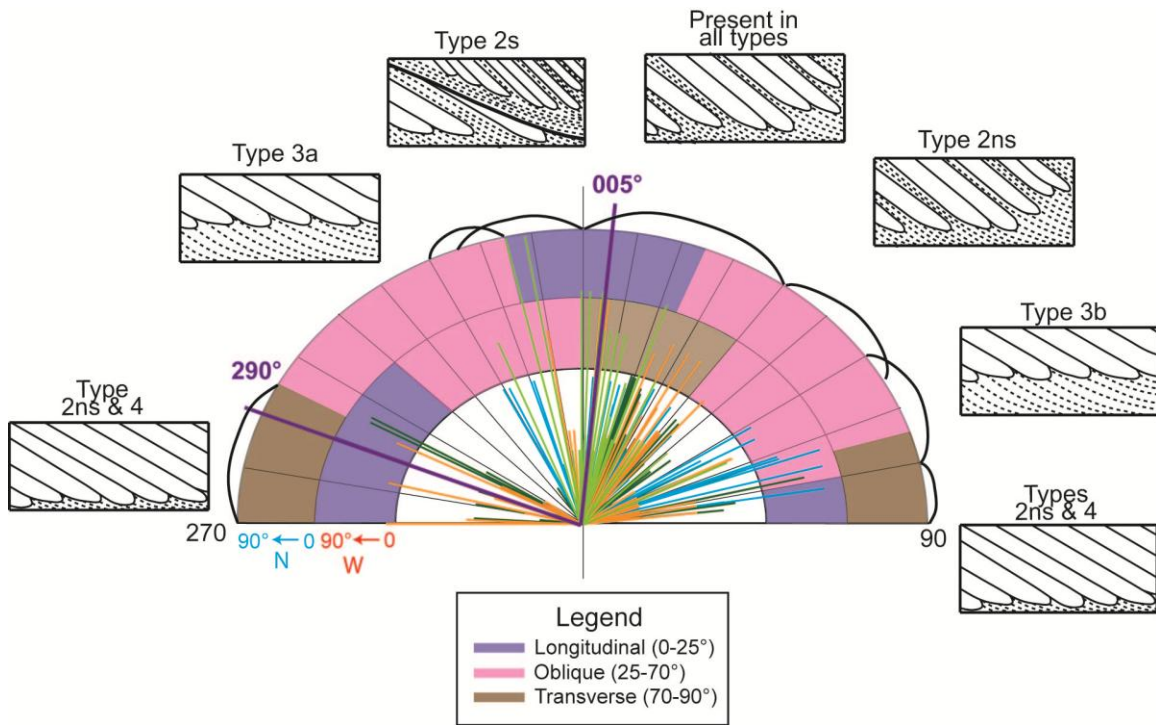


Figure 3.10. All crest orientations from the uppermost sequence of the Cedar Mesa Sandstone plotted on a wind rose diagram. Each crest orientation is scaled and color-coded by stratification type. Wind directions 290° and 005° are plotted, along with orientation of erosional reactivation surfaces. The wind rose diagram is segregated into erosional (0-15°), longitudinal (15-25°), oblique (25-65°), and transverse (65-90°) sections for the 005° wind (inner diagram) and the 290° wind (outer diagram).

Two varieties of Type 2 stratification result from the alternation of both wind regimes, with the transverse (290°) wind producing grainflow and the longitudinal or oblique (005°) wind producing wind ripples or an erosional reactivation surface. The difference between the varieties of Type 2 stratification is that with one variety, the 005° wind is more longitudinal to the bedforms and creates a truncation surface as opposed to a package of wind ripples. Type 2-surface (2s) bedforms are mainly oriented towards the north, which results in incidence angles that are longitudinal to the 005° wind and transverse to highly-oblique for the 290° wind. Type 2-non-surface (2ns) bedforms are oriented more towards the east and west, which results in incidence angles that are oblique to the 005° wind but still transverse to highly-oblique for the 290° wind. Two varieties of Type 3 stratification occur when bedforms are permanently oblique to both wind regimes (Type 3b), or oblique to one wind and oblique-longitudinal with the second wind (Type 3a). The occurrence of highly-oblique incidence angles for both wind directions ($45\text{-}60^\circ$) coincides with the range of incidence angles required to produce maximum thicknesses of basal wind ripples (Fig. 3.5), and Type 3 stratification contains the thickest deposits of basal wind ripples. Type 4 stratification contains deposits from a permanently transverse wind regime, with bedforms oriented transverse to one wind and longitudinal to the second wind. Transverse grainflow deposits in Type 4 are produced by both the 290° wind and the 005° wind. A subset of Type 4 stratification containing a basal grainfall wedge has been interpreted as the product of the 290° wind.

Type 2ns and Type 4 stratification can be found within south- and east-migrating dunes, while Type 2s and Type 3a&b stratification can only be found in east-migrating

dunes. Type 2ns and Type 4 stratifications share similar crest orientations; however, slight differences in these crest orientations control how far grainflow deposits reach towards the set base, and how high wind ripple deposits reach towards the set top. Type 2s stratification composes the majority of bedform crests oriented 0-20°. These crest orientations are permanently longitudinal to the 005° wind, resulting in abundant erosional reactivation surfaces within the Type 2s strata that is not seen elsewhere. Type 3a and 3b stratification are similar to Type 4 stratification; however, Type 3a&b stratification contain greater than 15 cm of basal wind ripples, while Type 4 stratification contains less than 15 cm. The difference between Type 3 and Type 4 stratification may also be a function of relative wind speed and/or dune size. Transverse grainflow deposits will reach further towards the dune base with relatively stronger winds and/or relatively smaller dunes.

5.2 Redefining Incidence Angle

Natural breaks in the crest orientation data within each stratification type (Fig. 3.10) are very similar to the ranges of incident angles responsible for producing different surface processes and stratification styles identified by Eastwood et al. (in review). Incidence angles between 65° and 90° produce grainflow. Grainflow is produced when the gravity load is greater than the traction load or at any time when the sediment flux over the dune crest is high. Wind ripples are produced for the range of incidence angles between 25° and 65° by tractional sediment transport. Longitudinal or bypass events occur when minimal wind ripples are produced (≤ 15 cm basal wind ripples) and the incidence angle is between 15° and 25°. Reactivation surfaces are typically overlain by

wind ripple deposits and underlain by grainflow deposits that have been truncated. The strike of erosional reactivation surfaces has been plotted in Figure 3.10. Erosional reactivation surfaces occur within 15° of both the 005° and the 290° wind, indicating that incidence angles between 0° and 15° are erosional, while depositional events occur at all incidence angles greater than 15° . These results coincide well with those in Eastwood et al. (in review), whose findings indicate that erosion occurs at incidence angles up to 13° , bypass occurs at angles between 13° and 26° , and deposition occurs at angles greater than 26° . The main difference between this work and that of Eastwood et al. (in review) is that grainflow and wind ripples preserved in the rock record occur over a narrower range of incidence angles than in modern dune fields. In modern fields, stratification can be observed at incidence angles between 0 and 25° ; however, this stratification is likely to be eroded and not preserved in the rock record.

Erosional reactivation surfaces were not identified in stratification types 3 and 4. However, one of the following explanations is likely: (1) even bevelling across the lee face will not produce an obvious truncation surface; (2) oblique bevelling, at an angle such that few or no grainflow deposits are truncated will not produce an obvious truncation surface; (3) reactivation surfaces occur between adjacent grainflow deposits, making them extremely difficult to identify in the field within Type 2, 3, or 4 stratification; or (4) tall dunes are less impacted by a change in the wind direction; as the eddy in the separation cell grows, it is unable to maintain momentum and grainflows without truncation surfaces are deposited.

5.3 Predicting Stratification Type

An ideal bedform is drawn in Figure 3.11, which identifies what processes are operating on the lee face for different ranges of incidence angles, given the results above and those from Eastwood et al (in review). These results are used to predict the stratification type that will develop based on the dune crest orientation and the primary wind directions. Outcrop wall panels from the Cedar Mesa Sandstone that contain multiple stratification types within a single set can be drawn on this ideal dune and used to test these predictions. The interpreted winds, 290° and 005°, give the correct aerodynamic configuration on the lee face to produce the distribution of stratification types seen in the field.

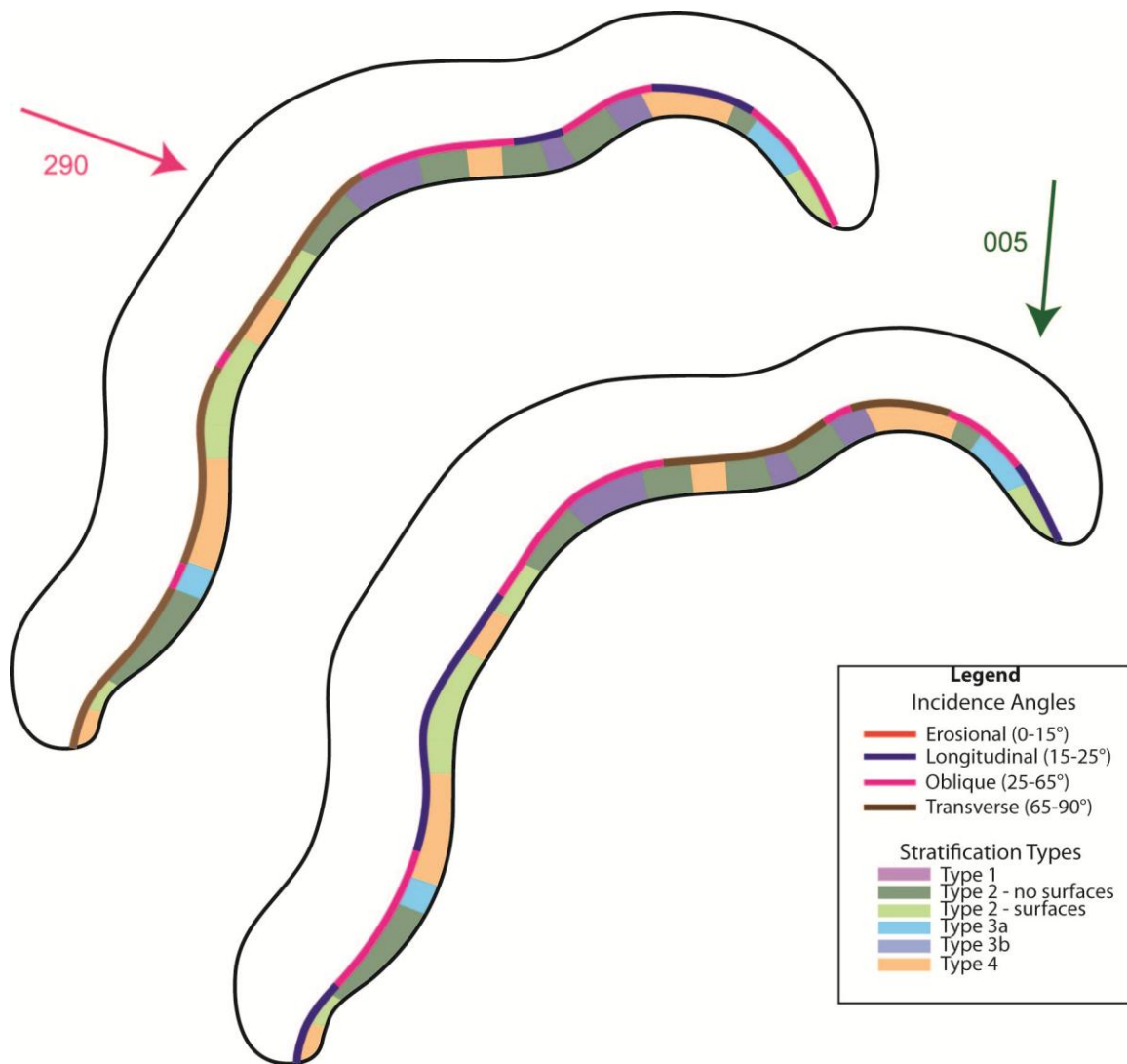


Figure 3.11. Ideal bedform for the Cedar Mesa Sandstone, predicting the stratification type that will develop at all crest orientations (360-90° northern hemisphere). Bedform is a real dune taken from LiDAR data of White Sands Dune Field, New Mexico and rotated to achieve the SE net migration direction seen in the Cedar Mesa Sandstone.

6. APPLICATION TO PALEOCLIMATE RECONSTRUCTIONS

Understanding the Pangean Permian icehouse climate is particularly useful because the steep temperature gradient between the equator and the poles during the Permian was

similar to today's temperate gradient (Patzkowski et al., 1991). Paleowind directions inferred from the dune migration directions in Peterson's (1988) dataset have been used to validate global circulation models for the Pangean supercontinent (Parrish and Peterson, 1988; Patzkowsky et al., 1991; Loope et al., 2004; Rowe et al., 2007). Pangean paleogeographic reconstructions, using paleomagnetic poles from igneous rocks, indicate a steady northward migration of the supercontinent from Permian (5°N) through Early Jurassic times (18°N) (Scotese, 1979 & 2003; Ziegler et al., 1997).

Parrish and Peterson (1988) used the paleogeography results obtained from Scotese (1979) and Early Permian (Wolfcampian) aeolian net migration direction data from Peterson (1988) to interpret global circulation models for the Colorado Plateau region. They interpret the dominant summer winds as monsoonal north-westerlies from a low-pressure cell in the paleocean to the northwest. Permian winter winds are interpreted as north-easterlies from a subtropical high-pressure cell to the northeast. These interpretations are supported by Dubiel et al. (1991), and Loope et al. (2001). Loope et al. (2004) used detrital hematite paleomagnetism from Steiner (2003) to say that the Colorado Plateau region remains near-equatorial through the Jurassic, as opposed to moving northward as Scotese (1979 & 2003) and Ziegler et al. (1997) have proposed. Loope et al. (2004) interpret the dominant summer winds as north-easterly trade winds that seasonally shift to tropical north-westerlies south of the equator. Kent and Tauxe (2005) showed that this alternate method of determining paleomagnetism using sedimentary rocks frequently underestimates paleolatitudes because it cannot account for sediment compaction. Rowe et al. (2007) interpreted the average Permian cross-strata dip

directions from Peterson (1988) as representing two different circulation belts within Pangea's monsoonal system. The northern portion of the Colorado Plateau records north-easterly trade winds that curve to become tropical westerlies south of the equator. While this interpretation is plausible for the near-equatorial Permian location of the Colorado Plateau, it does not hold for the Jurassic location at 18° N.

Reconstructed winds for the Permian Cedar Mesa Sandstone interpreted in this study, 290° (westerlies) and 005° (northerlies), have been reconstructed based on modern paleogeography and compass orientations. When the wind patterns obtained from global circulation models of Parrish and Peterson (1988) are compared to this study and corrected to modern-day orientations, the dominant summer monsoonal north-westerlies become westerlies and the winter subtropical north-easterlies become northerlies. Therefore, the global circulation model results of Parrish and Peterson (1988) are more accurate paleoclimate reconstructions for the Permian Colorado Plateau than those proposed by Loope et al. (2004) and Rowe et al. (2007). Loope et al. (2004) and Rowe et al. (2007) discount the widely-accepted paleolatitude information in order to fit the data to their model of seasonally-shifting circulation belts across the equator, without considering that the reconstructed paleowinds (average dip direction from aeolian cross-strata) could be the inaccurate data.

7. CONCLUSIONS

Two wind directions have been interpreted from the uppermost sequence of the Permian Cedar Mesa Sandstone near Hite, Utah; one direction of wind from 290° and one direction from 005°. For all 23 sets measured, the stratification type identified in the field

correlates with the incidence angle produced by these two winds. The gross-bedform normal resultant, or translation direction, is the net dune migration direction calculated from cross-strata dip directions measured in the field (305/125°), confirming that these two wind directions are correct. Reconstruction of wind speeds yield the “formative winds” most responsible for dune construction (20.1-23.1 mph), and two wind storms were recognized. Both storm events were a product of the west wind (290°), indicating that the west wind (290°) blew more intensely than the north wind (005°).

This study uses parameters from aeolian cross-strata deposits along with new methodology developed by Eastwood et al. (in review) regarding incidence angle and lee-face surface processes in sophisticated ways to reconstruct the paleowind direction. This methodology allows for quantification of the incidence angles corresponding to maximum obliquity and maximum thickness of basal wind ripples and erosional reactivation surfaces, and confirms the range of incidence angles over which grainflow and wind ripple stratification form and are preserved in the rock record. This method sets a new standard for producing specific and accurate paleowind reconstructions from aeolian cross-strata that can be used to interpret past climates, predict stratification types, and validate paleoclimate models.

8. MATHEMATICAL NOTATION

τ = boundary shear stress

w_s = settling or terminal fall velocity of a grain

u_* = mean shear velocity or strength of the wind

u_{*c} = critical shear stress/velocity required to initiate grain motion

u_{*i} = impact shear stress/velocity required to sustain grain motion

ρ_f = density of a fluid

ρ_s = density of sediment

$s = \rho_s/\rho_f$, ratio of sediment to fluid densities

g = gravitational force, 9.81 m/s^2

d = grain diameter

C_1 = theoretical constant (equal to 18 for typical sand grains)

C_2 = constant asymptotic value of the drag coefficient (equal to 1 for typical natural grains)

ν = kinematic viscosity

κ = von Karman's constant, value = 0.4

z = elevation above bed, in m

z_0 = roughness parameter, value = 1.05×10^{-4} for this study

u_z = time-averaged velocity at height z above the bed

α = angle of bedform trend (gross-bedform normal crest orientation)

D = dominant wind direction

S = subordinate wind direction

R = transport ratio between 2 wind directions

γ = divergence angle between 2 wind directions

9. REFERENCES

- Allen, J.R.L. (1982). *Sedimentary Structures: Their character and physical basis*, Volume 2: Amsterdam, Elsevier, 663 p.
- Bagnold, R. A., (1941). *The Physics of Blown Sand and Desert Dunes*. Methuen, New York.
- Bishop, S.R., Momiji, H., Carretero-Gonzalez, R. and Warren, A. (2002). Modeling Desert Dune Fields Based on Discrete Dynamics. *Discrete Dynamics in Nature and Society* 7: 7-17.
- Blakey, R.C. (1996). Permian eolian deposits, sequences and sequence boundaries, Colorado Plateau. In: *Paleozoic Systems of the Rocky Mountain Region* (Eds M.W. Longman and S.D. Sonnenfeld), pp. 405–426. Rocky Mountain Section SEPM (Society for Sedimentary Geology), Denver, CO.
- Condon, S.M. (1997) Geology of the Pennsylvanian and Permian Cutler Group and Permian Kaibab Limestone in the Paradox Basin, Southeastern Utah and Southwestern Colorado. U.S. Geol. Surv. Bull., 2000-P, 46 pp.
- Clemmensen, L.B., and K. Abrahamsen (1983), Aeolian stratification and facies association in desert sediments, Arran basin (Permian), Scotland. *Sedimentology* 30: 311-339.
- Curry, J.R., (1956). The analysis of two-dimensional orientation data. *Journal of Geology* 64: 117-131.
- Dott, R.H. and Roshardt, M.A. (1972). Analysis of Cross Stratification Orientation in the St. Peter Sandstone in Southwestern Wisconsin. *GSA Bulletin* 83: 2589-2596.
- Dott, R.H., Byers et al., C.W., Fielder, G.W., Stenzel, S.R., and Winfree, K.E. (1986). Aeolian to marine transition in Cambro-Ordovician cratonic sheet sandstone of the northern Mississippi valley, U.S.A. *Sedimentology* 33: 345-367.
- Dubiel, R.F., Parrish, J.T., Parrish, J.M. and Good, S.C. (1991). The Pangean megamonsoon: evidence from the Upper Triassic Chinle Formation. *Palaios* 6: 347-370.
- Eastwood, E.N., Kocurek, G., Mohrig, D. and T. Swanson (in review). A refined method for extracting wind direction and speed from aeolian cross-strata. *J. Geophys. Res.*
- Ferguson, R.I., and Church, M. (2004). A simple universal equation for grain setline velocity. *J. Sediment. Res.* 74: 933-937.
- Hintze, L.F. (1980) Geologic Map of Utah. Utah Geological and Mineral Survey, scale 1:500000.

- Howard, A.D. (1977). Effect of slope on the threshold of motion and its application to orientation of wind ripples. *GSA Bulletin* 88: 853-856.
- Hunter, R.E. (1977). Basic types of stratification in small eolian dunes. *Sedimentology* 24: 361-387.
- Hunter, R.E., and Rubin, D.M., (1983). Interpreting cyclic crossbedding, with an example from the Navajo Sandstone. in Brookfield ME, Ahlbrandt TS eds. *Developments in Sedimentology: Eolian Sediments and Processes* 38: 429-454.
- Huntoon, P.W., Billingsley, G.H., Jr and Breed, W.J. (1982) Geologic Map of Canyonlands National Park and Vicinity, Utah. The Canyonlands Natural History Association, scale 1:62000.
- Iverson, J.D. and B.R. White (1982). Saltation threshold on Earth, Mars, and Venus. *Sedimentology* 29: 111-119.
- Jerolmack, D.J., Mohrig, D., Grotzinger, J.P., Fike, D.A., and Watters, W.A. (2006), Spatial grain size sorting in eolian ripples and estimation of wind conditions on planetary surfaces: Application to Meridiani Planum, Mars: *Journal of Geophysical Research* 111: E03S90, doi:10.1029/2005JE002544.
- Jerolmack, D., M. Reitz, and R. Martin (2011), Sorting out abrasion in a gypsum dune field, *J. Geophys. Res.* 116: F02003, doi:10.1029/2010JF001821.
- Kent, D.V., and Tauxe, L., (2005). *Science* 307: 240.
- Kocurek, G., (1991). Interpretation of ancient eolian sand dunes. *Ann. Rev. Earth & Plan. Sci.* 19: 43-75.
- Kocurek, G., Knight, J., and Havholm, K.G., (1991). Outcrop and semi-regional three-dimensional architecture and reconstruction of a portion of the eolian Page Sandstone (Jurassic). *SEPM Concepts in Sedimentology and Paleontology* 3: 25-43.
- Langford, R.P., and Chan, M.A., (1989). Fluvial-aeolian interactions 2. Ancient Systems. *Sedimentology* 36: 1037-1051.
- Langford, R.P, Pearson, K.M., Duncan, K.A., Tatum, D.M., Adams, L., and Depret, P., (2008). Eolian topography as a control on deposition incorporating lessons from modern dunes seas: Permian Cedar Mesa Sandstone, SE Utah, U.S.A. *J. Sedim. Res.* 78: DOI: 10.2110/jsr.2008.045.
- Loope, D.B., (1984). Eolian origin of upper Paleozoic sandstone, southeastern Utah. *Journal of Sedim. Pet.* 54: 563-580.

- Loope, D.B., (1985). Episodic deposition and preservation of eolian sands – a late Paleozoic example from southeastern Utah. *Geology* 13: 73-76.
- Loope, D.B., Rowe, C.M., and Joeckel, R.M., (2001). Annual monsoon rains recorded by Jurassic dunes. *Nature* 412: 64.
- Loope, D.B., Steiner, M.B., and Rowe, C.M., (2004). Tropical westerlies over Pangean sand seas. *Sedimentology* 51: 315-322.
- Mountney, N.P., (2006). Periodic accumulation and destruction of aeolian erg sequences in the Permian Cedar Mesa Sandstone, White Canyon, southern Utah, USA. *Sedimentology* 53: 789-823.
- Mountney, N.P., and Jagger, A., (2004). Stratigraphic evolution of an aeolian erg margin system: the Permian Cedar Mesa Sandstone, SE Utah, USA. *Sedimentology* 51: 713-743.
- Nickling, W.G., McKenna Neuman, C. And N. Lancaster, (2002). Grainfall processes in the lee of transverse dunes, Silver Peak, Nevada. *Sedimentology* 49: 191-209.
- Nino, Y., F. Lopez, and M. Garcia (2003), Threshold for particle entrainment into suspension, *Sedimentology* 50: 247-263.
- Nishimura, K., and J.C.R. Hunt (2000), Saltation and incipient suspension above a flat particle bed below a turbulent boundary layer, *J. Fluid Mech.* 417: 77-102, doi:10.1017/S0022112000001014.
- Nuccio, V.F. and Condon, S.M. (1996) Burial and thermal history of the Paradox Basin, Utah and Colorado, and the petroleum potential of the Middle Pennsylvanian Paradox Formation. *U.S. Geol. Surv. Bull.* 2000-O: 41 pp.
- Parrish, J.T., and Peterson, F., (1988). Wind directions predicted from global circulation models and wind directions determined from eolian sandstones of the western United States – a comparison. *in: Kocurek, G. ed. Sedimentary Geology* 56: 261-282.
- Patzkowsky, M.E., Smith, L.H., Markwich, P.J., Engberts, C.J., and Gyllenhall, E.D. (1991). Application of the Fujita-Ziegler paleoclimatic model: Early Permian and Late Cretaceous examples. *Palaeogeog., Palaeoclim., Palaeoeco.* 86: 67-85.
- Peterson, F., (1988). Pennsylvanian to Jurassic eolian transportation systems in the western United States *in: Kocurek, G. ed. Sedimentary Geology* 56: 207-260.
- Poole, F.G., (1962). Wind directions in late Paleozoic to middle Mesozoic time on the Colorado Plateau. *U.S. Geol. Surv., Prof. Pap., 450-D: D147-D151.*
- Reiche, P., (1938). An analysis of cross-lamination, the Coconino Sandstone. *Journal of Geology* 46: 905-932.

- Rowe, C.M., Loope, D.B., Oglesby, R.J., Van der Voo, R., and Broadwater, C.E., (2007). Inconsistencies between Pangean reconstructions and basic climate controls. *Science* 318: 1284-1286.
- Rubin, D.M., and Hunter, R.E., (1987). Bedform alignment in directionally varying flows. *Science* 237: 276-278.
- Rubin, D.M., and Ikeda, H., (1990). Flume experiments on the alignment of transverse, oblique, and longitudinal dunes in directionally varying flows. *Sedimentology* 37: 673-684.
- Scherer, C.M.S. and K. Goldberg (2010). Cyclic cross-bedding in the eolian dunes of the Sergi Formation (Upper Jurassic), Reconcavo Basin: Inferences about the wind regime. *Palaeogeog., Palaeoclim., Palaeoeco* 296: 13-110.
- Scotese, C.R., Bambach, R.K., Barton, C., Van der Voo, R., and Ziegler, A.M., (1979). Paleozoic base maps. *J. Geol.* 87: 217-277.
- Scotese, C.R. (2003). PALEOMAP, Earth, History, Jurassic. URL <http://www.scotese.com/Jurassic.htm> (November 2008).
- Shao, Y. and H. Lu, 2000: A simplified expression for threshold friction velocity. *J. Geophys. Res.* 105: 22,437-22,443.
- Stanescio, J.D., and Campbell, J.A., (1989). Eolian and non-eolian facies of the Lower Permian Cedar Mesa Sandstone Member of the Cutler Formation, southeastern Utah. *U.S. Geol. Surv. Bull.* 1800-F.
- Steiner, M.B., (2003). A cratonic Middle Jurassic paleopole: Callovian-Oxfordian stillstand (J-2 cusp), rotation of the Colorado Plateau, and Jurassic North American apparent polar wander. *Tectonics* 22: 1020. doi:10.1029/2001TC001284
- Sweet, M.L., and Kocurek, G., (1990). An empirical model of aeolian dune lee-face air-flow. *Sedimentology* 37: 1023-1038.
- Tanner, W.F., (1965). Upper Jurassic paleogeography of the Four Corners region. *J. Sedim. Pet.* 35: 534-574.
- Tsoar H. (1983). Dynamic processes acting on a longitudinal (seif) sand dune. *Sedimentology* 30: 567-578.
- Walker, I.J., and Nickling, W.G., (2003). Simulation and measurement of surface shear stress over isolated and closely spaced transverse dunes in a wind tunnel. *Earth Surf. Proc. and Landf.* 28: 1111-1124.

- Werner, B.T. (1995). Eolian dunes: Computer simulations and attractor interpretation. *Geology* 23: 1107-1110.
- Werner, B.T. and Kocurek, G. (1997). Bedform dynamics: Does the tail wag the dog? *Geology* 25: 727-730.
- Ziegler, A.M., Hulver, M.L., and Rowley, D.B. (1997). Permian world topography and climate. In Martini, I.P. ed. *Late glacial and postglacial environmental changes: Pleistocene, Carboniferous-Permian, and Proterozoic*. Oxford, Oxford University Press: 111-146.

Chapter 4: Modelling Controls on Aeolian Dune-Field Pattern Evolution

ABSTRACT

A second-generation, source-to-sink cellular automaton-based model presented here captures and quantifies many of the factors controlling the evolution of aeolian dune-field patterns by varying only a small number of parameters. The role of sediment supply, sediment availability and transport capacity (together defined as sediment state) in the development and evolution of an aeolian dune-field pattern over long time scales is quantified from model simulations. Seven dune-field patterns can be classified from simulation results varying the sediment supply and transport capacity that control the type and frequency of dune interactions, the sediment availability of the system and, ultimately, the development of dune-field patterns. This model allows predictions to be made about the range of sediment supply and wind strengths required to produce the dune-field patterns seen in the real world. A new clustered dune-field pattern is identified from model results and used to propose an alternative mechanism for the formation of superimposed dunes. Bedforms are hypothesized to cluster together, simultaneously forming two spatial scales of bedforms without first developing a large basal dune with small superimposed dunes. Manipulation of boundary conditions produces evolving dune fields with different spatial configurations of sediment supply. Trends of spacing and crest length increase with decreasing variability as the dune field matures. This simple model is a valuable tool which can be used to elucidate the dominant control of aeolian sediment state on the construction and evolution of aeolian dune-field patterns.

1. INTRODUCTION

Aeolian dune fields exhibit some of the most striking and varied patterns on Earth and other planets. Because these patterns typically form over thousands of years, they are a record of climatic and geomorphic conditions. These records, however, are relatively under-utilized because of the inherent difficulties in extracting environmental information from geomorphic features. In order to extract information about climatic change and landscape evolution from aeolian dune fields, one must understand both the dune-field pattern development and its sensitivity to changes in environmental forcing. The environmental parameters that impact an evolving dune-field pattern are the boundary conditions of the system, as defined by Ewing and Kocurek (2010). One set of boundary conditions that impacts all dune fields is the sediment state of the system, which consists of the sediment supply, sediment availability, and transport capacity of the wind (Kocurek and Lancaster, 1999). Other well known boundary conditions include wind directionality, grain size, water-table height, and antecedent dune topography. Less explored boundary conditions include the geometry of the sediment source and the areal limits of the dune field (Ewing and Kocurek, 2010).

Although dune-field pattern characterization using satellite imagery (e.g., Ewing et al., 2006; Wilkins and Ford, 2007; Derickson et al., 2008; Dong et al., 2008) and time-series images (e.g., Ewing and Kocurek, in press; del Valle et al., 2008) provide snapshots of pattern evolution, the time range of pattern evolution in dune fields typically precludes direct observation. Recent studies have begun to connect sediment transport to

surface topography (Duran et al., 2009), but it remains difficult to collect direct measurements over long time frames. Numerical models, however, provide a tool that simulates the acceleration of time, permitting rapid investigations of multiple potential evolutions for a dune field.

In this paper, we present a simple second-generation cellular automaton (CA)-based source-to-sink model that incorporates temporal and spatial scales to simulate aeolian dune-field development through self-organization. This new model gives us insight into the controlling factors on aeolian systems by changing a small number of parameters that relate to the sediment state of the system and the configuration of the sand-source area. Results are in agreement with previous work (Ewing and Kocurek, 2010) that demonstrated source-area geometry strongly impacts dune-field pattern development. Quantification of the components of sediment state (sediment supply, availability, transport capacity of the wind) allows for their sensitivity testing in the model, yielding insights into their respective roles in basic dune-field configurations.

2. METHODS

2.1 Model Description

We simulate dune-field dynamics using a CA-based model adapted from the Werner (1995) algorithm. The Werner model successfully simulates barchan, crescentic, linear and star dunes as a function of sediment supply and wind-regime complexity. The algorithm is non-dimensional: simulated topography may represent ripples or dunes (Baas, 2007). Although our model is also non-dimensional, we chose model parameters, including sediment jump length, that more closely approximate dunes than ripples.

The model space is divided into a map grid of cells that contain stacks of sediment slabs (Fig. 4.1). As in the Werner (1995) model, our model consists of three simple, physically-based rules. The first rule governs erosion and subsequent deposition of slabs for sediment slab transport. Under this rule, a grid cell is randomly selected. The top slab either erodes or stays in place according to an erosion probability (P_e). If eroded, the slab moves downwind a constant transport length ℓ (Fig. 4.1). At the new location, the slab is deposited or remobilized according to the deposition probability (P_d). If the slab under transport is not deposited, it moves downwind another distance ℓ and the process is repeated. Unlike the erosion probability, the deposition probability varies from cell to cell. Bare cells have a lower probability of deposition than cells with sediment slabs. This rule mimics the tendency for grains to deposit when they land on sandy surfaces, since energy is dissipated upon impact with other grains (Bagnold, 1941). Different bedform topography forms under different sediment fluxes, and we assume the probability of deposition is proportional to sediment flux. The second rule forces deposition on the leeward side of bedforms within flow separation cells. Any slab transported into a shadow zone in the lee of a bedform, where the topographic slope is $\leq 15^\circ$, is automatically deposited ($P_e=0$ and $P_d=1$) (Fig. 4.1). In the third rule, the angle of repose is enforced through avalanches in the direction of steepest descent (Fig. 4.1). For further discussion of the applications of the rules within the algorithm, see Werner (1995), Baas (2002), and Nield and Baas (2008).

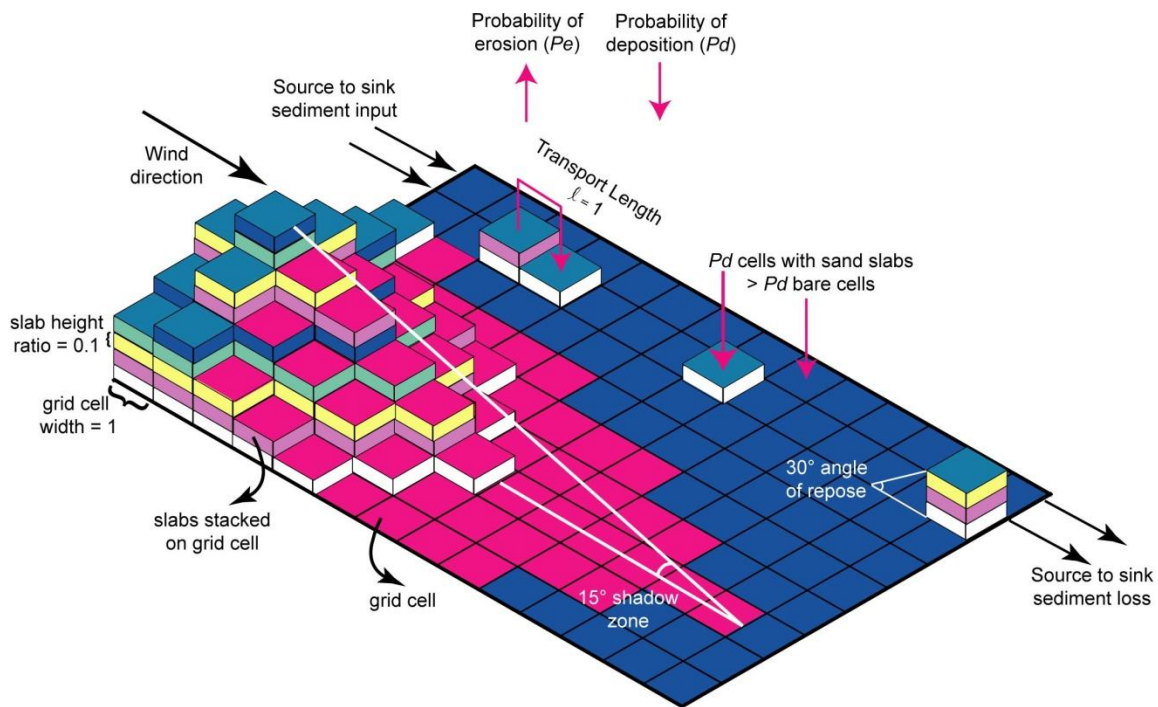


Figure 4.1. Schematic diagram of cellular model space. Sediment transport, flow separation, and avalanching rules used in algorithm are illustrated, as well as the source-to-sink sediment transport capability. Modified from Baas (1996).

Grid cells are randomly selected for erosion/deposition of slabs until the total number of grid cells in the model space has been selected, completing a single iteration. The process then repeats for a specified number of iterations. Following the definitions of Nield and Baas (2008), we select cells for erosion *without* replacement. This method randomly selects every cell once, and only once, per iteration, as opposed to selecting *with* replacement, which allows a slab at the same grid cell to be selected for transport multiple times within one iteration. It is important to note that the duration of one iteration is still much shorter than the characteristic time scales of dune formation, but it

is much larger than the characteristic time scale of individual sand-grain dynamics (Nishimori et al., 1998).

In order to understand the spatial and temporal evolution of dune fields, we modify Werner's model in two ways. First, Werner (1995) used a transport length of $\ell = 6$ grid cells, which resulted in reduced interactions by allowing moving slabs to jump over existing dunes. This second-generation model uses a transport length of $\ell = 1$ grid cell to ensure that moving slabs interact with all bedform topography. Second, the original Werner algorithm used periodic boundaries to simulate an internal sediment source and the conservation and recycling of sediment. The implication is that Werner's bedform topography repeats spatially; when a bedform migrates off the downwind edge of the model space it is immediately re-introduced along the upwind border. This innovative source-to-sink sediment transport adaption enables the exploration of variable sediment supply and non-periodic boundaries to explore diverse landscape patterns that vary in both time and space. Our second-generation model more accurately simulates the evolution of real-world dune fields because fresh sediment enters the model space along the upwind border and bedforms that migrate off the downwind edge of the model space are not re-introduced along the upwind edge.

2.2 Simulated Sediment State

Aeolian sediment state can be quantified by calculating the sediment supply, sediment availability, and the transport capacity of the wind, providing an instantaneous snapshot of the evolution of an individual dune field (Kocurek and Lancaster, 1999). Sediment supply is the sediment used to create the dune field. Transport capacity

represents the maximum amount of sediment that can be entrained for a given wind strength. Sediment availability is a measure of the availability of the sediment to entrainment by the wind, and is the dimensionless percentage of the dune-field surface covered by grains that can be entrained. In nature factors such as vegetation, surface moisture, armoring or cementation commonly limit entrainment. In this model, where there are no surface-limiting factors, sediment availability represents the specific case where the amount of sediment on the surface at any given time is a function of the sediment supply and transport capacity. In the model, therefore, at any one time it is the combination of the rate at which sediment is supplied to the surface (i.e., sediment supply) and the rate at which it is transported across the model space (i.e., transport capacity) that determines the amount of sediment available on the surface for dune construction (i.e., sediment availability). Not addressed in this study is accumulation, which requires the vertical stacking of dune deposits over time (Kocurek, 1999; Mounney and Russell, 2009).

Here we use model parameters that represent each of these real-world variables to quantify the simulated sediment state throughout the development and evolution of modeled dune fields. All three sediment state components can be calculated for each iteration. The sediment supply within each simulation is represented by the sprinkle density, defined as:

$$\rho_{sprinkle} = \frac{\# \text{ slabs added per iteration}}{\text{sprinkle area}} \quad (1)$$

where the sprinkle area determines the number of deposition cells along the downwind and lateral axes of the model space. For all simulations presented here, the downwind axis of the sprinkle area has been held constant to ensure that the sprinkle density can be equated to the sediment influx. Given the definition of one iteration within the algorithm, there is always a maximum volume of entrained slabs per iteration (equal to the total number of cells in the model space), but each entrained slab has a different displacement owing to the stochastic transport process. The mean path length (d_s), or average displacement of a single cell during one erosion/deposition event, is:

$$d_s = \frac{\ell}{P_d} \quad (2)$$

as defined by Nield and Baas (2008). The sediment flux over a perfectly flat surface, q_{\max} , is a measure of the transport capacity or potential transport rate of the wind and is defined by:

$$q_{(\max)} = \frac{P_e \cdot h_s \cdot \ell}{P_d \cdot I} \quad (3)$$

where P_e is the pre-defined probability of erosion parameter (default value is 1.0), h_s is the slab height ratio (default value is 0.1 of the cell width), and I is the length of time represented by one iteration (Baas, 1996; Nield and Baas, 2008). In the model the sediment availability, q_{avail} , can be best described by:

$$q_{(avail)} = \frac{\text{\# cells covered by slab(s)}}{\text{total \# cells over which migration has occurred}} \quad (4)$$

where the percentage of the surface covered by slabs is normalized by the extent of the downwind bedform migration. The only sediment influx within simulations occurs externally along the upwind border (source-to-sink sediment transport). We assume all slabs on the model surface are available for transport (i.e., when the sediment supply goes to zero, the availability goes to zero). All the sand within a dune is considered in transport, including sand temporarily trapped in a shadow zone.

2.3 Simulated Source-Area Geometry

The sediment supply can be manipulated by changing the source-area geometry (i.e., the configuration of the sediment influx to the system) by specifying the model boundary conditions and sediment-input distribution. Three types of source-area geometries have been recognized by Ewing and Kocurek (2010) and are simulated here: (1) a point source where sediment influx to the system occurs through a narrow wind gap (e.g., Siakhkikh Sands Dune Field, Afghanistan); (2) a line source, such as a beach (e.g., Guerrero Negro, Mexico); and (3) a plane source where a pre-existing source is mobilized for aeolian conditions (e.g., Taklimakan, China). Point and line sources were simulated using an external sediment source (source-to-sink sediment transport) and by providing a constant, contemporaneous sediment supply to the model space. Sediment can accumulate within the model space, creating a stored supply that can be reactivated as a lagged influx under favorable sediment availability and transport conditions (see Kocurek and Lancaster, 1999). The plane source was modeled using an internal sediment source (periodic boundaries) using sediment previously stored within the model space as a lagged sediment influx.

Following Ewing et al. (2006), basic measurable pattern parameters of crest spacing and crest length have been shown to be a viable approach to pattern analysis (e.g., Beveridge et al., 2006; Ewing et al., 2006; Derickson et al., 2008). Crest spacing is the distance between dune crests as measured in the net transport direction, whereas crest length is the distance along the crest between defects or dune terminations. Simulation results are used to investigate the trends of spacing and crest length through time for different source-area geometries using spacing and crest length metrics similar to those used by Ewing et al. (2006). Multiple time slices were analyzed to record the evolution of each dune-field pattern. Five transects were measured across each simulated time slice to calculate the spacing. Crest length was calculated for each dune that intersected a transect drawn through the center of each time slice. The spacing between each pair of dune crests, plus all crest lengths, were measured and plotted as a function of the distance from the upwind edge of the model space.

3. RESULTS AND DISCUSSION

3.1 Simulated Bedforms

Our simple CA-based model has produced simulated bedforms and dune-field patterns that are similar in shape to real-world bedforms and dune-field patterns (Fig. 4.2). Barchans and crescentic dunes have been simulated before with similar models (e.g. Werner, 1995; Bishop et al., 2002; Baas, 2002; Nield and Baas, 2008). However, our adapted algorithm has generated new shapes, examples of which can be found in real world dune-fields on Earth and Mars (Fig. 4.2). The dune-field patterns associated with these new shapes are discussed later in the Simulated Patterns section.

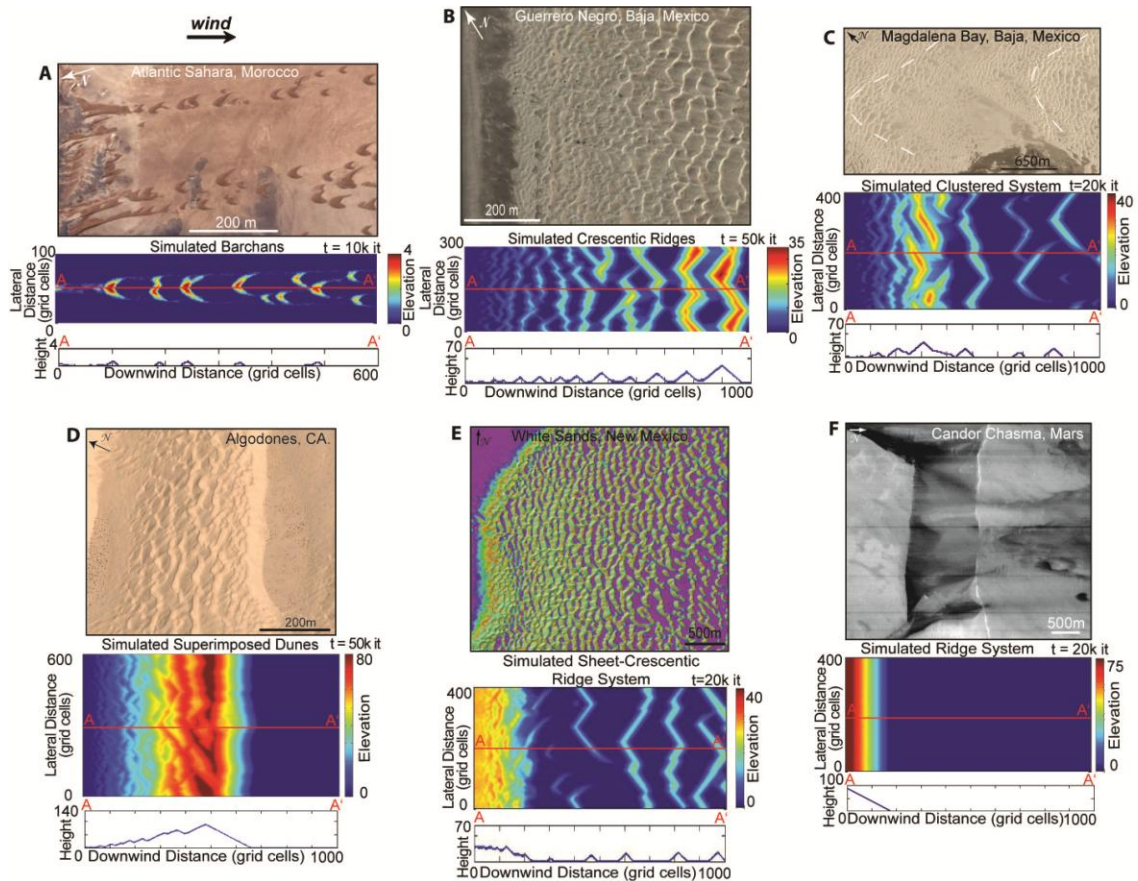


Figure 4.2. Examples of simulated and real-world dune-fields showing similar shapes and dune-field patterns. Sediment transport is from left to right in each image. All images from Google Earth unless otherwise noted. (A) Simulated barchans and barchans from the Atlantic Sahara, Morocco ($27^{\circ}47'N$, $12^{\circ}41'W$). (B) Simulated crescentic ridges and crescentic ridges from Guerrero Negro, Baja, Mexico ($27^{\circ}51'N$, $114^{\circ}18'W$). (C) Simulated clustered pattern and clustered pattern from Magdalena Bay, Baja, Mexico ($24^{\circ}48'N$, $112^{\circ}14'W$). (D) Simulated superimposed dunes and superimposed dunes from the Algodones Dune Field, California ($32^{\circ}47'N$, $114^{\circ}56'W$). (E) Simulated sheet-crescentic ridge pattern and a sheet-crescentic ridge pattern from the White Sands Dune Field, New Mexico, LiDAR image ($32^{\circ}48'N$, $106^{\circ}16'W$). (F) Simulated ridge pattern or falling dune and falling dune from Candor Chasma, Mars. MOC image E03-00746 ($7.01^{\circ}S$, $72.69^{\circ}W$), modified from Bourke et al. 2004.

3.2 Source-Area Geometries

3.2.1 Point and Line Sources

The evolution of transverse point and line source patterns occurs spatially as dunes grow, migrate, and increase in size over time (Figs 4.3A to C and 4.4A to C). Modeling results allow examination of the trends of spacing and crest length vs. migration distance as a function of simulation time. Point and line source areas both show an increase in spacing and crest length with distance in the transport direction (Figs 4.3D to E and 4.4D to E).

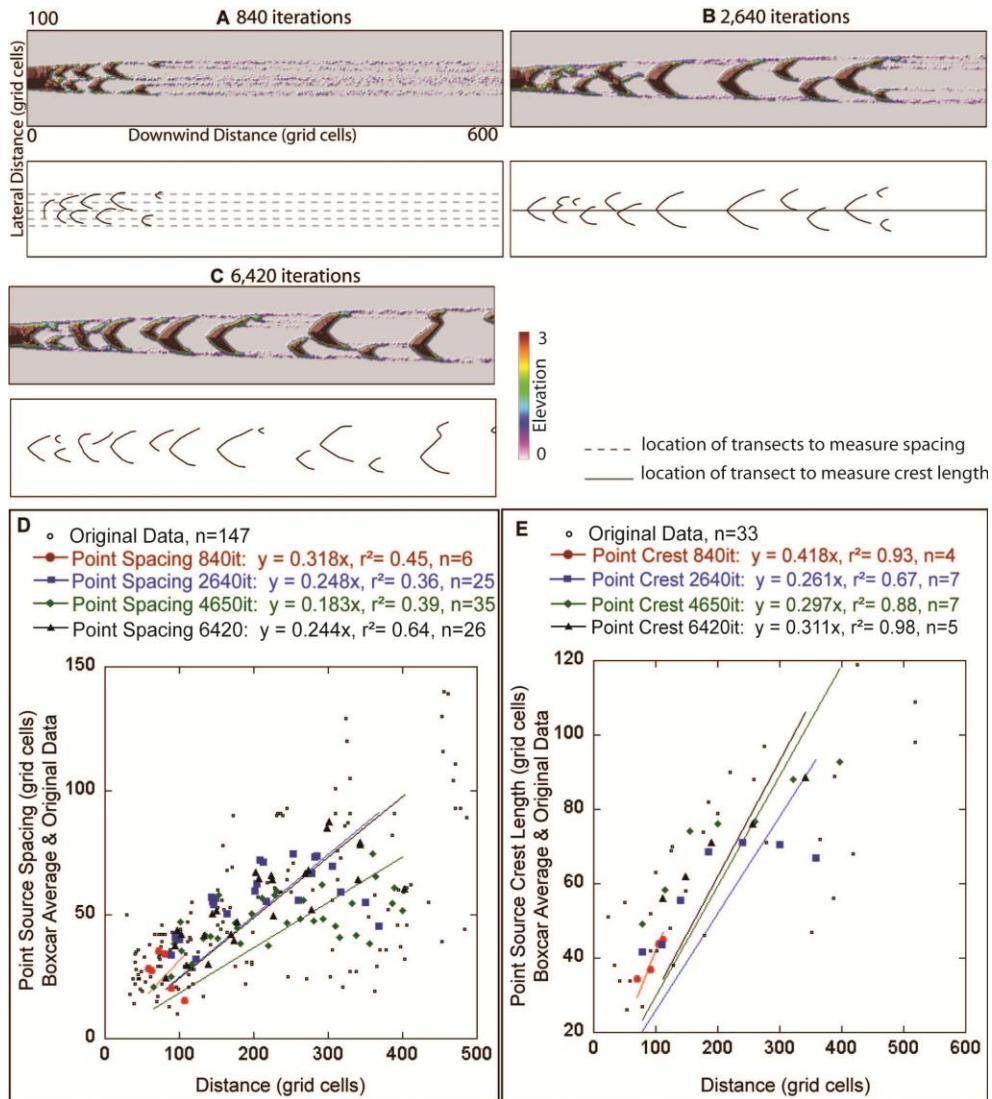


Figure 4.3. Simulation of transverse point source-area geometry over 5000 iterations. Images (A) to (C) include landscape patterns and tracings of dune crest lines at multiple time slices, illustrating the evolution of the dune field. (A) Landscape after 840 iterations and the location of the 5 equally-spaced transects used in each time slice to calculate the spacing vs. distance values in plot D. (B) Landscape after 2640 iterations and the location of the single transect through the dune field center, used to calculate the crest length vs. distance values in plot E. (C) Landscape after 6420 iterations. (D) Plots of spacing vs. distance for each time slice. (E) Plot of crest length vs. distance for each time slice. The linear regression coefficients (r^2 values) for each time slice and the number of data used are listed along the top portion of the graph. Data were smoothed using a boxcar average with a bin size of 4.

With respect to spacing, regression slope coefficients range from 0.18 to 0.32 over the 5,000 iterations of dune-field development for point sources (Fig. 4.3D), and these coefficients range from 0.24 to 0.26 over the 20,000 iterations of dune-field development for line sources (Fig. 4.4D). Spacing increases at a similar rate through time for both point and line sources. Variability exists in the spacing vs. distance measurements and is a result of the creation of new defects (i.e., dune terminations) and bedforms from dune interactions. For example, small barchans can be shed from the horns of another larger barchan, resulting in small spacing values. These interactions can happen at any location within the dune field in both point and line sources, disrupting the trend of increased spacing with distance across the dune field. The variability of the spacing vs. distance measurements decreases with increasing development time, as evidenced by higher r^2 values for most time periods (Figs 4.3D and 4.4D). This is likely indicative of a decrease in the frequency of dune interactions as the dune-field pattern matures and stabilizes.

Model results for crest length, both over time and with migration distance, show a trend similar to that of spacing (Figs 4.3E and 4.4E). Regression slope coefficients range from 0.26-0.42 throughout the 5000 iterations of dune-field development for point sources (Fig. 4.3E), and slope coefficients range from 0.66-0.98 throughout the 20,000 iterations of line-source dune-field construction (Fig. 4.4E). Crest length increases with distance at a greater rate for line sources than point sources. Both source-area geometries

show a general decrease in the variability of crest length measurements with increasing development time (Figs 4.3E and 4.4E).

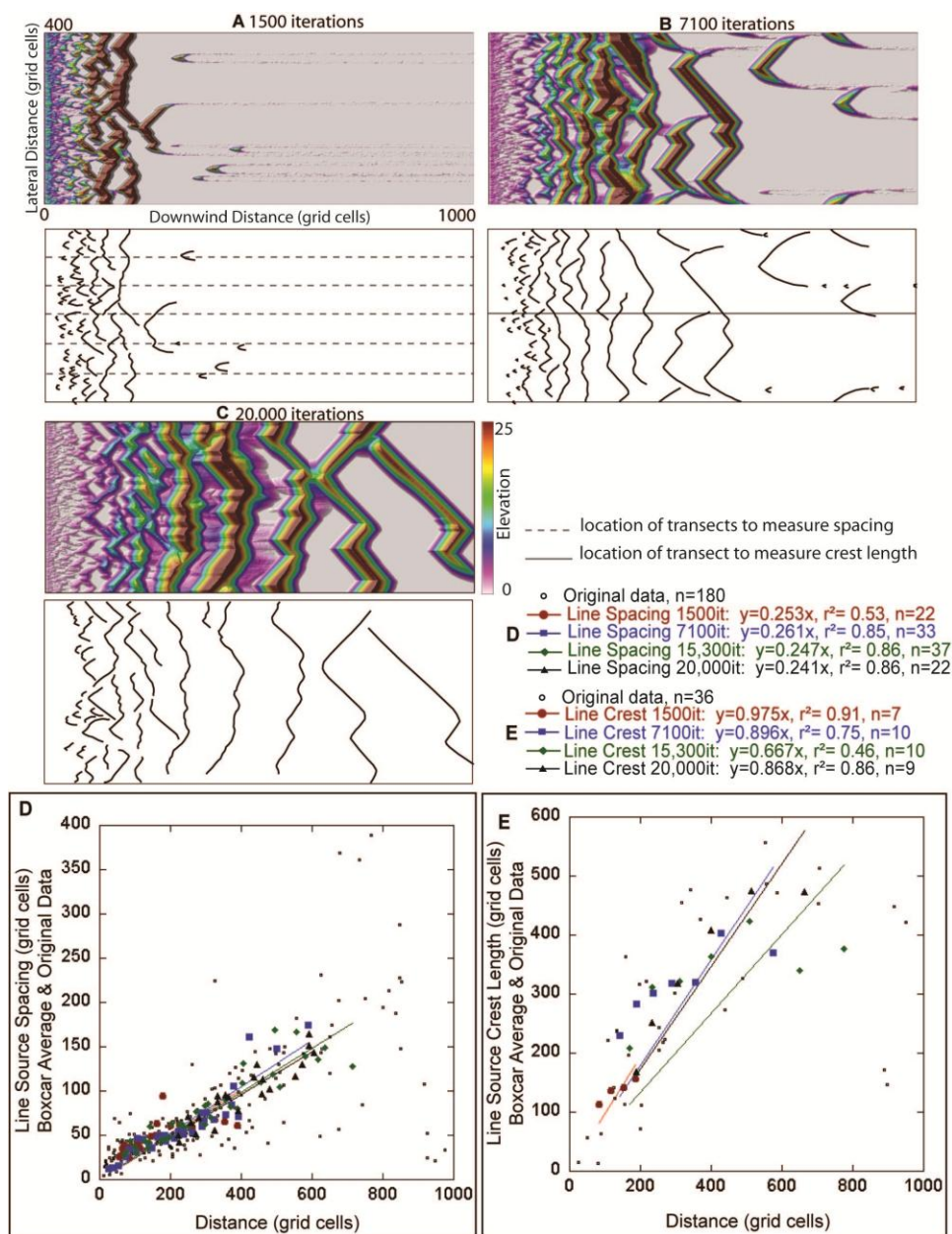


Figure 4.4. Simulation of transverse line source-area geometry over 20,000 iterations. Images (A) to (C) include landscape patterns and dune crest lines at multiple time slices. (A) Landscape after 1500 iterations and the 5 transects used in each time slice to calculate the values in plot D. (B) Landscape after 7100 iterations and the transect location used to calculate the values in plot E. (C) Landscape after 20,000 iterations. (D) Plots of spacing vs. distance for each time slice. (E) Plot of crest length vs. distance for each time slice. Data were smoothed using a boxcar average with a bin size of 4.

3.2.2 Plane Source

In contrast to the point and line source patterns, the transverse plane source pattern emerges simultaneously across the dune field and coarsens over time as the dunes grow and become more distally spaced (Fig. 4.5A to C). Spacing and crest length is compatible with a logarithmic increase in average spacing and average crest length over downwind distance as a function of time (Fig. 4.5D and E) (Anderson, 1990; Werner and Gillespie, 1993; Maske, 2000). The increase in spacing is also indicated in Fig. 4.5A to C by a decrease in the number of dunes within the model space as the dune field develops. However, the variability also increases with time (Fig. 4.5D), which is likely a result of dune interactions occurring along the five fixed transects used to measure spacing. These dune interactions introduce variability and appear to be a fundamental control on spacing.

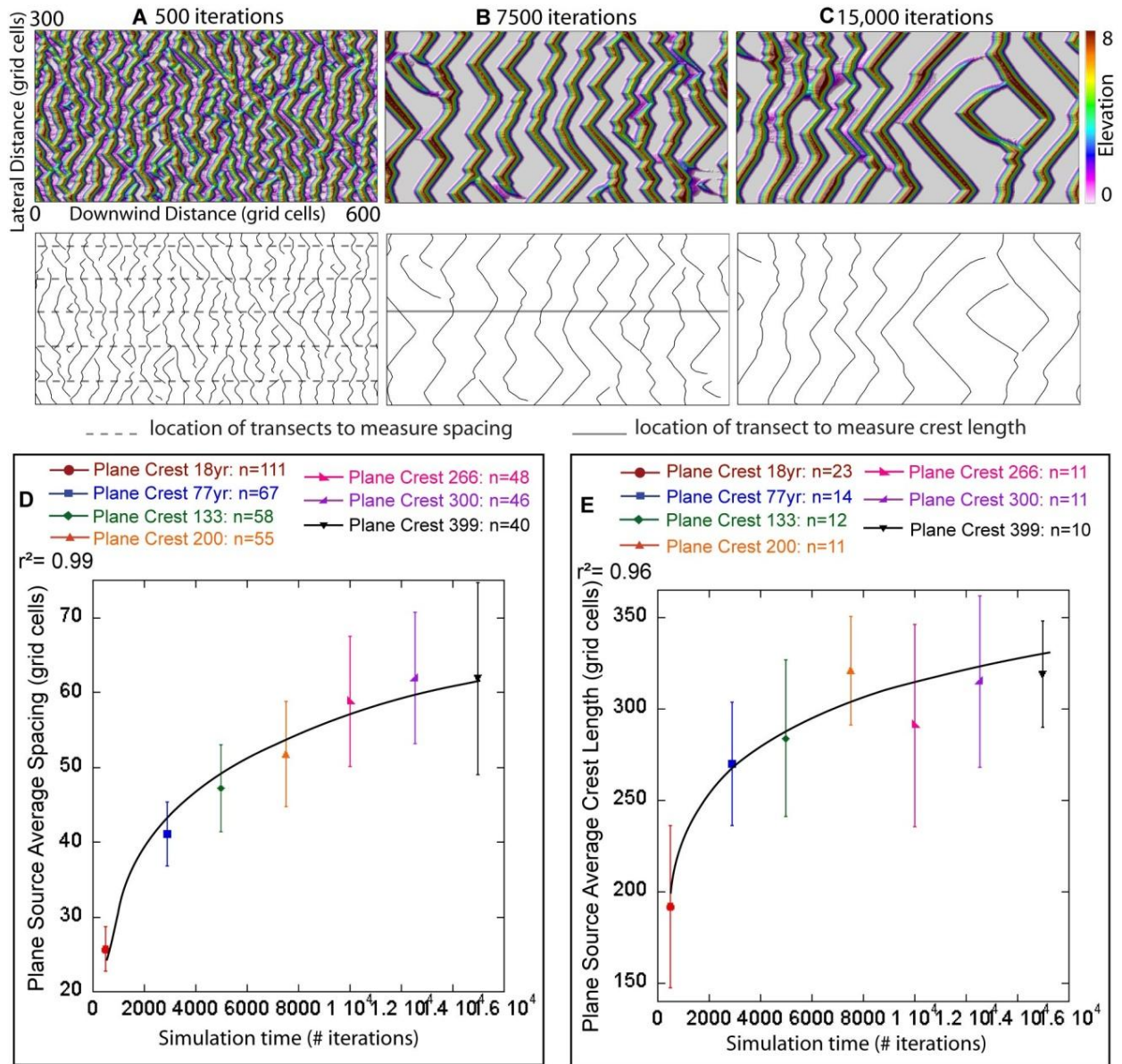


Figure 4.5. Simulation of transverse plane source-area geometry over 15,000 iterations of simulation time. Images (A) to (C) include landscape patterns and dune crest lines at multiple time slices. (A) Landscape after 500 iterations and the 5 equally-spaced transects used in each time slice to calculate the spacing vs. distance values in plot D. (B) Landscape after 7500 iterations and the location of the single transect, drawn through the center of the dune field, used in each time slice to calculate the crest length vs. distance values in plot E. (C) Landscape after 15,000 iterations. (D) Plot of average spacing vs. distance for each time slice. (E) Plot of average crest length vs. distance for 6 time slices. Error bars for plots D and E are $\frac{1}{2}$ std.

3.2.3 Source-Area Pattern Evolution

The simulation results provide insights into aeolian dune-field pattern development over long time scales, which previously have been postulated only from the evolution snapshots recorded in modern dune fields. All three types of source-area geometries demonstrate that spacing, and to a lesser extent, crest length increase with decreasing variability as the dune-field matures. Werner and Kocurek (1997) and Huntley et al. (2008) have shown that dune fields with a lower defect density produce a more stable dune-field pattern. This reduction in the number of defects, and, therefore, fewer dune interactions as a dune field matures can explain the observed stabilized spacing increases for the three simulated source-area geometries. Trends of pattern variables with distance for simulated patterns agree with real-world dune fields (Ewing and Kocurek, 2010).

4. MODELING CHANGES IN SEDIMENT SUPPLY AND TRANSPORT CAPACITY

A large range in basic dune-field configurations is observed when only the sediment supply and transport capacity of the wind are changed in an aeolian system with contemporaneous (steady) influx and no previously stored sediment supply. The $\rho_{sprinkle}$ is the simulated parameter for the sediment supply. The d_s variable is a proxy for the transport capacity of the simulated system, because it is the only variable within Equation 3 that changes between simulations. Approximately 90 scenarios were run for 20,000 iterations modeling a line source with standard parameters under unidirectional wind, while systematically changing the sediment supply and transport capacity values. Each system reached a steady state within the 20,000 iterations and simulation results are

independent of the downwind length of the model grid. Simulations were run using an arbitrarily-sized 1000x400 grid (downwind cells x lateral cells) to examine initial dune-field construction dependence on sediment flux. All simulations were produced using the same set of simple rules (see Model Description section). Simulated patterns were classified based on visual characteristics, dune morphology, and system dynamics. The diversity of patterns simulated using source-to-sink sediment transport can be divided into seven categories according to the magnitude of the sediment supply and transport capacity: non-development, barchan, crescentic ridge, clustered, superimposed, sheet-crescentic ridge, and ridge patterns (Fig. 4.2 and 4.6).

5. SEDIMENT SUPPLY AND TRANSPORT CAPACITY CONTROLS ON DUNE-FIELD DEVELOPMENT

Figure 4.6 shows a phase diagram describing the simulated patterned landscapes after 20,000 iterations as a function of the sediment supply and the transport capacity. When all other model parameters are held constant, large volumes of sediment supply may simulate transport-limited conditions and can produce a stored sediment source within the model space as seen in the superimposed, sheet-crescentic ridge, and ridge patterns (Fig. 4.2 and 4.6 D, E, and F, respectively). Small volumes of sediment supply simulate supply-limited conditions. The non-development pattern contains the smallest volume of sediment supply and represents the extreme end-member of supply- and availability-limited conditions because all of the sediment influx to the system is available for entrainment, yet the volume of influx is quite small (Fig. 4.6). Ridge patterns represent the extreme end-member of transport-limited conditions because the

rate of sediment supply is large enough to completely overwhelm sediment transport. The remaining patterns represent a continuum between these end-members and evolve as a function of increasing sediment supply, which in turn controls the type and frequency of dune interactions. For a constant transport capacity, increasing the sediment supply increases the rate of pattern development and reduces pattern development time, while a large increase in sediment supply forces the system to a different dune-field configuration (Fig. 4.6). For example, barchans form under a range of sediment supply and transport conditions, but at some point, given any transport capacity, crescentic ridges will develop instead of barchans because the sediment supply is so high.

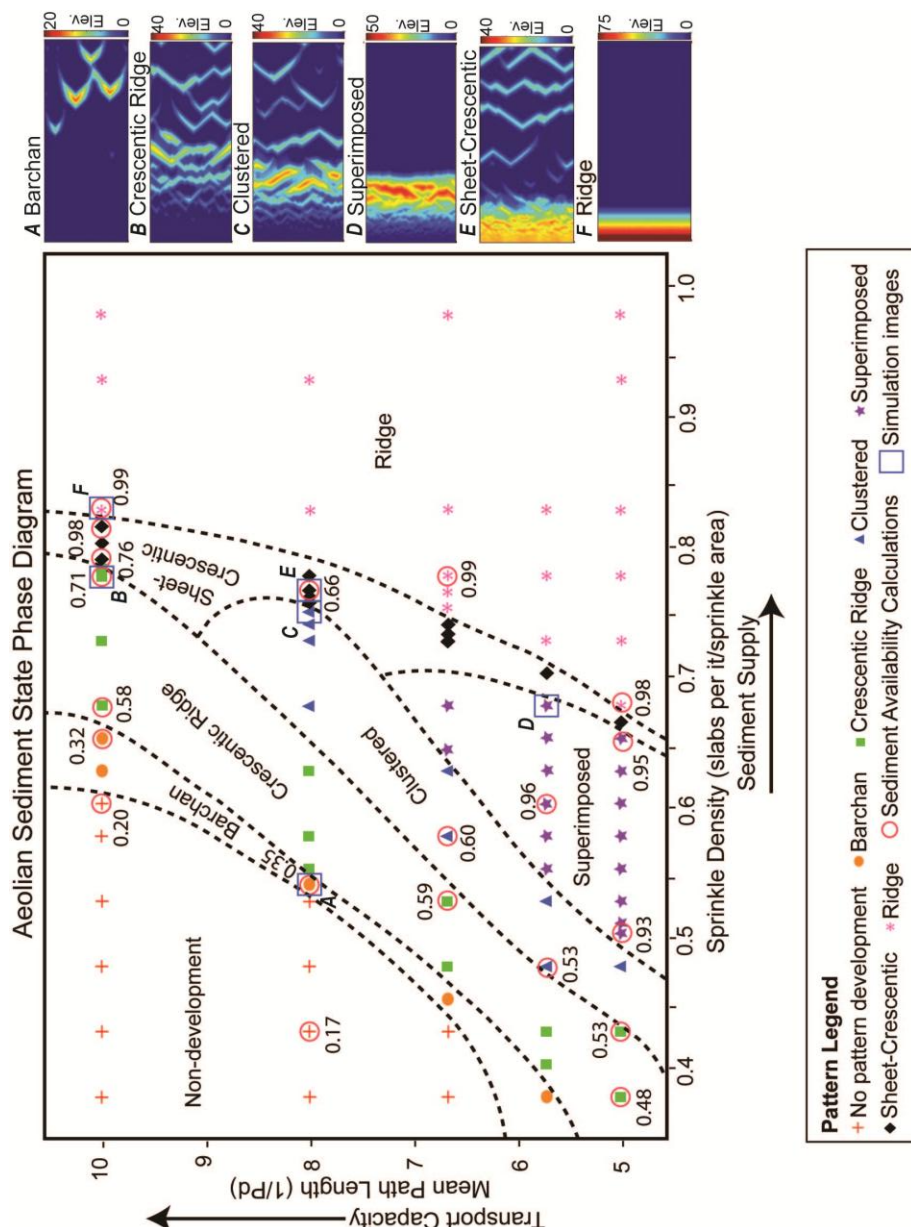


Figure 4.6. The range of landscape patterns seen in simulations as a function of the sediment supply and transport capacity of the wind. Lines of constant sediment availability separate the different pattern categories. Values of sediment availability calculated using Eqn. 4 are shown for specific (circled) simulations. (A)-(F) Transverse model simulations of pattern evolution resulting from changes in the sediment supply and transport capacity of the wind. Patterns are shown as a function of increasing sediment supply, with lowest influx at the top and greatest influx at the bottom. Each simulation was modeled on a 1000x400 grid (downwind cells x lateral cells).

The phase diagram in Fig. 4.6 indicates that, in order to continue developing the same pattern, the transport capacity must be exponentially increased as the sediment supply is linearly increased; this non-linear relationship reflects the basic relationship of $q \approx u_*^3$ (Bagnold, 1941) where transport (q) increases as the cube of the shear stress (u_*). The relative combination of both sediment supply and transport capacity values determines the style of dune-field construction. It is the transport capacity, for each value of sediment supply, that determines how much sediment is on the surface at any one time available for dune construction (Fig. 4.6).

5.1 Simulated Patterns

Detailed descriptions of the seven categories of simulated patterns are listed below, in order of increasing sediment supply and represent fields in Fig. 4.6.

5.1.1 Non-development Pattern

Non-development simulations represent conditions with high transport capacity (i.e., wind) and very little sediment supply, resulting in extreme supply-limited conditions. Throughout the simulation small amounts of sediment are transported across the model space, but the spatial density of sediment required to create bedforms is never reached.

5.1.2 Barchan Pattern

Simulated barchan patterns (Fig. 4.2 and 4.6A) consist of crescentic dunes of various sizes that frequently undergo merging, lateral linking, and calving interactions and are produced under conditions of limited sediment availability for a wide range of

transport rates. The barchan pattern quickly assumes a dynamic steady state, with no subsequent evolution to other configurations. This modeling result is supported by the dynamic steady-state of barchan fields in the flume experiments of Hersen and Douady (2005), and in natural aeolian systems (Fig. 4.2A) (Elbelrhiti et al., 2008).

5.1.3 Crescentic Ridge Pattern

Simulated crescentic ridge patterns (Fig. 4.2 and 4.6B) show a large variability in the shapes, sizes, and frequency of crescentic ridges. The crescentic ridges develop through the lateral linking and merging of small barchan dunes under conditions of adequate sediment availability, across all transport capacity values and all but the highest sediment supply values used in the simulations. The transformation of barchan dunes to crescentic dunes with an increased sediment availability has been well documented in nature (e.g., Bagnold, 1941) and simulated previously (e.g., Werner, 1995). Lateral linking occurs throughout the simulation on time scales of 550-950 iterations per interaction event.

5.1.4 Clustered Pattern

What is termed here as a clustered pattern (Fig. 4.2 and 4.6C) represents a transitional phase between the crescentic ridges (Fig. 4.2 and 4.6B) and superimposed patterns (Fig. 4.2 and 4.6D), and contains elements of both pattern types at somewhat different spatial scales. This pattern is produced using sediment supply values slightly higher than those in the crescentic pattern, except at the largest transport capacity values. In the clustered pattern, crescentic ridges of various sizes and small superimposed dunes migrate over a basal sand accumulation that lacks development of a true slipface. This

basal accumulation acts as a slow-migrating feature over which the superimposed dunes migrate, fundamentally controlling the spacing of clusters across the dune field. This dune-field configuration appears similar to complexes of dunes in southern Afghanistan (Fig. 4.7A) and Magdalena Bay, Baja, Mexico (Fig. 4.2C), as discussed below in the Bedform Clustering section.

5.1.5 Superimposed Pattern

Simulated superimposed patterns (Fig. 4.2 and 4.6D) contain abundant sediment stored as a large, basal crescentic ridge with smaller, superimposed crescentic dunes and ridges that migrate up the stoss slope of the larger bedform. This pattern is produced under higher sediment supply conditions than the clustered pattern, with relatively lower transport capacity values (i.e., wind speeds). This combination of sediment supply and transport capacity results in crescentic ridges migrating up and over a basal sediment accumulation with a true slipface. Although this is not the classic way superimposed dunes form, there are situations where this process may occur. For example, in the Guerrero Negro Dune Field in Baja, Mexico, crescentic dunes and ridges and superimposed bedforms are produced by onshore winds that experience both a decrease in the transport rate and a significant increase in the supply of sand (Fig. 4.7B). This simulated superimposed pattern also resembles the mega-bedforms found in the Atlantic Sahara, Morocco (Fig. 4.7C).

The scalings of simulated superimposed dunes match well with the large superimposed transverse bedforms at the Algodones Dune Field, California (Fig. 4.2D and 4.8) and are most comparable to the upwind dune that has an external sediment

source. Line-source simulations have produced only one superimposed dune; as an aeolian system that lacks an internal sediment source, the only sediment within the model space is added as contemporaneous sediment supply. Once a single superimposed dune develops, the large basal dune spans the entire lateral width of the model space, limiting sediment migration past this bedform and prohibiting further migration of defects (and bedforms) downwind. As a result there is no sediment available to create an additional superimposed dune downwind. Development of a train of superimposed bedforms requires sediment from the bed and this work requires further investigation.

5.1.6 Sheet-Crescentic Ridge Pattern

The sheet-crescentic ridge pattern consists of an upwind stored sand sheet feeding downwind transverse crescentic ridges (Fig. 4.2 and 4.6E). This pattern is produced under relatively high sediment supply conditions and across the entire range of transport capacity values, and evolves differently from both the superimposed and cluster patterns. Unlike the superimposed pattern, dunes in the sheet-crescentic ridge pattern migrate downwind across the entire model space because the increased transport capacity causes more dune migration and diminishes the tendency for a slipface to form. This relative abundance of sediment supply, greater than for superimposed and clustered dunes, creates an upwind supply of stored sediment that feeds downwind bedforms. This sheet-crescentic ridge pattern of a sediment supply sourcing dunes downwind is similar to a beach ridge (foredune) feeding migrating parabolic dunes (Hesp, 1988; 2002), except the simulation produces crescentic ridges instead of parabolic dunes owing to the absence of vegetation. This pattern is also similar to the White Sands Dune Field, New Mexico,

where gypsum sediment is sourced from an upwind playa lake and is entrained by the wind along an ancient beach ridge and natural line source-area (Kocurek et al., 2007). Sediment is first transported from the playa to the ridge where it forms the tallest dunes in the dune field, and is later shed downwind to feed smaller dunes in the center of the basin (Fig. 4.2E).

5.1.7 Ridge Pattern

A very high sediment supply that out-paces the transport capacity of the wind at any speed results in a ridge, which mainly consists of a stored sediment supply, but one with an angle of repose downwind edge (Fig. 4.2 and 4.6F). This ridge pattern grows slowly over time but is limited by the angle of repose and sediment input volume; however, this limitation does not occur in other patterns because they are not saturated with sediment. Dunes do not develop downwind because sediment is piling up faster than it can be transported by the wind. In the real world this extreme combination of high sediment supply with respect to the transport capacity that yields abrupt deposition is analogous to falling dunes on the downwind side of a topographic obstacle (e.g., mountain or valley; Liu et al., 1999; Seppala, 1993). These falling dunes have most frequently been recognized within Martian craters (Bourke et al., 2004) (Fig. 4.2F).

5.2 Sediment Availability Controls On Dune-field Development

The different simulated patterns best reflect sediment availability, which in this cellular model is a function of sediment supply and transport capacity. Discrete calculations for sediment availability values of specific simulations calculated using Equation 4 are plotted in Fig. 4.6. Divisions between categories equal approximately

constant availability values. When the transport capacity is held constant, sediment availability increases with increasing sediment supply (Fig. 4.6). When the sediment supply is held constant, sediment availability decreases with increasing transport capacity. In the case of no dune-field development, sediment availability is extremely low. Simple bedforms are created under conditions of low sediment availability in the barchan pattern and increase in the case of the crescentic ridge pattern. Model results are in good agreement with the well-documented transition between barchans and crescentic ridges as a function of increasing sediment availability. Clusters of crescentic ridges, superimposed dunes, and mega-bedforms are created under conditions of high sediment availability in the clustered and superimposed dune-field patterns. Source areas represent the stored sand produced under the highest sediment availability conditions in the sheet-crescentic ridge and ridge patterns. For these simulations the sediment supply was greater than the transport capacity, producing a pile of stored sediment within the model space.

5.3 Bedform Clustering

The clustered pattern has been previously overlooked, most likely because it is a non-traditional morphology and pattern and, therefore, not a focus of previous investigations. The clustered pattern (Fig. 4.2 and 4.6C) forms under conditions very similar to those of the superimposed pattern (Fig. 4.2 and 4.6D); however, the spatial scales of the bedforms have been slightly offset from those in the superimposed pattern -- either increasing the size of the superimposed dunes or decreasing the size of the basal bedform.

Figure 4.6 indicates that superimposed patterns will form under conditions of greater sediment supply and lower transport capacity, relative to the clustered pattern. For the superimposed pattern at Guerrero Negro Dune Field (Fig. 4.7B), previous studies have identified a highly-fluctuating water table (Fryberger et al., 1990), suggesting that an increase in the sediment supply/availability after a drop in the water table elevation was likely responsible for creating the mega-bedform. In contrast, for the clustered pattern at Magdalena Bay (Fig. 4.2C) model results indicate that a lower sediment supply and/or higher transport capacity with lower sediment availability than the superimposed pattern is responsible for this pattern development. If the sediment supply and availability were to increase and/or the transport capacity of the wind were to decrease, the basal sand sheet could develop a slipface and create a superimposed, compound mega-bedform within these clusters of crescentic ridges.

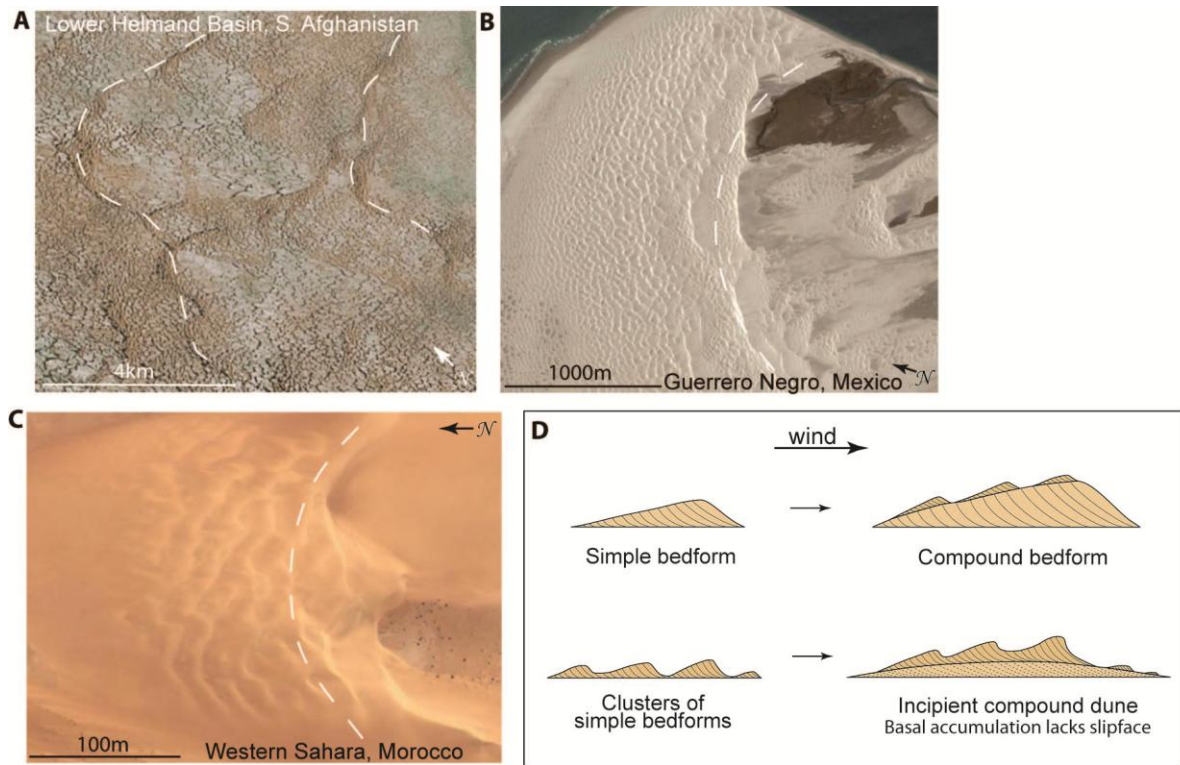


Figure 4.7. Real world examples of clustered and superimposed patterns. Images from Google Earth. White dashed lines mark approximate location of downwind extent of each bedform cluster. (A) Compound, clustered bedforms, Lower Helmand Basin, southern Afghanistan ($30^{\circ}46'N$, $62^{\circ}06'E$). (B) Mega-compound bedform, Guerrero Negro, Baja, México ($27^{\circ}51'N$, $114^{\circ}18'W$). (C) Megabarchan, Atlantic Sahara, Morocco ($21^{\circ}14'N$, $16^{\circ}48'W$). (D) Schematic diagram for the formation of compound dunes. Top panel depicts the commonly-envisioned evolution in which a simple bedform grows large enough to support superimposed dunes. The lower panel depicts an alternate mechanism of bedform clustering with an incipient compound dune. Basal accumulation lacks slipface.

Bedform clustering may represent an incipient compound dune. This is an alternate mechanism to that commonly envisioned for compound dunes in which a simple bedform grows large enough and subsequently supports superimposed dunes (Fig. 4.7D). These two formation mechanisms for superimposed dunes have the potential to develop similar dune-field pattern shapes and scalings (Fig. 4.8).

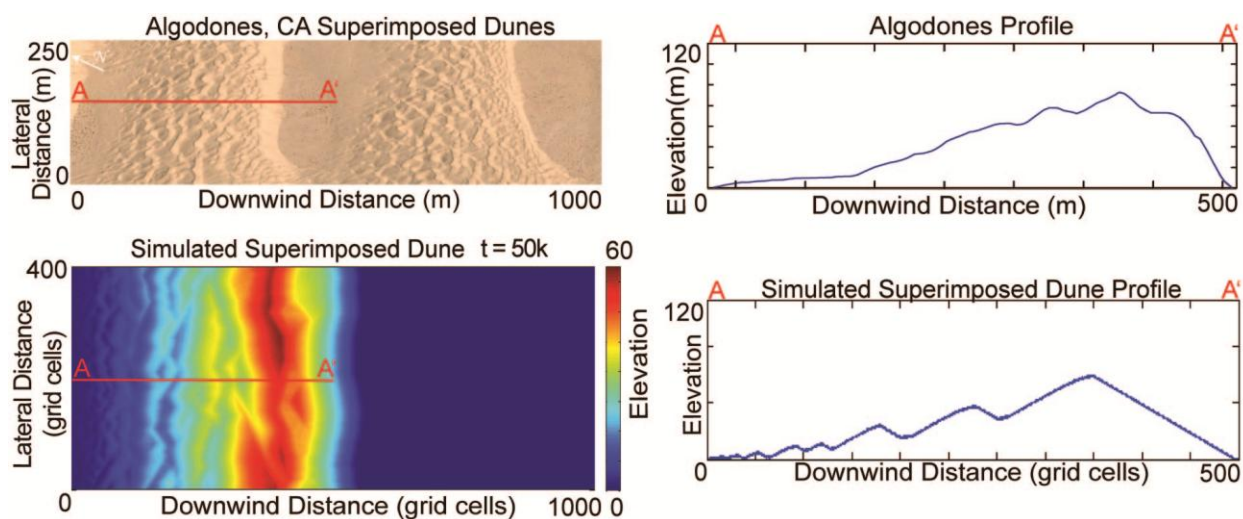


Figure 4.8. Map and plan views of both real-world and simulated superimposed dunes. (A) Algodones Dune Field, California ($32^{\circ}47'N$, $114^{\circ}56'W$). (B) Simulated superimposed dunes. Note similarity of dune morphologies, patterns, and spatial scales. Simulations are explicitly associated with line source simulations. See the Simulated Patterns section for additional discussion.

6. CONCLUSIONS

The simulated aeolian dune-field patterns presented here capture a wide variety of the landscape patterns seen in the real world and were produced by a cellular algorithm composed of a few simple, physically-based rules that do not simulate grain-scale interactions. Simulation results indicate that our cellular model captures the fundamental system components required for aeolian dune-field construction, allowing classification of simulated patterns as a function of sediment supply and transport capacity. This simple, yet versatile model acts as a stimulus to find dune-field patterns and bedform morphologies in nature that resemble simulation results and identify sediment state conditions of formation for these real-world dune fields.

Aeolian sediment state fundamentally controls the development and evolution of dune-field patterns. Much of the diversity of aeolian dune-field patterns seen in the real world is a function of the sediment supply and transport capacity, which in turn determine the sediment availability of the system. The amount of sediment availability within the system has a profound effect on the dune-field pattern produced. Simple bedforms are produced under lower sediment availability conditions when compared to mega-bedforms, which form under high sediment availability conditions. Extremely high sediment availability produces source areas of stored sediment. The clustered pattern is newly identified and may represent incipient or alternative development of superimposed dunes, in which clusters of bedforms develop superimposed dunes without requiring prior development of a large basal dune. Previous studies suggest this conclusion (Andreotti et al., 2009; Raudkivi and Witte, 1991), and simulations here argue for the feasibility of forming superimposed compound bedforms by bedform clustering.

Evaluating the trends of the crest spacing and crest length over long time scales allows insight into and quantification of the evolution of aeolian dune-field patterns. Simulation results from point and line source-area geometries indicate that spacing and crest length increase over distance at a constant rate through time, while spacing and crest length are compatible with logarithmic time behavior over distance with increasing time for plane source-area geometries. The increase in spacing stabilizes as the dune-field pattern matures for all three source-area geometries as a result of a reduction in the number of defects and associated dune interactions.

7. MATHEMATICAL NOMENCLATURE

d_s = average displacement of a single cell during one polling event

h_s = slab height ratio

ℓ = transport length of one slab

I = length of time represented by one iteration

P_d = pre-defined probability of deposition

P_e = pre-defined probability of erosion

ρ_{spr} = sprinkle density, equivalent to the sediment supply

q_{max} = transport capacity, defined as the sediment flux over a perfectly flat surface

q_{avail} = sediment availability, percent of the surface covered by grains

sprinkle area = number of deposition cells along the downwind & lateral axes of
the model space

8. REFERENCES

- Anderson, R.S. (1990) Eolian ripples as examples of self-organization in geomorphological systems. *Earth-Science Reviews*, 29, 77-96.
- Andreotti, B., Fourriere, A., Ould-Kaddour, F., Murray, B., Claudin, P. (2009) Giant aeolian dune size determined by the average depth of the atmospheric boundary layer. *Nature*, 457, doi:10.1038/nature07787.
- Baas, A.C.W. (1996) Stochastic dune model for the simulation of dune landscapes under desert and coastal conditions. Unpublished MS thesis, University of Amsterdam, Amsterdam, 47p.
- Baas, A.C.W. (2002) Chaos, fractals and self-organization in coastal geomorphology: simulating dune landscapes in vegetated environments. *Geomorphology*, 48, 309-328.
- Baas, A.C.W. (2007) Complex systems in aeolian geomorphology. *Geomorphology*, 91, 311-331.
- Bagnold, R.A. (1941) *The Physics of Blown Sand and Desert Dunes*. Methuen and Co., London, UK, 265 pp.
- Beveridge, C., Kocurek, G., Ewing, R.C., Lancaster, N., Mortekai, P., Singhvi, A.K. and Mahan, S. (2006) Development of spatially diverse and complex dune-field patterns: Gran Desierto Dune Field, Sonora, Mexico. *Sedimentology*, 53, 1391-1409.
- Bishop, S.R., Momiji, H., Carretero-Gonzalez, R. and Warren, A. (2002) Modeling Desert Dune Fields Based on Discrete Dynamics. *Discrete Dynamics in Nature and Society*, 7, 7-17.
- Bourke, M.C., Bullard, J.E. and Barnouin-Jha, O.S. (2004) Aeolian sediment transport pathways and aerodynamics at troughs on Mars. *J. Geophys. Res.*, 109, E07005, doi: 10.1029/2003JE002155.
- del Valle, H.F., Rostagno, L.M., Coronato, F.R., Bouza, P.J. and Blanco, P.D. (2008) Sand dune activity in north-eastern Patagonia. *J. Arid Environ.*, 72, 411-422.
- Derickson, D., Kocurek, G., Ewing, R.C. and Bristow, C. (2008) Origin of a complex and spatially diverse dune-field pattern, Algodones, southeastern California. *Geomorphology*, 99, 186-204.
- Dong, Z., Qian, G., Luo, W., Zhang, Z., Xiao, S. and Zhao, A. (2008) Geomorphological hierarchies for complex mega-dunes and their implications for mega-dune evolution in the Badain Jaran Desert. *Geomorphology*, doi: 10.1016/j.geomorph.2008.10.015.
- Duran, O., Schwammle, V., Lind, P.G., Herrmann, H.J. (2009) The dune size distribution and scaling relations of barchan dune fields. *Granular Matter*, 11: 7-11.
- Elbelrhiti, H., Andreotti, B. and Claudin, P. (2008). Barchan dune corridors: Field characterization and investigation of control parameters. *J. Geophys. Res.*, 113, doi: 10.1029/2007JF000767.
- Ewing, R.C. and Kocurek, G. (in press) Aeolian dune interactions and dune-field pattern formation: White Sands Dune Field, New Mexico. *Sedimentology*.
- Ewing, R.C. and Kocurek, G. (2010) Aeolian dune-field pattern boundary conditions. *Geomorphology*, 114, 175-187.
- Ewing, R.C., Kocurek, G. and Lake, L.W. (2006) Pattern analysis of dune-field parameters. *Earth Surf. Proc. Land.*, 31, 1176-1191.

- Fryberger, S.G., Krystinik, L.F. and Schenk, C.J. (1990) Tidally flooded back-barrier dunefield, Guerrero Negro area, Baja California, Mexico. *Sedimentology*, 37, 23-43.
- Hesp, P. (1988) Morphology, dynamics and internal stratification of some established foredunes in southeast Australia. *Sedimentary Geology*, 55, 17-41.
- Hesp, P. (2002) Foredunes and blowouts: initiation, geomorphology and dynamics. *Geomorphology*, 48, 245-268.
- Hersen, P. and Douady, S. (2005) Collision of barchan dunes as a mechanism of size regulation. *Geophys. Res. Lett.*, 32, L21403, doi:10.1029/2005GL024179.
- Huntley, D.A., Coco, G., Bryan, K.R. and Murray, A.B. (2008) Influence of “defects” on sorted bedform dynamics. *Geophys. Res. Lett.*, 35, L02601.
- Kocurek, G. (1999) The aeolian rock record (Yes, Virginia, it exists, but it really is rather special to create one). In: *Aeolian Environments Sediments and Landforms* (Eds A.S. Goudie, I. Livingstone and S. Stokes), pp. 239-259. John Wiley and Sons, Chichester.
- Kocurek, G. and Lancaster, N. (1999) Aeolian system sediment state: theory and Mohave Desert Kelso dune field example. *Sedimentology*, 46, 505-515.
- Kocurek, G., Carr, M., Ewing, R., Havholm, K.G., Nagar, Y.C. and Singhvi, A.K. (2007) White Sands Dune Field, New Mexico: Age, dune dynamics and recent accumulations. *Sedimentary Geology*, 197, 313-331.
- Liu X.,W., Li, S. and Shen, J. Y. (1999) Wind tunnel simulation experiment of mountain dunes. *J. Arid Environ.*, 42, 49– 59.
- Maske, H.A. (2000). Grain segregation mechanism in aeolian sand ripples. *Eur. Phys.J. E*, 1, 127-135.
- Mountney, N.P. and Russell, A.J. (2009) Aeolian dune-field development in a water table-controlled system: Skeidararsandur, Southern Iceland. *Sedimentology*, 56, 2017-2131.
- Nield, J.M. and Baas, A.C.W. (2008) Investigating parabolic and nebkha dune formation using a cellular automaton modeling approach. *Earth Surf. Proc. Land.*, 33, 724-740.
- Nishimori, H., Yamasaki, M. and Andersen, K.H. (1998) A simple model for the various pattern dynamics of dunes. *Intern. J. Modern Physics B*, 12, 257-272.
- Raudkivi, A.J. and Witte, H.H. (1991) Development of bed features. *Journal of Hydraulic Engineering*, 116, 1063-1079.
- Seppala, M. (1993) Climbing and falling sand dunes in Finnish Lapland. In: Pye, K. (Ed), *The Dynamics and Environmental Context of Aeolian Sedimentary Systems: Geol. Soc. Spec Publ.*, 72, 269– 274.
- Werner, B.T. (1995) Eolian dunes: Computer simulations and attractor interpretation. *Geology*, 23, 1107-1110.
- Werner, B.T. and Gillespie, D.T. (1993) Fundamentally discrete stochastic model for wind ripple dynamics. *Physical Review Letters*, 71, 3230-3233.
- Werner, B.T. and Kocurek, G. (1997) Bedform dynamics: Does the tail wag the dog? *Geology*, 25, 727-730.
- Wilkins, D.E. and Ford, R.L. (2007) Nearest neighbor methods applied to dune field organization: The Coral Pink Sand Dunes, Kane County, Utah, USA. *Geomorphology*, 83, 48-57.

Chapter 5: Conclusions

Chapter 2 presents results from field studies at the White Sands Dune Field, NM, that are used to assemble a toolset to reconstruct both wind direction and wind speed from sets of aeolian cross-strata. Surface processes and the resultant style of stratification arise from the secondary lee-face flow, which is a function of the incidence angle formed between the local crestline and the primary wind direction. Although local dune sinuosity, wind speed, and dune height impact the styles of stratification, incidence angle emerges as a robust tool to bracket the primary wind direction. Rates of erosion/deposition on the lee face also track with incidence angle, such that rates of deposition increase with increasing incidence angles. Grain-size samples show that grain size is not uniform over a dune lee face, but rather the total sediment load traveling over the dune is sorted by the secondary flow and the surface transport. Grainflow is most representative of the total sediment load, whereas grainfall is enriched in grains that traveled in incipient suspension and depleted in grains that traveled in creep. Wind ripples are the least diagnostic surface process because they may form on any lee sediment subject to traction reworking.

Chapter 3 applies the new methodology developed in Chapter 2 to the uppermost sequence of the Permian Cedar Mesa Sandstone on the Colorado Plateau in the southwestern USA. The objective is to demonstrate the utility of this methodology in reconstructing the range of wind directions and wind speeds that gave rise to this portion of the Cedar Mesa dune field. Trial-and-error fit in the Cedar Mesa demonstrated that no single wind direction could account for the sequence of stratification styles observed

along segments of crestlines, but all could be accounted for by two primary winds (from 290° and 005°). In order to satisfy the gross bedform-normal crest orientation and yield net migration of the dunes to the SE, the west wind (290°) would have to have been twice the magnitude (in either duration or intensity) of the north wind (005°). Two wind storms were recognized in the rock record, identified by the presence of basal grainfall deposits. Both storm events were a product of the west wind (290°), indicating that the west wind (290°) blew more intensely than the north wind (005°). Wind speed estimates for typical transporting winds range from 9.0-10.3 m/s (20.1-23.1 mph, while storm wind speeds responsible for deposition of the basal grainfall deposits range from 25.1-32.9 m/s (56.3-73.6 mph).

In Chapter 4 the role of sediment supply, sediment availability and transport capacity in the development and evolution of an aeolian dune-field pattern over long time scales is quantified from numerical simulations. Seven dune-field patterns can be classified from simulation results varying the sediment supply and transport capacity that control the type and frequency of dune interactions, the sediment availability of the system and, ultimately, the development of dune-field patterns. This model allows predictions to be made about the range of sediment supply and wind strengths required to produce the dune-field patterns seen in the real world.

Chapters 2 and 3 used stratification type, cross-strata orientation, set boundaries, and grain sizes collected from aeolian deposits to reconstruct the wind direction and wind speed for individual wind events. These same parameters also control the flow of hydrocarbons in aeolian reservoirs. The permeability and porosity in aeolian reservoirs

are a function of the sorting, packing, and size of the individual grains. As a result, different stratification styles contain very different permeabilities and porosities. Chandler et al. (1989) recorded up to five orders of magnitude difference in permeability between grainflow, wind ripple, and interdune/extra-erg deposits. Grainflow deposits contain the highest permeability, interdune/extra-erg deposits contain the lowest permeability, and wind ripples deposits are located between these end members. Wind ripple deposits help to orient the migration of hydrocarbons and other fluids parallel to the aeolian stratification (Chandler et al., 1989). It is possible to estimate the hydrocarbon fluid flow through a reservoir if the stratification types are known, and to predict baffles and barriers to fluid flow.

Given 3-D seismic reflection data, core samples, and dipmeter and resistivity well logs, it is possible to reconstruct bedform morphologies, cross-strata orientations, stratification types, and bounding surfaces for an aeolian reservoir. These data also allow predictions to be made regarding the percentage of grainflow vs. wind ripples vs. interdune/extra-erg deposits within an aeolian reservoir. This information can be used as a stepping stone to reconstruct the internal architecture of aeolian dunes within the reservoir, and to predict the reservoir architecture away from the well bore. These ideas make the assumption that the aeolian dunes within the reservoir do not change shape through time.

Characterizing the reservoir architecture is a critical step in planning the development and production of an aeolian hydrocarbon reservoir. The results from this dissertation can be used, as described above, to plan the spacing of wells in a

development project and to improve the recovery factor of hydrocarbons from the reservoir.

Chapter 4 used sensitivity analyses and numerical simulations to describe the control of sediment state on the dune-field pattern development, and to predict the sediment supply and transport capacity for modern aeolian dune field patterns. The sediment supply, sediment availability, transport capacity, and paleoclimate information obtained from aeolian deposits as described in Chapters 2 and 3 can be combined to predict the paleolandscape and surface dune-field patterns for specific ancient dune fields. Knowledge of the wind speed, wind direction, bedform morphologies, and sediment supply can be used in numerical simulations to predict the dune-field pattern and spatial extent (or aerial limits) of a specific ancient dune field. Knowledge of the paleolandscape and surficial dune-field pattern is useful for hydrocarbon exploration when an initial wildcat discovery is made. Applying the methods and results from Chapters 2, 3, and 4 can begin to predict the spatial extent of the reservoir both laterally and vertically, and can aid in selecting sites for additional exploration targets and well locations.

This dissertation documents that the surface processes and resulting styles of stratification on the lee faces of aeolian dunes is chiefly a function of the incidence angle between the dune crest and the primary wind direction. Dune sinuosity, wind speed, and dune height are identified as important factors that influence the stratification styles produced by different incidence angles. This dissertation does not address the impact of dune height on stratification styles, because all three dunes measured at White Sands

Dune Field, NM, were of similar heights. Future work should quantitatively investigate the importance of dune height and relative wind speed on lee face stratification and provide any adjustments necessary to use this methodology to reconstruct wind regimes from ancient aeolian cross-strata.

Several potential improvements could be made to the numerical model used in Chapter 4 to enhance the model's capability to simulate specific ancient aeolian sequences: (1) algorithm modifications to include paleotopography on the model surface; (2) the ability to track dune stratigraphy created by the migration of simulated dunes; and (3) the addition of a rule to simulate compression of the fluid flow over the tops of dunes, and to increase the wind speed as it travels up the stoss side of a dune.

Appendix A: Estimating Percentages of Grainflow and Wind Ripples, Cedar Mesa Sandstone

| Set | Strat Type | Numerical Estimates (%) | | Field Estimates (%) | |
|-----|------------|-------------------------|----------------|---------------------|----------------|
| | | % grainflow | % wind ripples | % grainflow | % wind ripples |
| 2Ja | 1 | 0 | 100 | 0 | 100 |
| 2Jb | 1 | 0 | 100 | 0 | 100 |
| 5B | 2 | 19.8 | 80.2 | 20 | 80 |
| 2B | 2 | 32.2 | 67.8 | 40 | 60 |
| 3D | 2 | 9.3 | 90.7 | 40 | 60 |
| 2K | 2 | 19.5 | 80.5 | 40 | 60 |
| 2Jd | 2 | 15.7 | 84.2 | 60 | 40 |
| 2Jc | 2 | 49.4 | 50.6 | 70 | 30 |
| 6G | 2 | 74.2 | 25.8 | 40 | 60 |
| 5B | 2 | 43.5 | 56.5 | 70 | 30 |
| 2E | 2 | 41.2 | 58.8 | 40 | 60 |
| 3C | 2 | 40.2 | 59.8 | 40 | 60 |
| 3D | 2 | 49.2 | 50.8 | 60 | 40 |
| 1F | 2 | 62.5 | 37.5 | 60 | 40 |
| 2H | 2 | 78.2 | 21.8 | 70 | 30 |
| 3D | 2 | 15.8 | 84.2 | 60 | 40 |
| 1C | 2 | 14 | 86 | 5 | 95 |
| 1B | 2 | 45.3 | 54.7 | 60 | 40 |
| 5B | 2 | 41.7 | 58.3 | 80 | 20 |
| 6B | 2 | 47.4 | 52.6 | 40 | 60 |
| 3D | 3 | 34.5 | 65.5 | 70 | 30 |
| 1F | 3 | 62.5 | 37.5 | 55 | 45 |
| 2B | 3 | 26.3 | 73.7 | 30 | 70 |
| 3C | 3 | 69 | 31 | 70 | 30 |
| 1E | 3 | 11.8 | 88.2 | 10 | 90 |
| 4B | 3 | 14.9 | 85.1 | 5 | 95 |
| 1J | 4 | 90.2 | 9.8 | 98 | 2 |
| 4F | 4 | 54.8 | 45.2 | 90 | 10 |
| 3B | 4 | 83.6 | 16.4 | 90 | 10 |
| 2C | 4 | 90.8 | 9.2 | 90 | 10 |
| 2B | 4 | 96.8 | 3.2 | 98 | 2 |

Table A1. Estimating percentages of grainflow and wind ripple stratification within individual aeolian sets, Permian Cedar Mesa Sandstone, SE Utah. Percentages estimated in the field using visual estimates, and estimated numerically by quantifying the aerial portions of JPEG images using Adobe Illustrator and ArcGIS.

Appendix B: Maximum Set Thickness, Cedar Mesa Sandstone

| Maximum Thickness of Individual Sets - Permian Cedar Mesa Sandstone | |
|--|---------------|
| Set | Thickness (m) |
| 1B | 1.553 |
| 1C | 1.519 |
| 1E | 2.123 |
| 1F | 6.013 |
| 1J | 2.113 |
| 2B | 4.0925 |
| 2C | 3.935 |
| 2E | 2.331 |
| 2H | 3.348 |
| 2Ja | 0.81 |
| 2Jb | 0.164 |
| 2Jc | 0.724 |
| 2Jd | 0.758 |
| 2Je | 0.327 |
| 2K | 0.778 |
| 3B | 4.552 |
| 3C | 2.4885 |
| 3D | 2.813 |
| 4B | 2.649 |
| 4F | 5.388 |
| 5B | 4.5365 |
| 6B | 3.535 |
| 6G | 3.269 |

Table A2. Maximum thickness of different aeolian sets measured using topographic survey data, Permian Cedar Mesa Sandstone, SE Utah.

Appendix C: Average Thickness of Individual Grainflows, Cedar Mesa Sandstone

| Permian Cedar Mesa Sandstone | | |
|---------------------------------------|--------------------|---|
| Set | Strat Type | Average Individual Grainflow Thickness (cm) |
| 2B | 2 | 2.25 |
| 2B | 3 | 2.50 |
| 2B | 4 (with ga) | 2.25 |
| 2B | 4 | 1.59 |
| 2B | 2 (2nd occurrence) | 1.24 |
| 3C | 2 | 1.63 |
| 3C | 3 | 2.00 |
| 3D | 2 | 2.38 |
| 3D | 3 | 3.03 |
| 4F | 4 | 1.50 |
| 1F | 2 | 2.84 |
| 5B | 2 (with ga) | 2.60 |
| 2H | 4 | 2.39 |
| 2H | 2 | 2.00 |
| 2Jd | 2 | 1.83 |
| 2Jc | 2 | 1.70 |
| 1J | 4 | 2.00 |
| 6B | 4 | 2.27 |
| 6G | 4 | 2.38 |
| 1C | 2 | 1.36 |
| 1B | 2 | 3.04 |
| 4B | 2 | 2.40 |
| 3B | 4 | 3.09 |
| 2C | 4 | 2.28 |
| 1E | 3 | 2.57 |
| 2E | 2 | 1.76 |
| average across all sets & strat types | | 2.18 |

Table A3. Average thickness of individual grainflow avalanches from different aeolian sets in the Permian Cedar Mesa Sandstone, SE Utah.

References

- Allen, J.R.L. (1982). *Sedimentary Structures: Their character and physical basis*, Volume 2: Amsterdam, Elsevier, 663 p.
- Allmendinger, R.J. (1972), Hydrologic control over the origin of gypsum at Lake Lucero, White Sands National Monument, New Mexico. *M.S. Thesis*, New Mexico Institute of Mining and Technology, Socorro, New Mexico, 182 p.
- Anderson, R.S. (1990) Eolian ripples as examples of self-organization in geomorphological systems. *Earth-Science Reviews*, 29, 77-96.
- Andreotti, B., Fourriere, A., Ould-Kaddour, F., Murray, B., Claudin, P. (2009) Giant aeolian dune size determined by the average depth of the atmospheric boundary layer. *Nature*, 457, doi:10.1038/nature07787.
- Baas, A.C.W. (1996) Stochastic dune model for the simulation of dune landscapes under desert and coastal conditions. Unpublished MS thesis, University of Amsterdam, Amsterdam, 47p.
- Baas, A.C.W. (2002) Chaos, fractals and self-organization in coastal geomorphology: simulating dune landscapes in vegetated environments. *Geomorphology*, 48, 309-328.
- Baas, A.C.W. (2007) Complex systems in aeolian geomorphology. *Geomorphology*, 91, 311-331.
- Bagnold, R. (1941), *The Physics of Blown Sand and Desert Dunes*, Methuen, London.
- Bagnold, R. (1966), An approach to the sediment transport problem from general physics, *Geol. Surv. Prof. Paper*, 422-I.
- Beveridge, C., Kocurek, G., Ewing, R.C., Lancaster, N., Mortekai, P., Singhvi, A.K. and Mahan, S. (2006) Development of spatially diverse and complex dune-field patterns: Gran Desierto Dune Field, Sonora, Mexico. *Sedimentology*, 53, 1391-1409.
- Bishop, S.R., H. Momiji, R. Carretero-Gonzalez, and A. Warren (2002), Modeling desert dune fields based on discrete dynamics, *Discrete Dynamics in Nature and Society*, 7, 7-17.
- Blakey, R.C. (1996). Permian eolian deposits, sequences and sequence boundaries, Colorado Plateau. In: *Paleozoic Systems of the Rocky Mountain Region* (Eds M.W. Longman and S.D. Sonnenfeld), pp. 405–426. Rocky Mountain Section SEPM (Society for Sedimentary Geology), Denver, CO.
- Blakey, R.C., and L.T. Middleton (1983), Permian shoreline eolian complex in Central Arizona: Dune changes in response to cyclic sealevel changes. in *Developments in Sedimentology: Eolian Sediments and Processes*, v. 38, edited by M.E. Brookfield and T.S. Ahlbrandt, p. 551-581

- Bourke, M.C., Bullard, J.E. and Barnouin-Jha, O.S. (2004) Aeolian sediment transport pathways and aerodynamics at troughs on Mars. *J. Geophys. Res.*, 109, E07005, doi: 10.1029/2003JE002155.
- Chandler, M.A., Kocurek, G., Goggin, D.J., and L.W. Lake (1989), Effects of stratigraphic heterogeneity on permeability in eolian sandstone sequence, Page Sandstone, Northern Arizona, *AAPG Bulletin*, 73, 658-668.
- Clemmensen, L.B., and K. Abrahamsen (1983), Aeolian stratification and facies association in desert sediments, Arran basin (Permian), Scotland, *Sedimentology*, 30, 311-339.
- Clemmensen, L.B. and R.C. Blakey (1989), Erg deposits in the Lower Jurassic Wingate Sandstone, northern Arizona: oblique dune sedimentation, *Sedimentology*, 36, 449-470.
- Condon, S.M. (1997) Geology of the Pennsylvanian and Permian Cutler Group and Permian Kaibab Limestone in the Paradox Basin, Southeastern Utah and Southwestern Colorado. U.S. Geol. Surv. Bull., 2000-P, 46 pp.
- Curry, J.R., (1956), The analysis of two-dimensional orientation data, *Journal of Geology*, 64, 117-131.
- del Valle, H.F., Rostagno, L.M., Coronato, F.R., Bouza, P.J. and Blanco, P.D. (2008) Sand dune activity in north-eastern Patagonia. *J. Arid Environ.*, 72, 411-422.
- Derickson, D., Kocurek, G., Ewing, R.C. and Bristow, C. (2008) Origin of a complex and spatially diverse dune-field pattern, Algodones, southeastern California. *Geomorphology*, 99, 186-204.
- Dong, Z., Qian, G., Luo, W., Zhang, Z., Xiao, S. and Zhao, A. (2008) Geomorphological hierarchies for complex mega-dunes and their implications for mega-dune evolution in the Badain Jaran Desert. *Geomorphology*, doi: 10.1016/j.geomorph.2008.10.015.
- Dott, R.H. and Roshardt, M.A. (1972). Analysis of Cross Stratification Orientation in the St. Peter Sandstone in Southwestern Wisconsin. *GSA Bulletin* 83: 2589-2596.
- Dott, R.H., C.W. Byers, G.W. Fielder, S.R. Stenzel, and K.E. Winfree (1986), Aeolian to marine transition in Cambro-Ordovician cratonic sheet sandstone of the northern Mississippi valley, U.S.A, *Sedimentology*, 33, 345-367.
- Dubiel, R.F., Parrish, J.T., Parrish, J.M. and Good, S.C. (1991). The Pangean megamonsoon: evidence from the Upper Triassic Chinle Formation. *Palaios* 6: 347-370.
- Duran, O., Schwammle, V., Lind, P.G., Herrmann, H.J. (2009) The dune size distribution and scaling relations of barchan dune fields. *Granular Matter*, 11: 7-11.

- Eastwood, E.N., Kocurek, G., Mohrig, D. and T. Swanson (in review). A refined method for extracting wind direction and speed from aeolian cross-strata. *J. Geophys. Res.*
- Elbelrhiti, H., Andreotti, B. and Claudin, P. (2008). Barchan dune corridors: Field characterization and investigation of control parameters. *J. Geophys. Res.*, 113, doi: 10.1029/2007JF000767.
- Ewing, R.C., and Kocurek, G. (2010a), Aeolian dune interactions and dune-field pattern formation: White Sands Dune Field, New Mexico, *Sedimentology*, 57, 1199-1219.
- Ewing, R.C. and Kocurek, G. (2010b) Aeolian dune-field pattern boundary conditions. *Geomorphology*., 114, 175-187.
- Ewing, R.C., Kocurek, G. and Lake, L.W. (2006) Pattern analysis of dune-field parameters. *Earth Surf. Proc. Land.*, 31, 1176-1191.
- Ferguson, R.I., and Church, M. (2004). A simple universal equation for grain setline velocity. *J. Sediment. Res.* 74: 933-937.
- Frank A. & Kocurek G. 1994. Effects of atmospheric conditions on wind profiles and aeolian sand transport with an example from White Sands National Monument. *Earth Surf. Proc. and Landf.* 19, 735-745.
- Fryberger, S.G. (2003), Geology of White Sands National Monument web page: www2.nature.nps.gov/geology/parks/whsa/.
- Fryberger, S.G., and C.J. Schenk (1988), Pin stripe lamination: A distinctive feature of modern and ancient eolian sediments, *Sedimentary Geology*, 55, 1-15.
- Fryberger, S.G., Krystinik, L.F. and Schenk, C.J. (1990) Tidally flooded back-barrier dunefield, Guerrero Negro area, Baja California, Mexico. *Sedimentology*, 37, 23-43.
- Gilbert, G. K., 1914, The transportation of debris by running water: U.S. Geological Survey Professional Paper 86, 263 p.
- Grass, A.J. (1971) Structural features of turbulent flow over smooth & rough boundaries, *J. Fluid Mechanics*, 50, 233-255.
- Hesp, P. (1988) Morphology, dynamics and internal stratification of some established foredunes in southeast Australia. *Sedimentary Geology*, 55, 17-41.
- Hesp, P. (2002) Foredunes and blowouts: initiation, geomorphology and dynamics. *Geomorphology*, 48, 245-268.
- Hersen, P. and Douady, S. (2005) Collision of barchan dunes as a mechanism of size regulation, *Geophys. Res. Lett.*, 32, L21403, doi:10.1029/2005GL024179.
- Hintze, L.F. (1980) Geologic Map of Utah. Utah Geological and Mineral Survey, scale 1:500000.

- Howard, A.D. (1977), Effect of slope on the threshold of motion and its application to orientation of wind ripples, *GSA Bulletin* 88, 853-856.
- Hunter, R.E. (1977), Basic types of stratification in small eolian dunes, *Sedimentology*, 24, 361-387.
- Hunter, R.E. (1981), Stratification styles in eolian sandstones: some Pennsylvanian to Jurassic examples from the Western Interior U.S.A. in Recent and ancient nonmarine depositional environments: models for exploration, v. 31, edited by F.G. Ethridge and R.M. Flores, p. 315-329.
- Hunter, R.E., and B.M. Richmond (1987), Daily cycles in coastal dunes, *Sedimentary Geology*, 55, 43-67.
- Hunter, R.E., and D.M. Rubin (1983), Interpreting cyclic crossbedding, with an example from the Navajo Sandstone. in *Developments in Sedimentology: Eolian Sediments and Processes*, v. 38, edited by M.E. Brookfield and T.S. Ahlbrandt, p. 429-454.
- Huntley, D.A., Coco, G., Bryan, K.R. and Murray, A.B. (2008) Influence of “defects” on sorted bedform dynamics. *Geophys. Res. Lett.*, 35, L02601.
- Huntoon, P.W., Billingsley, G.H., Jr and Breed, W.J. (1982) Geologic Map of Canyonlands National Park and Vicinity, Utah. The Canyonlands Natural History Association, scale 1:62000.
- Iverson, J.D. and B.R. White (1982), Saltation threshold on Earth, Mars and Venus, *Sedimentology*, 29, 111-119.
- Jerolmack, D.J. and T.A. Brzinski, (2010), Equivalence of abrupt grain-size transitions in alluvial rivers and eolian sand seas: A hypothesis, *Geology*, 38, 719-722.
- Jerolmack, D., D. Mohrig, J. Grotzinger, D. Fike, and W. Watters (2006), Spatial grain size sorting in eolian ripples and estimation of wind conditions on planetary surfaces: Application to Meridiani Planum, Mars, *J. Geophys. Res.*, 111, E12S02, doi:10.1029/2005JE002544.
- Jerolmack, D., M. Reitz, and R. Martin (2011), Sorting out abrasion in a gypsum dune field, *J. Geophys. Res.*, 116, F02003, doi:10.1029/2010JF001821.
- Kent, D.V., and Tauxe, L., (2005). *Science* 307: 240.
- Kerr, D.R., and R.H. Dott, (1988), Eolian dune types preserved in the Tensleep Sandstone (Pennsylvanian-Permian) north-central Wyoming, *Sedimentary Geology*, 56, 383-402.
- Kocurek, G. (1981), Significance of interdune deposits and bounding surfaces in aeolian dune sands, *Sedimentology*, 28, 753-780.
- Kocurek, G. (1991), Interpretation of ancient eolian sand dunes, *Annu. Rev. Earth Planet. Sci.*, 19, 43-75.

- Kocurek, G. (1996), Desert aeolian systems. in *Sedimentary Environments: Processes, Facies and Stratigraphy*, 3rd ed, edited by H.G. Reading, p. 125-133.
- Kocurek, G. (1999) The aeolian rock record (Yes, Virginia, it exists, but it really is rather special to create one). In: *Aeolian Environments Sediments and Landforms* (Eds A.S. Goudie, I. Livingstone and S. Stokes), pp. 239-259. John Wiley and Sons, Chichester.
- Kocurek, G. and R.H. Dott (1981), Distinctions and uses of stratification types in the interpretation of eolian sand, *J. Sedim. Pet.*, 51, 579-595.
- Kocurek, G., J. Knight, and K. G. Havholm (1991), Outcrop and semi-regional three-dimensional architecture and reconstruction of a portion of the eolian Page Sandstone (Jurassic), *SEPM Concepts in Sedimentology and Paleontology*, 3: 25-43.
- Kocurek, G. and Lancaster, N. (1999) Aeolian system sediment state: theory and Mohave Desert Kelso dune field example. *Sedimentology*, 46, 505-515.
- Kocurek, G., Carr, M., Ewing, R., Havholm, K.G., Nagar, Y.C., and A.K. Singhvi (2007), White Sands Dune Field, New Mexico: Age, dune dynamics and recent accumulations, *Sedimentary Geology*, 197, 313-331.
- Kottowski, F.E. (1958), Lake Otero: second phase in formation of New Mexico's gypsum dunes, *GSA Bulletin*, 69, 1733-1734.
- Langford, R. (2003), The Holocene history of the White Sands dune field and influences on eolian deflation and playa lakes, *Quat. Int.*, 104, 31-39.
- Langford, R.P., and Chan, M.A., (1989). Fluvial-aeolian interactions 2. Ancient Systems. *Sedimentology* 36: 1037-1051.
- Langford, R.P, K.M. Pearson, K.A. Duncan, D.M. Tatum, L. Adams, and P. Depret (2008), Eolian topography as a control on deposition incorporating lessons from modern dunes seas: Permian Cedar Mesa Sandstone, SE Utah, U.S.A, *J. Sedim. Res.*, 78, 410-422, doi: 10.2110/jsr.2008.045.
- Laursen, E.M. (1958), The total sediment load of streams, *Proceedings of the American Society of Civil Engineers, Journal Hydraulics Division*, 84, 1530-1536.
- Liu X., W., Li, S. and Shen, J. Y. (1999) Wind tunnel simulation experiment of mountain dunes, *J. Arid Environ.*, 42, 49– 59.
- Loope, D.B., (1984). Eolian origin of upper Paleozoic sandstone, southeastern Utah. *Journal of Sedim. Pet.* 54: 563-580.
- Loope, D.B., (1985). Episodic deposition and preservation of eolian sands – a late Paleozoic example from southeastern Utah. *Geology* 13: 73-76.
- Loope, D.B., Rowe, C.M., and Joeckel, R.M., (2001). Annual monsoon rains recorded by Jurassic dunes. *Nature* 412: 64.

- Loope, D.B., Steiner, M.B., and Rowe, C.M., (2004). Tropical westerlies over Pangean sand seas. *Sedimentology* 51: 315-322.
- Maske, H.A. (2000). Grain segregation mechanism in aeolian sand ripples. *Eur. Phys.J. E*, 1, 127-135.
- McKee, E.D. (1966), Structures of dunes at White Sands National Monument, New Mexico (and a comparison with structures of dune from other selected areas), *Sedimentology*, 7, 3-69, doi:10.1111/j.1365-3091.1966.tb01579.x.
- McKee, E.D. and J.R. Douglass (1971), Growth and movement of dunes at White Sands National Monument, New Mexico, *U.S.G.S. Prof. Paper 750-D*, p. D108-D114.
- McKee, E.D., and R.J. Moiola (1975), Geometry and growth of the White Sands Dune Field, New Mexico. *U.S.G.S. J. Res.* 3, 59-66.
- Mountney, N.P. (2006). Periodic accumulation and destruction of aeolian erg sequences in the Permian Cedar Mesa Sandstone, White Canyon, southern Utah, USA, *Sedimentology*, 53, 789-823.
- Mountney, N.P., and A. Jagger (2004), Stratigraphic evolution of an aeolian erg margin system: the Permian Cedar Mesa Sandstone, SE Utah, USA, *Sedimentology*, 51, 713-743.
- Mountney, N.P. and Russell, A.J. (2009) Aeolian dune-field development in a water table-controlled system: Skeidararsandur, Southern Iceland. *Sedimentology*, 56, 2017-2131.
- Nickling, W.G., McKenna Neuman, C. And N. Lancaster, (2002), Grainfall processes in the lee of transverse dunes, Silver Peak, Nevada, *Sedimentology* 49, 191-209.
- Nield, J.M. and Baas, A.C.W. (2008) Investigating parabolic and nebkha dune formation using a cellular automaton modeling approach. *Earth Surf. Proc. Land.*, 33, 724-740.
- Nino, Y., F. Lopez, and M. Garcia (2003), Threshold for particle entrainment into suspension, *Sedimentology*, 50, 247-263.
- Nishimori, H., Yamasaki, M. and Andersen, K.H. (1998) A simple model for the various pattern dynamics of dunes. *Intern. J. Modern Physics B*, 12, 257-272.
- Nishimura, K., and J.C.R. Hunt (2000), Saltation and incipient suspension above a flat particle bed below a turbulent boundary layer, *J. Fluid Mech.*, 417, 77-102, doi:10.1017/S0022112000001014.
- Nuccio, V.F. and Condon, S.M. (1996) Burial and thermal history of the Paradox Basin, Utah and Colorado, and the petroleum potential of the Middle Pennsylvanian Paradox Formation. *U.S. Geol. Surv. Bull.* 2000-O: 41 pp.
- Parrish, J.T., and F. Peterson (1988), Wind directions predicted from global circulation models and wind directions determined from eolian sandstones of the western

- United States – a comparison, in *Sedimentary Geology* 56, edited by G. Kocurek, p. 261-282.
- Patzkowsky, M.E., Smith, L.H., Markwich, P.J., Engberts, C.J., and Gyllenhall, E.D. (1991). Application of the Fujita-Ziegler paleoclimatic model: Early Permian and Late Cretaceous examples. *Palaeogeog., Palaeoclim., Palaeoeco.* 86: 67-85.
- Peterson, F., (1988). Pennsylvanian to Jurassic eolian transportation systems in the western United States *in: Kocurek, G. ed. Sedimentary Geology* 56: 207-260.
- Poole, F.G., (1962). Wind directions in late Paleozoic to middle Mesozoic time on the Colorado Plateau. *U.S. Geol. Surv., Prof. Pap., 450-D: D147-D151.*
- Raudkivi, A.J. and Witte, H.H. (1991) Development of bed features. *Journal of Hydraulic Engineering*, 116, 1063-1079.
- Reiche, P. (1938), An analysis of cross-lamination the Coconino Sandstone, *J. of Geology*, 46, 905-932.
- Reitz, M.D., Jerolmack, D.J., Ewing, R.C., and R.L. Martin (2010), Barchan-parabolic dune pattern transition from vegetation stability threshold, *Geophys. Res. Lett.*, 37, L19402, doi:10.1029/2010GL044957.
- Rowe, C.M., Loope, D.B., Oglesby, R.J., Van der Voo, R., and Broadwater, C.E., (2007), Inconsistencies between Pangean reconstructions and basic climate controls, *Science* 318, 1284-1286.
- Rubin, D.M., and R.E. Hunter (1982), Bedform climbing in theory and nature, *Sedimentology*, 29, 121-138.
- Rubin, D. and R.E. Hunter (1983), Reconstructing bedform assemblages from compound crossbedding, in *Eolian sediments and processes*, edited by M.E. Brookfield, and T.S. Ahlbrandt, p. 407-427, Elsevier, Amsterdam, Netherlands.
- Rubin, D.M., and R.E. Hunter (1987), Bedform alignment in directionally varying flows, *Science*, 237, 276-278.
- Rubin, D.M., and H. Ikeda (1990), Flume experiments on the alignment of transverse, oblique, and longitudinal dunes in directionally varying flows, *Sedimentology*, 37, 673-684.
- Scherer, C.M.S. and K. Goldberg (2010), Cyclic cross-bedding in the eolian dunes of the Sergi Formation (Upper Jurassic), Reconcavo Basin: Inferences about the wind regime, *Palaeogeography, Palaeoclimatology, Palaeoecology*, 296, 103-110.
- Scotese, C.R., Bambach, R.K., Barton, C., Van der Voo, R., and Ziegler, A.M., (1979). Paleozoic base maps. *J. Geol.* 87: 217-277.
- Scotese, C.R. (2003). PALEOMAP, Earth, History, Jurassic. URL <http://www.scotese.com/Jurassic.htm> (November 2008).

- Seppala, M. (1993) Climbing and falling sand dunes in Finnish Lapland. In: Pye, K. (Ed), *The Dynamics and Environmental Context of Aeolian Sedimentary Systems: Geol. Soc. Spec Publ.*, 72, 269– 274.
- Shao, Y. (2000), *Physics and modeling of wind erosion*, Atms. and Oceano. Sci. Library, 23, Kluwerk, Dordrecht.
- Shao, Y. and H. Lu (2000), A simplified expression for threshold friction velocity, *J. Geophys. Res.*, 105, 22,437-22,443.
- Smith, J.D., and T.S. Hopkins (1972), Sediment transport on the continental shelf off of Washington and Oregon in light of recent current measurements. in *Shelf Sediment Transport: Process and Patterns*, edited by D.J.P. Swift, D.B. Duane, and O.H. Pilkey. Dowden, p. 143-179, Hutchinson & Ross, Stroudsburg, PA.
- Stanescio, J.D., and Campbell, J.A., (1989). Eolian and non-eolian facies of the Lower Permian Cedar Mesa Sandstone Member of the Cutler Formation, southeastern Utah. *U.S. Geol. Surv. Bull.* 1800-F.
- Steiner, M.B., (2003). A cratonic Middle Jurassic paleopole: Callovian-Oxfordian stillstand (J-2 cusp), rotation of the Colorado Plateau, and Jurassic North American apparent polar wander. *Tectonics* 22: 1020. doi:10.1029/2001TC001284.
- Sweet, M.L., and G. Kocurek (1990), An empirical model of aeolian dune lee-face air-flow, *Sedimentology*, 37, 1023-1038.
- Szykiewicz, A., Ewing, R.C., Moore, C.H., Glamoclija, M. Bustos, D., and L. Pratt (2010), Origin of terrestrial gypsum dunes – Implications for Martian gypsum-rich dunes of Olympia Undae, *Geomorphology*, 121, 69-83.
- Taggart, S. Hampson, G.J., and M.D. Jackson (2010), High-resolution stratigraphic architecture and lithological heterogeneity within marginal aeolian reservoir analogues, *Sedimentology*, 57, 1246-1279.
- Tanner, W.F., (1965). Upper Jurassic paleogeography of the Four Corners region, *J. Sedim. Pet.*, 35, 534-574.
- Tsoar, H. (1983), Dynamic processes acting on a longitudinal (seif) sand dune, *Sedimentology*, 30, 567-578.
- Van Rijn, L.C. (1984), Sediment transport part I: Bed load transport, *J. Hydr. Engin.*, 110, 1431-1456.
- Walker, I.J., and W.G. Nickling (2002), Dynamics of secondary airflow and sediment transport over and in the lee of transverse dunes, *Progress in Physical Geography*, 26, 47-75.

- Walker, I.J., and W.G. Nickling (2003), Simulation and measurement of surface shear stress over isolated and closely spaced transverse dunes in a wind tunnel, *Earth Surface Processes and Landforms*, 28, 1111-1124.
- Werner, B.T. (1995), Eolian dunes: Computer simulations and attractor interpretation, *Geology*, 23, 1107-1110.
- Werner, B.T. and Gillespie, D.T. (1993) Fundamentally discrete stochastic model for wind ripple dynamics. *Physical Review Letters*, 71, 3230-3233.
- Werner, B.T. and G. Kocurek (1997), Bedform dynamics: Does the tail wag the dog? *Geology*, 25, 727-730.
- Wilkins, D.E. and Ford, R.L. (2007) Nearest neighbor methods applied to dune field organization: The Coral Pink Sand Dunes, Kane County, Utah, USA. *Geomorphology*, 83, 48-57.
- Ziegler, A.M., Hulver, M.L., and Rowley, D.B. (1997). Permian world topography and climate. In Martini, I.P. ed. *Late glacial and postglacial environmental changes: Pleistocene, Carboniferous-Permian, and Proterozoic*. Oxford, Oxford University Press: 111-146.

Vita

Erin was born in Laramie, Wyoming. She grew up in Flagstaff, Arizona, hiking and backpacking in the Grand Canyon. Her love of the Grand Canyon led her to study geology at Northern Arizona University with Dr. Ron Blakey where she received a B.S. in Geology and a minor in Physics. Erin has always been intrigued by earth surface processes and the physics that drive sediment-fluid interactions, and chose to pursue her doctorate at The University of Texas at Austin to work with Dr. Gary Kocurek. Erin met her fiancé, Andrew, as a teaching assistant for GEO 416M Sedimentary Rocks during the 3rd year of her PhD while Andrew was studying petroleum engineering. Outside of geology, Erin enjoys spending time outside, traveling, exercising, and being with family. She is a former competitive swimmer and currently a competitive triathlete and cyclist. Erin plans to fulfill her lifelong dream of completing an Ironman Triathlon now that she has finished her PhD!

Permanent email: erin.eastwood@utexas.edu

This manuscript was typed by Erin N. Eastwood.